学位論文

Nonequilibrium current fluctuation in interacting mesoscopic systems

（相互作用のあるメゾスコピック系における非平衡電流揺らぎ）

平成28年12月博士(理学)申請

東京大学大学院理学系研究科
物理学専攻

鈴木　貴文

Thesis

Nonequilibrium current fluctuation in interacting mesoscopic systems

Takafumi Suzuki

Department of Physics, Graduate School of Science
The University of Tokyo

February 2017

Acknowledgements

I would like to express my deepest gratitude to my supervisor Prof. Seiji Miyashita for providing me fruitful discussions and wonderful opportunities to work through my Ph.D. course. I had many discussions with Dr. Takashi Mori, and was always stimulated by his deep insight into the physics. I am also greatly in debt to all the other current, previous, and quasi members of Miyashita group; Tatsuhiko Shirai, Taichi Hinokihara, Eriko Kaminishi, Sergio Andraus, Adrien Bolens, Takuya Hatomura, Hiroki Ikeuchi, Moriaki Sugita, Yuta Goto, and Kaoru Yamamoto. I am grateful to Prof. Takeo Kato in Institute for Solid State Physics (ISSP) for leading me to the field of mesoscopic physics. After I started my Ph.D. course, I often had no idea what I should do. I really appreciate Dr. Rui Sakano in ISSP for kindly guiding me into the right direction at such times.

During my Ph.D. course, I experienced two long-term visits to different organizations. Large parts of this thesis are based on the study performed during these visits. First, I spent at Prof. Volker Meden's group in RWTH Aachen University from January to March in 2015. I started research on the functional renormalization group with Prof. Volker Meden and Dr. Dante Marvin Kennes. I was always helped by their full knowledge of the method and warm hospitality. I realized delight in research through the collaborative work with them. For the last two months in the same year, I stayed at Prof. Hisao Hayakawa's group in Yukawa Institute for Theoretical Physics (YITP) to launch the study on non-Gaussian noise. The visit was financially supported by Atom visiting program held by YITP. During the visit, I had opportunities to have discussion with Dr. Kiyoshi Kanazawa in Tokyo Institute of Technology and Prof. Yasuhiro Utsumi in Mie University. I greatly acknowledge Prof. Hisao Hayakawa for his stimulating discussions and providing me this opportunity. I also acknowledge Dr. Tomohiko G. Sano and Dr. Satoshi Takada, who were Ph.D. students in the Kyoto University at that time, for their warm hospitality.

I acknowledge financial support provided by the Advanced Leading Graduate Course for Photon Science (ALPS). Finally, I would like to express my indebtedness to my family for their understanding and continuous supports.

Publication List

1. “Non-Gaussianity in a quasiclassical electronic circuit”, Takafumi J. Suzuki and Hisao Hayakawa, arXiv:1609.01325. [Chapter 4]

2. “Current noise of the interacting resonant level model”, Takafumi J. Suzuki, Dante Marvin Kennes, and Volker Meden, Phys. Rev. B **93**, 085306 (2016). [Chapter 5]

3. “Effects of Coulomb interaction on photon-assisted current noise through a quantum dot”, Takafumi J. Suzuki and Takeo Kato, Phys. Rev. B **91**, 165302 (2015)

Abstract

Current fluctuation in mesoscopic conductors is of increasing importance along with the development of nanotechnology. The current fluctuation provides interesting and unique information on nonequilibrium interacting systems. The distribution of the current has also been extensively studied from a viewpoint of the nonequilibrium statistical physics. In this thesis, we shed light on two important aspects of the current fluctuation in interacting systems: (i) a detection scheme of the current distribution in a mesoscopic conductor and (ii) renormalization effect on current noise through an interacting mesoscopic system. The difficulty of analyzing the fluctuation in interacting systems arises from the absence of a systematic framework. We utilize a path integral approach based on the Keldysh formalism to provide microscopic understanding of the current fluctuation.

(i) Detection scheme of current distribution in a mesoscopic conductor

Owing to the rapid development of on-chip devices, it becomes realistic to characterize nonequilibrium transport in mesoscopic conductors by the distribution of current through the system. The first purpose of this thesis is to substantiate a detection scheme of the current distribution by using a simple LC circuit. We use a stochastic method of describing the dynamics of the detector LC circuit, which can be understood as a stochastic particle subject to non-Gaussian noise. We show that the current distribution is fully determined by the steady-state probability density function of the degrees of freedom in the detector circuit in the classical-to-quantum crossover regime. At sufficiently low temperatures, the effect of the quantum fluctuation in the detector circuit becomes significant to correctly estimate the current distribution.

(ii) Renormalization effect on current noise in a charge-fluctuating quantum dot

Among mesoscopic conductors, quantum dot systems offer an ideal arena to study nonequilibrium transport of interacting fermions. One of the most prominent many-body effects in the quantum dot system is the strong renormalization of the transmission between the quantum dot and the reservoirs due to their capacitive coupling. The second purpose of this thesis is to elucidate the renormalization effect on current noise in the charge-fluctuating quantum dot system. We develop a functional renormalization group method to systematically investigate the current noise in the quantum dot system in wide parameter regions. It is found that the current noise shows power-law behavior at large bias voltages. This is a manifestation of the renormalization effect in the nonequilibrium situation.

Table of contents

Chapter 1

Introduction

1.1 Current fluctuation in mesoscopic conductors

Mesoscopic physics deals with condensed matters of an intermediate length scale [1]. The characteristic lengthscale lies between the microscale where the system is considered as an isolated quantum system and the macroscale where fluctuation is suppressed in the thermodynamic limit. Hence, the mesoscopic systems offer an ideal arena for research into both the quantum and statistical physics. The mesoscopic physics has been developed along with the rapid advance in nanotechnology. In particular, novel transport phenomena have been investigated in artificially-fabricated mesoscopic conductors. They are easily driven out of equilibrium by an applied electric field in a controllable manner. Such availability of the mesoscopic conductors paves the way to understanding the nonequilibrium statistical physics.

The importance of current fluctuation in mesoscopic conductors has been widely appreciated in a field of the mesoscopic physics, leading to a vast amount of experimental and theoretical studies [2, 3]. The intrinsic sources of the current fluctuation are classified into two types: thermal noise and shot noise. While the thermal noise is determined by the equilibrium nature of the system, the shot noise has a nonequilibrium origin. It is a consequence of the granularity of carrier particles, and reveals unique information which is averaged out in conductance. The experimental demonstration of a fractional charge in fractional quantum Hall systems is a good example to illustrate the usefulness of the shot noise [4, 5]. The informative role of the noise is expressed as "The noise is the signal" by Rolf Landauer, who made a significant contribution to research into the mesoscopic physics [6].

As the current fluctuation essentially reflects a correlation of particles, it can be utilized to elucidate the properties of a low-energy excitation which is intrinsic to the system. Among various mesoscopic conductors, quantum dot systems form an ideal test stage for investigating the nonequilibrium transport of interacting electrons. At low temperatures, the quantum dot exhibits the Kondo effect [7], where an elementary excitation is described by the Fermi liquid interacting with each other via the residual interaction [8]. The current fluctuation in the quantum dot system in the Kondo regime helps us to understand the microscopic scattering processes of the Fermi liquid [9]. Another prominent example of quantum many-body effects is the Fermi-edge singularity [10, 11]. The Coulomb interaction between a local electron and surrounding conduction electrons

can lead to singularities of the resonant tunneling close to the Fermi energy [12–15]. It is closely related to the instability of the Fermi sea against a localized perturbation [16], and generalization of the problem to the nonequilibrium transport provides nontrivial and challenging issues.

Largely owing to the great advance in measurement techniques, the interest in the current fluctuation has been extended beyond the Gaussian distribution [17–20]. The first significant step was made by L. S. Levitov and G. B. Lesovik, who laid a foundation of the full counting statistics [17]. They considered the counting statistics of electrons which are transferred from one reservoir to another in a sufficiently long time interval. The histogram thus obtained fully characterizes the microscopic scattering processes in the mesoscopic conductor. The current distribution has attracted much attention also from a viewpoint of nonequilibrium statistical mechanics. The combination of the equilibrium property of the reservoir and the microscopic reversibility of the quantum dynamics requires the current distribution to satisfy a special symmetry, which is known as the fluctuation theorem [21]. The fluctuation theorem reproduces the fluctuation-dissipation relation and the Onsager-Casimir reciprocal relations in the linear-response regime. What is surprising is that the fluctuation theorem is valid far from the equilibrium state, imposing strict constraints on the current distribution. Another important consequence of the fluctuation theorem is the appearance of the universal relations among nonlinear transport coefficients [22]. Experimental verification of the fluctuation theorem in the mesoscopic conductors is currently in progress [23–27].

The fundamental question as to the full counting statistics is whether and how it can be detected in a feasible measurement. The measuring device was first proposed by considering an ideal spin $1/2$ galvanometer that is exposed to a magnetic field produced by current through a conductor [18]. In this setup, the number of the transferred charge in a given time interval is directly related to the precession angle of the spin. Later, a simple LC circuit started to be employed as a realistic detector circuit for the current through the conductor [28–30]. The detector was also quantum mechanically treated to ascertain the measurability of the full counting statistics [19, 31–33]. Now, the subject on the measurement of the full counting statistics is not just a theoretical matter because of the remarkable development of on-chip detection schemes [34–45]. In various experiments, the detector consists of another electronic circuit fabricated on the same chip. In the classical regime, it is even possible to count the number of the transferred electrons [25, 46, 47], and the histogram is qualitatively compared with the theoretical prediction [25].

Motivated by the theoretical and experimental progresses on the current fluctuation in mesoscopic conductors, we investigate the following topics in this thesis.

Detection scheme of non-Gaussian current fluctuation

We investigate a realistic detection scheme of non-Gaussian current fluctuation in a mesoscopic conductor by using a simple LC circuit as a detector circuit. In previous works, the explicit relations between the cumulants of the current distribution and those of the detector LC circuit have been known only for the first three cumulants. It is still an open question whether and how the LC circuit can characterize all the cumulants of the current. In this thesis, we establish the relations for all the higher-order cumulants by developing a stochastic method of incorporating the thermal, non-Gaussian, and quantum noise in the detector circuit. It is shown that there is a one-to-one correspondence between the distribution of the current and the detector

in the quasi-classical regime. We also clarify how the quantum dynamics of the detector circuit affects the estimation of the current fluctuation.

Renormalization effect on current noise in a charge-fluctuating quantum dot

We investigate current noise through a quantum dot system dominated by charge fluctuation. It is well established that the capacitive coupling between the quantum dot and the reservoir introduces power-law singularities in $I-V$ characteristics due to the renormalization effect [48–54]. However, little is known about the current noise except for a special parameter point where the model exhibits self-duality [55–57]. In this thesis, we clarify the renormalization effect on the current noise in the charge-fluctuating quantum dot system. The functional renormalization group (FRG) is one of the promising theoretical schemes which can incorporate the two-body interaction in nonequilibrium situations [51, 58]. We develop an FRG scheme to gain a comprehensive understanding on the current noise in the interacting quantum dot system in wide parameter regions.

1.2 Full counting statistics

In contrast to bulk systems where the fluctuation is suppressed in the thermodynamic limit, the fluctuation of current in mesoscopic conductors is of the same order as its mean value. This fact is crucial from a viewpoint of application as the signal-to-noise ratio determines the performance of the device. On the other hand, unique properties of the fluctuation have also been appreciated and utilized for a long time. The current fluctuation has rich information on carrier particles and dynamics of a system [2]. The noise measurement has now become an indispensable tool to investigate equilibrium and nonequilibrium systems. Substantially supported by the rapid development of fine processing and measuring technologies, the trend is gradually being shifted to the current fluctuation beyond the Gaussian approximation, namely the current distribution. It is closely related to the fundamental aspects of nonequilibrium phenomena, such as the fluctuation theorem [21]. This also requires us to develop a suitable framework to describe the current fluctuation in all orders. The full counting statistics is such a theory to conveniently and totally characterize the current distribution [18].

In this section, we review the theory of the full counting statistics, and provide basic knowledge on the current fluctuation. In subsection 1.2.1, we provide a general framework to describe the fluctuation of current through a mesoscopic conductor. In subsection 1.2.2, the full counting statistics is applied to the simplest model in order to elucidate the fundamental microscopic processes lying behind the nonequilibrium transport phenomena. In subsection 1.2.3, the fluctuation theorem and its consequences are discussed.

1.2.1 Stage of nonequilibrium transport

Let us consider a generic setup which consists of the system coupled to the left and right reservoirs (Fig. 1.1). The full Hamiltonian reads $H = H_0 + H_T$. The isolated regions are described by the Hamiltonian $H_0 = H_S + H_L + H_R$, where H_S, H_L, and H_R are the Hamiltonian of the isolated system, the left reservoir, and the right reservoir, respectively.

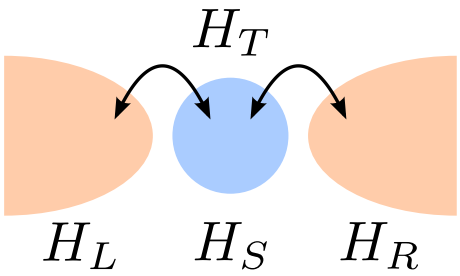

Fig. 1.1 Schematic of a generic setup of mesoscopic conductors.

Each reservoir is connected to the system via the tunneling Hamiltonian H_T, which describes the hopping of an electron from the system to the left and right reservoirs.

The idea of the counting statistics has roots in the photodetection, which reveals that the higher-order correlation functions carry fundamental information on the coherence of photons [59]. The full counting statistics is an electronic analog of the photodetection: The number of the electrons transferred from one reservoir to another in a given time interval is counted to obtain the histogram which is intrinsic to the transport. The theory of the counting statistics of the electronic current was pioneered by L. S. Levitov and G. B. Lesovik [17, 18]. There are several ways to establish the full counting statistics: the spin 1/2 galvanometer [18], the Keldysh formalism [60, 61], the system-detector coupled system [19], and the two-point measurement [62].

The central object in the full counting statistics is the probabilities $p_\tau(n)$ associated with the transfer of n electrons from the left to the right reservoir in the time interval $[0,\tau]$. One of the intuitive ways to determine the probabilities is to use the two-point measurement scheme [62]. In this approach, we project a many-body state to the eigenstate of the numbers of electron in the right reservoir N_R at $t=0$ and $t=\tau$. The outputs at $t=0$ and $t=\tau$ are denoted by $n_R(0)$ and $n_R(\tau)$, respectively. The number of transferred electrons is associated with the difference between the outputs of the two measurements, i.e. $n=n_R(\tau)-n_R(0)$. An alternative formulation of the full counting statistics based on a field-theoretical method [60, 61] is discussed in the next chapter.

Once the probabilities $p_\tau(n)$ are determined, it is possible to evaluate the expectation value of the measurable function $g(n)$ as

$$\boldsymbol{E}_\tau[g(n)] \equiv \sum_{m=-\infty}^{\infty} g(n)p_\tau(n). \tag{1.1}$$

It is convenient to define the characteristic function of the counting process associated with the transfer probabilities $p_\tau(n)$ $(n \in \mathbf{Z})$ as

$$\begin{aligned}\chi_\tau(\lambda) &\equiv \boldsymbol{E}_\tau[e^{in\lambda}] \\ &= \sum_{n=-\infty}^{\infty} e^{in\lambda} p_\tau(n).\end{aligned} \tag{1.2}$$

The auxiliary parameter λ is called the counting field in the theory of the full counting statistics. The moments of the numbers of the transferred charge n can be generated by

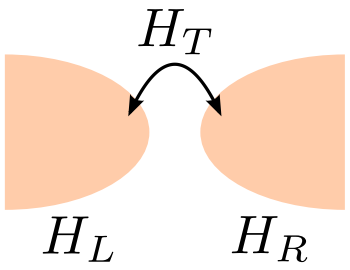

Fig. 1.2 Schematic of a tunneling junction.

differentiating the characteristic function with respect to the counting field λ;

$$\boldsymbol{E}_\tau[n^k] = \frac{\partial^k \chi_\tau(\lambda)}{i^k \partial \lambda^k}\bigg|_{\lambda=0}. \tag{1.3}$$

As the number of the transferred charge n is expected to grow asymptotically in proportional to the observation time interval τ, it is useful to introduce the scaled cumulant-generating function

$$\mathcal{S}(\lambda) \equiv \lim_{\tau\to\infty} \frac{1}{\tau} \ln \chi_\tau(\lambda). \tag{1.4}$$

Then, cumulants of the steady-state current is defined as

$$\bar{I^k} \equiv e^k \frac{\partial^k}{i^k \partial \lambda^k} \mathcal{S}(\lambda)\bigg|_{\lambda=0}, \tag{1.5}$$

with the elementary charge e.

1.2.2 Levitov-Lesovik formula

The theory of the full counting statistics has achieved great success in varieties of mesoscopic conductors such as diffusive conductors [61, 63], quantum Hall systems [64], chaotic cavities [65], Aharonov-Bohm rings [22], Coulomb blockade system [66], Kondo systems [9], charge fluctuating quantum dot [67], superconductors [68–70], and conductors under a time-periodic driving field [71]. One of the cornerstones of the full counting statistics is the Levitov-Lesovik formula [17, 18].

In order to illustrate the usefulness of the full counting statistics, let us consider the simplest model: the noninteracting fermionic system which is composed of weakly coupled left and right reservoirs (Fig. 1.2). The isolated reservoirs are described by the Hamiltonian $H_0 = H_L + H_R$ with

$$H_\alpha = \sum_{\boldsymbol{k}} \varepsilon_{\alpha\boldsymbol{k}} c^\dagger_{\alpha\boldsymbol{k}} c_{\alpha\boldsymbol{k}}, \tag{1.6}$$

for $\alpha = L, R$. Here, $c^\dagger_{L(R)\boldsymbol{k}}$ and $c_{L(R)\boldsymbol{k}}$ are the creation and the annihilation operators of the electrons in the left (right) reservoir with momentum $\boldsymbol{k}$, and the dispersion relation $\varepsilon_{\alpha\boldsymbol{k}}$.

These reservoirs are coupled to each other with the tunneling Hamiltonian

$$H_T = \sum_{\boldsymbol{k}\boldsymbol{k}'} \left(t c^\dagger_{R\boldsymbol{k}} c_{L\boldsymbol{k}'} + t^* c^\dagger_{L\boldsymbol{k}'} c_{R\boldsymbol{k}} \right), \tag{1.7}$$

with the transmission amplitude t. The left and right reservoirs are assumed to be in equilibrium at the inverse temperature β. The chemical potentials of the left and right reservoir are $\mu_L = \varepsilon_F + eV/2$ and $\mu_R = \varepsilon_F - eV/2$, respectively, with the Fermi energy ε_F and the bias voltage V. Then, the distribution of the electrons in reservoir α $(= L, R)$ is characterized by the Fermi-Dirac distribution;

$$f_\alpha(\omega) = \frac{1}{e^{\beta(\omega-\mu_\alpha)}+1}. \tag{1.8}$$

Since the total Hamiltonian $H = H_0 + H_T$ is quadratic in terms of the fermionic degrees of freedom, the characteristic function $\chi_\tau(\lambda)$ is exactly evaluated. According to the field-theoretic analysis discussed in subsection 2.3.2, the scaled cumulant-generating function is obtained as

$$\begin{aligned} \mathcal{S}_{\mathrm{LL}}(\lambda) = \frac{1}{2\pi\hbar} \int d\omega \ln \Big[1 + T_{LR} \Big[& f_L(\omega)(1-f_R(\omega))(e^{i\lambda}-1) \\ & + f_R(\omega)(1-f_L(\omega))(e^{-i\lambda}-1) \Big] \Big], \end{aligned} \tag{1.9}$$

with the transmission coefficient $T_{LR} = 4\pi^2 t^2 \rho_L(\varepsilon_F)\rho_R(\varepsilon_F)$. Here, we have neglected the energy dependence of the density of states $\rho_{\alpha=L,R}(\omega)$, for simplicity. The result is known as the Levitov-Lesovik formula [18].

The first and the second cumulants of the current [see Eq. (1.5) for the definition] are computed respectively as

$$\bar{I} = \frac{e}{2\pi\hbar} \int d\omega T_{LR}(f_L(\omega) - f_R(\omega)), \tag{1.10}$$

$$\begin{aligned} \bar{I^2} = \frac{e^2}{2\pi\hbar} \int d\omega \, [& T_{LR} [f_L(\omega)(1-f_L(\omega)) + f_R(\omega)(1-f_R(\omega))] \\ & + T_{LR}(1-T_{LR})(f_L(\omega) - f_R(\omega))^2]. \end{aligned} \tag{1.11}$$

The first expression is known as the Landauer formula, which represents the current through the transport channels lying within the bias window $f_L(\omega) - f_R(\omega)$. The linear conductance $G \equiv d\bar{I}/dV|_{V=0}$ is obtained as

$$G = \frac{e^2 T_{LR}}{2\pi\hbar}. \tag{1.12}$$

The first two terms in the second-order cumulant (1.11) are the thermal noise because $f_\alpha(\omega)$ and $(1 - f_\alpha(\omega))$ are overlapped at finite temperatures. It is also known as the Johnson-Nyquist noise. The last term in the same equation is called the shot noise, which is finite in the presence of a bias voltage. The factor $T_{LR}(1-T_{LR})$ originates from the partition process of the carriers: The injected electron is transmitted through or reflected at

the scattering region. After performing the energy integration, we have

$$\bar{I^2} = \frac{1}{\pi\hbar}\left[2k_BTT_{LR} + eV\coth\left(\frac{eV}{2k_BT}\right)T_{LR}(1-T_{LR})\right], \tag{1.13}$$

with the Boltzmann constant k_B and the absolute temperature T. When the thermal noise is dominant ($eV \ll k_BT$), we obtain the fluctuation dissipation relation

$$\bar{I^2} = 4k_BTG, \tag{1.14}$$

which connects the thermal noise to the conductance with the universal factor k_BT. In the zero temperature limit, on the other hand, the current noise is dominantly given by the partition process at the scattering region:

$$\bar{I^2} = \frac{e^3V}{\pi\hbar}T_{LR}(1-T_{LR}), \tag{1.15}$$

which increases linearly with the bias voltage. In the weak tunneling regime ($T_{LR} \ll 1$), the shot noise is related to the averaged current as

$$\bar{I^2} = 2e\bar{I}. \tag{1.16}$$

This is identical to Schottky's result for the shot noise induced by uncorrelated injections of particles with the charge e. The ratio between the shot noise and the current can be utilized to detect the effective charge of the quasiparticle which is intrinsic to the system [2]. The property is elegantly utilized by identifying the fractional charge in quantum Hall systems [4, 5].

While the second-order cumulant of the current has already elucidated the unique properties of the carriers, the Levitov-Lesovik formula (1.9) contains much information on the microscopic transport processes beyond that obtained with the Gaussian treatment. Actually, it is possible to understand the stochastic processes underlying the transport phenomena by comparing the characteristic function for the transport with that of the basic stochastic distributions. In order to discuss this point, we consider the three cases (i) at zero-temperature, (ii) with small transmission coefficient and (iii) away from these regimes.

At zero temperature, the scaled cumulant-generating function (1.9) becomes

$$\begin{aligned}\mathcal{S}_{\mathrm{LL}}^{T=0}(\lambda) &= \frac{eV}{2\pi\hbar}\ln\left[1+T_{LR}(e^{i\lambda}-1)\right] \\ &= \frac{eV}{2\pi\hbar}\mathcal{S}_B(\lambda;T_{LR}),\end{aligned} \tag{1.17}$$

where $\mathcal{S}_B(\lambda;p)$ is the cumulant-generating function of the Bernoulli distribution with the success probability p;

$$\mathcal{S}_B(\lambda;p) = \ln\left[1-p+pe^{i\lambda}\right]. \tag{1.18}$$

The stochastic interpretation is as follows. At zero temperature, electrons are unidirectionally injected from the source reservoir to the drain one. The electron succeeds to transmit

through the scattering region with the probability T_{LR}, otherwise it is reflected back to the source reservoir. Within the bias window eV, there are $eV/2\pi\hbar$ numbers of available energy channels, in which the Bernoulli trial occurs independently.

Another important case is the electron transmission in the weak tunneling regime $T_{LR} \ll 1$, where the scaled cumulant-generating function (1.9) becomes

$$\mathcal{S}_{\mathrm{LL}}^{T_{LR}\ll 1}(\lambda) = \mu_+(e^{i\lambda}-1) + \mu_-(e^{-i\lambda}-1), \tag{1.19}$$

with $\mu_+ \equiv \frac{eVT_{LR}}{2\pi\hbar}\int d\omega f_L(\omega)(1-f_R(\omega))$ and $\mu_- \equiv \frac{eVT_{LR}}{2\pi\hbar}\int d\omega f_R(\omega)(1-f_L(\omega))$. This is equivalent to the cumulant generating function for the Skellam distribution [72]

$$\mathcal{S}_S(\lambda;\mu_1,\mu_2) = \mu_1(e^{i\lambda}-1) + \mu_2(e^{-i\lambda}-1), \tag{1.20}$$

which describes the difference of the two independently Poisson-distributed random variables with the rate parameters μ_1 and μ_2. It is also called the bidirectional Poisson process in the context of nonequilibrium transport. The equality $\mathcal{S}_{\mathrm{LL}}^{T_{LR}\ll 1}(\lambda) = \mathcal{S}_S(\lambda;\mu_+,\mu_-)$ can be interpreted as follows. In the weak tunneling limit, the electron transmission is dominated by the lowest-order processes, in which a single electron is transferred from the left (right) to the right (left) reservoir with the transition probability μ_+ (μ_-). These processes are considered to be rare events characterized by the Poisson distribution with the rate parameter $\mu_\pm$ and to have opposite contributions to the current. If the system is further assumed to be at zero-temperature $T = 0$ with a finite bias voltage, the cumulant-generating function is reduced to the Poissonian one

$$\mathcal{S}_P(\lambda;\mu_n) = \mu_n(e^{in\lambda}-1), \tag{1.21}$$

with $n = V/|V|$.

We can extend the above argument to the strong tunneling regime by decomposing the microscopic transport events into the Poisson processes. By noting that $(a(e^{i\lambda}-1)+b(e^{-i\lambda}-1))^n$ can be expanded with respect to $e^{im\lambda}-1$ ($m=-n,\,-n+1,\,\cdots,\,n$), the Levitov-Lesovik formula (1.9) can be generally expressed as the summation of the Poissonian cumulant generating functions;

$$\begin{aligned}\mathcal{S}_{\mathrm{LL}}(\lambda) &= \sum_{n=-\infty}^{\infty} W_n(e^{in\lambda}-1) \\ &= \sum_{n=-\infty}^{\infty} \mathcal{S}_P(\lambda;W_n),\end{aligned} \tag{1.22}$$

where the transition matrices W_n are defined as the coefficient of the $(e^{in\lambda}-1)$ term. According to the probability theory, the cumulant generating function of the linear combination of independent random variables is described by the summation of each one. In our case, the number of the transferred charge m obeying the Levitov-Lesovik formula is expressed as the summation of the random variables m_n which obey the Poisson distribution with the rate parameter W_n. From a different point of view, we rewrite the scaled

cumulant-generating function as

$$\begin{aligned}\mathcal{S}_{\mathrm{LL}}(\lambda) &= \mu_P \sum_{n=-\infty}^{\infty} w_n (e^{in\lambda} - 1) \\ &= \mu_p \left[e^{\mathcal{S}_w(\lambda)} - 1 \right] \\ &= \mathcal{S}_P(-i\mathcal{S}_w(\lambda); \mu_P),\end{aligned} \tag{1.23}$$

by introducing the rate parameter $\mu_P = \sum_{n=-\infty}^{\infty} W_n$, the probability $w_n \equiv W_n/\mu_P$, and the cumulant generating function $\mathcal{S}_w(\lambda) = \ln \sum_{n=-\infty}^{\infty} w_n e^{i\lambda n}$. This is equivalent to the cumulant generating function of the compound Poisson distribution.

1.2.3 Fluctuation theorem

As was discussed in the previous subsection, the current distribution contains much information on the microscopic transport processes beyond the second cumulant. One of the illuminating properties that hold in the higher-order cumulants is the fluctuation theorem, which is derived from the microscopic reversibility of the system and the equilibrium nature of the reservoirs [21].

The fluctuation theorem states that the distribution $p_\tau(\sigma)$ with the time-averaged entropy production rate σ and the time interval τ must be related to the time-reversed probability $p_\tau^{\mathrm{TR}}(\sigma)$ as

$$p_\tau^{\mathrm{TR}}(-\sigma) = p_\tau(\sigma) e^{-\sigma\tau}. \tag{1.24}$$

This imposes a universal relation between the typical processes with the entropy production and the rare ones with the entropy consumption. While both the entropy-producing and entropy-consuming processes are allowed in the short time interval, the former dominates the latter for $\tau \to \infty$. Thus, Eq. (1.24) can be viewed as a quantitative description of the second law of thermodynamics. Indeed, the non-negativity of the expectation value of the entropy production rate $\boldsymbol{E}[\sigma] \geq 0$ is proved by using the Jarzynski equality

$$\boldsymbol{E}[e^{-\sigma\tau}] = 1, \tag{1.25}$$

which is readily confirmed by integrating the left- and right- hand sides of Eq. (1.24) with respect to σ, and Jensen's inequality

$$\boldsymbol{E}[e^{-\sigma\tau}] \geq e^{-\boldsymbol{E}[\sigma\tau]}. \tag{1.26}$$

The fluctuation theorem (1.24) is also expressed as

$$\chi_\tau(\lambda) = \chi_\tau^{\mathrm{TR}}(i\tau - \lambda), \tag{1.27}$$

with the characteristic functions $\chi_\tau(\lambda) = \int d\sigma e^{i\lambda\sigma} p_\tau(\sigma)$ and $\chi_\tau^{\mathrm{TR}}(\lambda) = \int d\sigma e^{i\lambda\sigma} p_\tau^{\mathrm{TR}}(\sigma)$. In the long-time limit, the fluctuation theorem takes the form

$$\lim_{\tau\to\infty} \frac{1}{\tau} \ln \frac{p_\tau(\sigma)}{p_\tau^{\mathrm{TR}}(-\sigma)} = \sigma, \tag{1.28}$$

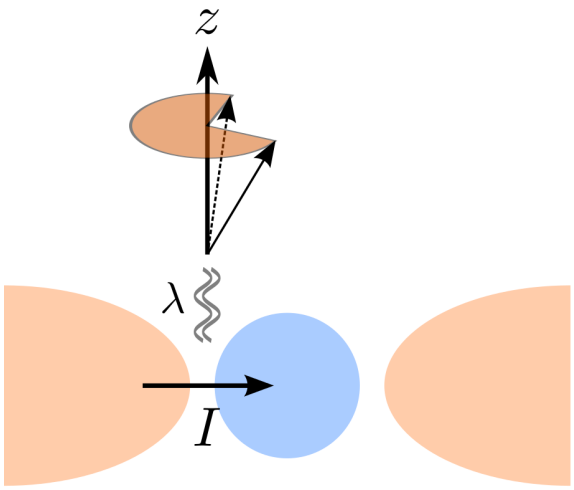

Fig. 1.3 Schematic of a spin $1/2$ galvanometer.

which is also equivalently represented with respect to the (time-reversed) scaled cumulant-generating function $\mathcal{S}(\lambda)$ ($\mathcal{S}^{\mathrm{TR}}(\lambda)$) as

$$\mathcal{S}(\lambda) = \mathcal{S}^{\mathrm{TR}}(i-\lambda). \tag{1.29}$$

What is nontrivial about the fluctuation theorem is that the general results obtained in the linear-response theory, such as the fluctuation-dissipation theorem and the Onsager-Casimir reciprocal relation, are recovered systematically [21].

The general discussion as to the fluctuation theorem holds true for the electron transport phenomena, in which the entropy production is related to the Joule heating. When an electron is transferred through the scattering region with the applied bias voltage V, the Joule heat eV is generated. The corresponding entropy production is $\sigma = \beta eV$ with the inverse temperature β. The fluctuation theorem can be verified in the simple model discussed in the previous subsection. By noting the identity $f_L(\omega)(1-f_R(\omega)) = e^{\beta eV} f_R(\omega)(1-f_L(\omega))$, the scaled cumulant-generating function (1.9) is shown to satisfy the symmetry

$$\mathcal{S}_{\mathrm{LL}}(\lambda) = \mathcal{S}_{\mathrm{LL}}(i\beta eV - \lambda). \tag{1.30}$$

The time-reversed scaled cumulant-generating function is identical to the original one in the simple model ($\mathcal{S}_{\mathrm{LL}}(\lambda) = \mathcal{S}^{\mathrm{TR}}_{\mathrm{LL}}(\lambda)$) because of its time-reversal symmetry.

1.3 Detection scheme of current distribution

The current distribution discussed in the previous section is introduced with a purely theoretical motivation. A natural question is whether and how we can observe the distribution. In order to fill the gap between theory and practice, a gedanken measurement scheme for the current fluctuation was proposed by using a spin $1/2$ galvanometer [18]. A magnetic moment placed near a conductor precesses due to the electromagnetic field emitted by electrons flowing through the conductor. The total precession angle during a time interval τ is associated with the number of the transferred electrons.

Let us consider a virtual spin $1/2$ galvanometer which is placed near a mesoscopic conductor (see Fig. 1.3). According to Ampere's law, the current flowing through the conductor generates a magnetic field, which exerts a torque on the magnetic moment. The spin $1/2$ starts to precess around the z axis according to the interaction Hamiltonian

$$H_{\rm int} = \frac{\lambda}{2} I \sigma_z, \tag{1.31}$$

with the current I, the Pauli matrices $\sigma_{x,y,z}$, and the coupling constant λ. The total Hamiltonian is given by

$$H = H_{\rm sys} \otimes 1 + H_{\rm int} = \begin{pmatrix} H_{\rm sys} + \lambda I/2 & 0 \\ 0 & H_{\rm sys} - \lambda I/2 \end{pmatrix} = \begin{pmatrix} H_\uparrow & 0 \\ 0 & H_\downarrow \end{pmatrix}, \tag{1.32}$$

with the Hamiltonian of the system $H_{\rm sys}$. The total Hamiltonian is diagonal in the spin space, and the components are denoted by $H_\uparrow$ and $H_\downarrow$. If the spin is coupled to the conductor during the time interval $[0,\tau)$, the expectation value of the transverse component $\sigma_+ = \sigma_x + i\sigma_y$ is

$$\begin{aligned} {\rm Tr}\left[\sigma_+ \rho(\tau)\right] &= {\rm Tr}\left[\sigma_+ e^{-iH\tau}\left(\rho_{\rm el}\otimes\rho_{\rm spin}\right)e^{iH\tau}\right] \\ &= {\rm Tr}\left[e^{+iH_\uparrow\tau}e^{-iH_\downarrow\tau}\rho_{\rm el}\right]{\rm Tr}\left[\sigma_+\rho_{\rm spin}\right], \end{aligned} \tag{1.33}$$

with the initial density matrix $\rho_{\rm ini} = \rho_{\rm el}\otimes\rho_{\rm spin}$. In the classical picture, the precession angle of the magnetic moment is estimated as $\theta = \lambda n$, when n electrons are transferred through the system. If we consider that the electron transport is decomposed into such stochastic processes which occur with the probability $p_\tau(n)$, the precession-angle part in Eq. (1.33) is identical to the characteristic function (1.2);

$${\rm Tr}\left[e^{+iH_\uparrow\tau}e^{-iH_\downarrow\tau}\rho_{\rm el}\right] = \sum_n p_\tau(n)e^{i\lambda n} = \chi_\tau(\lambda), \tag{1.34}$$

which is also consistent with the result obtained in the two-point measurement scheme without the initial correlation [62]. The similarity between the above characteristic function and the partition function defined in the Keldysh formalism is discussed in the next chapter.

The spin $1/2$ galvanometer was an illuminating idea to understand the full counting statistics, but, at the same time, left some questions on its applicability. For instance, the current distribution through superconducting junctions does not allow a probabilistic interpretation because it can be negative [69]. This difficulty was solved by considering a quantum mechanical description of the detector [19]. The authors of the paper found that the probabilistic interpretation of the characteristic function is valid only in the presence of the gauge symmetry. They also pointed out the importance of back action originating from the dynamics of the detector. As the current fluctuation requires high accuracy of the measurement, the detailed analysis of detector dynamics is a practically important problem.

1.4 Related Experiments

Mesoscopic circuits are promising arenas to test the fundamental aspects of nonequilibrium statistical physics. In particular, the current distribution attracts much attention in the context of the fluctuation theorem. In the following, we review two important experimental works which examined the fluctuation theorem in the classical and quantum regimes.

Fluctuation theorem in the classical regime

The fluctuation theorem has been tested in Ref. [25] by using a double quantum-dot (DQD) system in the classical tunneling regime. The experimental setup is shown in Fig. 1.4(a). The DQD structure marked by the white circles is fabricated between the drain and source reservoirs. The position of an electron in the DQD is monitored by a detector quantum point contact (QPC) which is asymmetrically coupled to the left and right dots. Figure 1.4(b) shows the QPC conductance $G_{\rm QPC}$, from which we can resolve the possible charge states of the QPC; the left (right) occupied state "L" ("R") and the empty state "0". The experiment was performed in a parameter region where the doubly occupied state is not allowed. By counting the number of transitions between L and R during a time interval τ, we can obtain the probability $p_\tau(n)$ with the number n of electrons transferred from the source to drain.

The probabilities obtained at the bias voltage $V_{\rm DQD} = 0\mu V$ and $V_{\rm DQD} = 20\mu V$ are shown in the upper and lower panels in Fig. 1.4(c), respectively. The distribution is clearly shifted in the presence of $V_{\rm DQD}$. Nevertheless, a charge flow against the source-drain voltage $n < 0$ can occur with a finite probability. According to the fluctuation theorem reviewed in subsection 1.2.3, the forward and backward probability should be related as

$$\ln \frac{p_\tau(n)}{p_\tau(-n)} = neV_{\rm DQD}/k_BT, \tag{1.35}$$

with the temperature T of the DQD system. This relation is directly tested in Fig. 1.4(d) for various T and $V_{\rm DQD}$. The experimental data shows linear behavior in accordance with the theoretical prediction plotted as the solid lines though the discrepancies of 20% to 30% are found in the slope. These discrepancies can be removed within the statistical uncertainty of the data when we take into account the limited bandwidth of the detector circuit (dashed lines).

This clear demonstration of the fluctuation theorem in the classical regime shows that the recent technology has reached a stage of experimental verification of the full counting statistics. The above result also suggests that a detailed analysis of the detector circuit is indispensable to achieve good agreements between the theory and the experiment. The detector cannot react to charge-switching events which occur much faster than the inverse of the detector bandwidth. The missing events results in the correction of the fluctuation theorem. We note that the discrepancies found in this experiment are explained not by the QPC backaction [73] but by the imperfectness of the detector. The former scenario implies excitation in the DQD system perturbed by the detector while the microscopic scattering processes are not perturbed in the latter one.

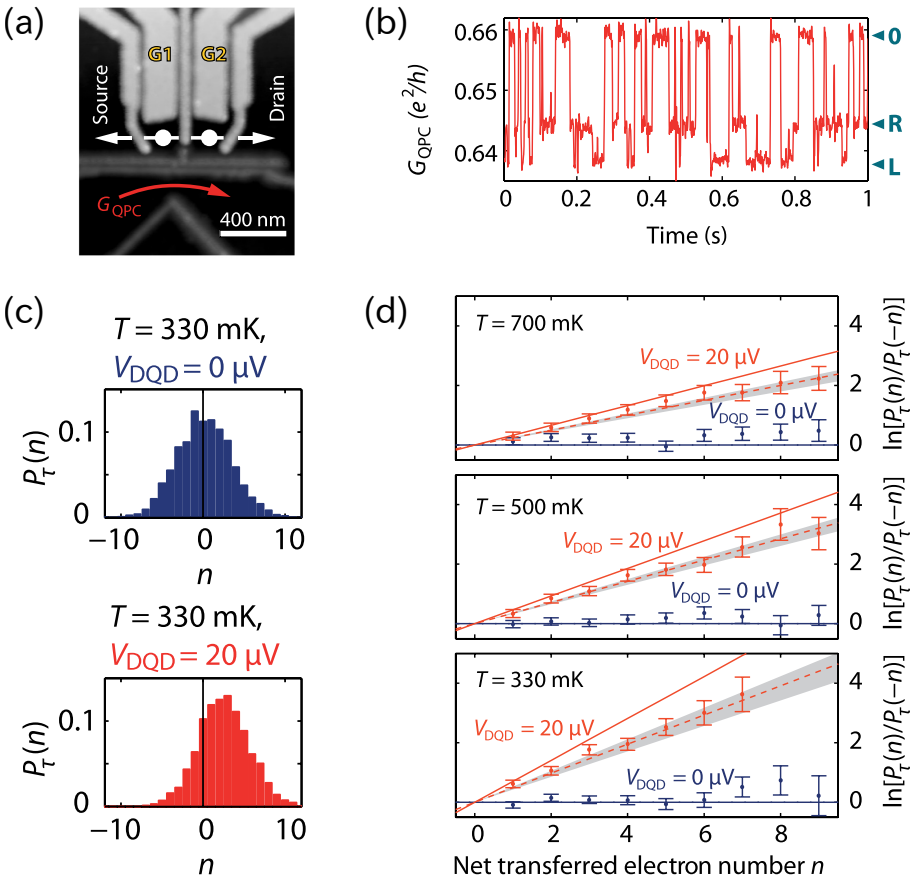

Fig. 1.4 (a) DQD system with a detector QPC. (b) Conductance of the QPC. (c) Probabilities of the transferred electron number n. (d) Test of the fluctuation theorem (1.35). [Reprinted from "Irreversibility on the Level of Single-Electron Tunneling" by B. Küng *et al.*, Phys. Rev. X **2**, 011001 (2012) under the terms of the Creative Commons Attribution 3.0 License.]

Fluctuation theorem in the quantum regime

The fluctuation theorem results in novel consequences also in the quantum regime. At near equilibrium, the current I and the current noise S can be expanded in terms of the bias voltage V as

$$I(V,B) = G_1(B)V + \frac{1}{2}G_2(B)V^2 + \frac{1}{3!}G_3(B)V^3 + \cdots, \tag{1.36}$$

$$S(V,B) = S_0(B) + S_1(B)V + \frac{1}{2}S_2(B)V^2 + \cdots, \tag{1.37}$$

under an applied magnetic field B. The first coefficients of the current and noise are related by the Johnson-Nyquist relation as $S_0(B) = 4k_BTG_1(B)$. The Onsager-Casimir reciprocity states that the lowest-order coefficients are symmetric with respect to B, i,e, $G_1(B) = G_1(-B)$ and $S_1(B) = S_1(-B)$. Remarkably, the fluctuation theorem further imposes relations for nonlinear coefficients of the current and noise [22–24]. We introduce the symmetrized and antisymmetrized components of the nonlinear coefficients with

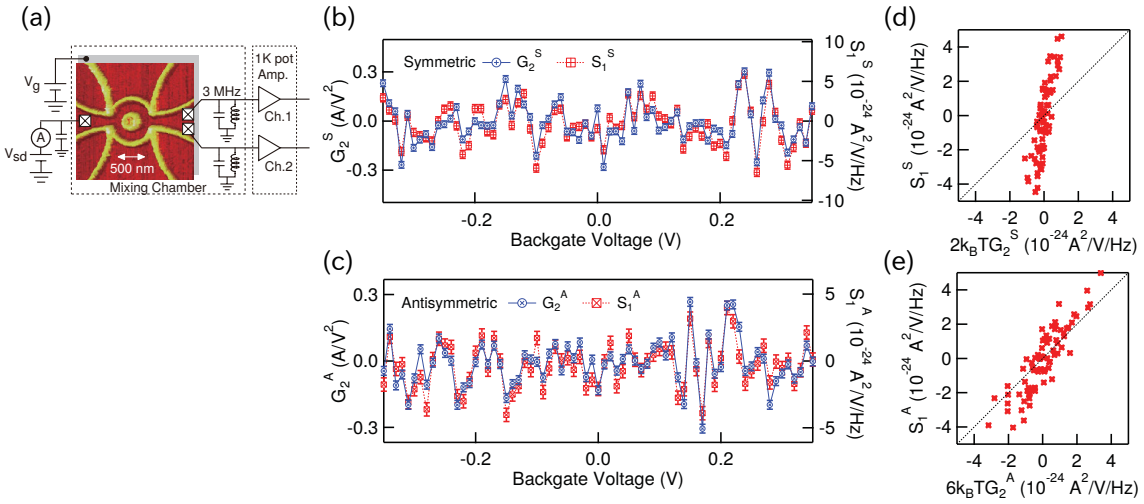

Fig. 1.5 (a) Aharonov-Bohm ring with the measurement setup. (b) Symmetric components G_2^S and S_1^S. (c) Antisymmetric components G_2^A and S_1^A. (d) S_1^S plotted against G_2^S. (e) S_1^A plotted against G_2^A. [Reprinted with permission from "Fluctuation theorem and microreversibility in a quantum coherent conductor" by S. Nakamura *et al.*, Phys. Rev. B **83**, 155431 (2011). Copyright 2011 by The American Physical Society.]

respect to the magnetic field as

$$G_2^{S,A} \equiv G_2(B) \pm G_2(B), \tag{1.38}$$

$$S_1^{S,A} \equiv S_1(B) \pm S_1(B). \tag{1.39}$$

Here, $+$ and $-$ are taken for S and A, respectively. The fluctuation theorem requires the relations

$$S_1^S = 2k_BTG_2^S, \tag{1.40}$$

$$S_1^A = 6k_BTG_2^A. \tag{1.41}$$

These results are beyond the consequence of the Onsager-Casmir reciprocal relation and the fluctuation dissipation theorem.

The consequences of the fluctuation theorem have been directly tested in a quantum coherent conductor [23, 24]. The experimental setup is given by using an Aharonov-Bohm ring fabricated on a GaAs/AlGaAs 2DEG. Atomic force microscope image of the system is shown in Fig. 1.5(a). The back-gate voltage V_g tunes the electron density in the Aharonov-Bohm ring. Figures 1.5(a) and (b) show the V_g-dependence of the symmetric components G_2^S (S_1^S) and antisymmetric components G_2^A (S_1^A) in the left (right) axis, respectively. The symmetric and antisymmetric quantities are found to have a strong correlation independently. Indeed, the proportionality between G_2^S and S_1^S and between G_2^A and S_1^A are clearly seen in Fig. 1.5(d) and (e), respectively. More quantitatively speaking, the factors are estimated as $S_1^S/2k_BTG_2^S = 6.00^{+0.94}_{-0.98}$ and $S_1^A/6k_BTG_2^S = 1.61^{+0.22}_{-0.20}$ in Ref. [24]. Unfortunately, there are discrepancies between the theoretical predictions and the experimental results for the moment.

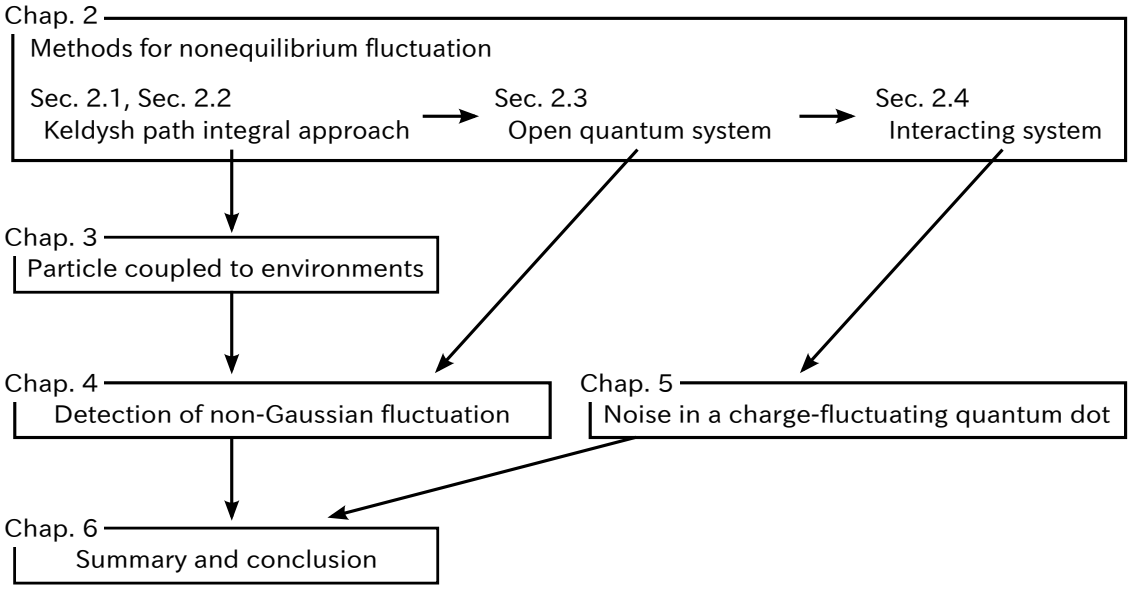

Fig. 1.6 Flow chart of this thesis.

The experiment reviewed here has demonstrated that there exists nontrivial proportionality between the nonlinear response and the nonequilibrium fluctuation in the coherent mesoscopic conductor. This is the first experimental verification of the fluctuation theorem in the quantum regime. In spite of this remarkable achievement, the reason of the observed discrepancy has not yet been clarified. Recalling that a similar problem found in the incoherent transport through the DQD required the detailed analysis of the detector circuit, there is a possibility to explain this discrepancy by taking into account the realistic situation of the system. This is an important question for future studies.

1.5 Organization of this thesis

As have been reviewed above, the current distribution has fundamental information on the microscopic processes underling the nonequilibrium transport through the mesoscopic conductors. With strong support from the recent progress in nanotechnology, it is feasible to experimentally characterize the higher cumulants of the current both in the classical and quantum regimes. It is an urgent need to refine the theoretical detection framework for the current distribution. Another important viewpoint in the full counting statistics is the modification of the current distribution itself due to many-body effects. It is known that the transmission through mesoscopic conductors is strongly renormalized by the interaction with the surrounding environments [60]. As the current fluctuation is sensitive to the correlation of quasi-particles, it can be utilized to elucidate the intrinsic properties of the interacting systems.

In this thesis, we investigate twofold topics on the current fluctuation in mesoscopic conductors: a detection scheme of the full counting statistics and a renormalization effect on the current fluctuation. These topics are subjects of nonequilibrium transport in interacting mesoscopic systems. In order to utilize accumulated knowledge of such challenging systems, we need an integrated framework which can treat the two-body

interaction in both the classical and quantum regimes. In chapter 2, we develop a path integral method for nonequilibrium transport in interacting systems based on the Keldysh formalism. The current fluctuation can be transparently written in terms of the field-theoretic language. The full counting statistics and the renormalization structure are systematically incorporated in the framework. In chapter 3, we review recent insights on a "particle" under Gaussian and non-Gaussian noises. Such a particle can work as an effective detector for the fluctuation in the system of interest. Chapters 4 and 5 concern the two main topics of this thesis. In chapter 4, a detection scheme of the current distribution is discussed based on a stochastic method. We show that the current distribution in a mesoscopic conductor is fully characterized by the steady-state distribution of the detector circuit. Detailed analysis of detector dynamics is indispensable to correctly estimate the current distribution. In chapter 5, we discuss the renormalization effect on the current fluctuation in an interacting quantum dot system, i.e. the interacting resonant level model. The current noise is found to exhibit a universal power-law behavior as a consequence of the renormalization effect. In chapter 6, we summarize the results and state concluding remarks of this thesis. The flow chart of this thesis is presented in Fig. 1.6.

References

[1] Y. Imry, *Introduction to mesoscopic physics*, 2 (Oxford University Press on Demand, 2002).

[2] Y. M. Blanter and M. Büttiker, Phy. Rep. **336**, 1 (2000).

[3] C. Beenakker and C. Schönenberger, Phys. Today **56**, 37 (2003).

[4] R. De-Picciotto, M. Reznikov, M. Heiblum, V. Umansky, G. Bunin, and D. Mahalu, Nature **389**, 162 (1997).

[5] L. Saminadayar, D. Glattli, Y. Jin, and B. Etienne, Phys. Rev. Lett. **79**, 2526 (1997).

[6] R. Landauer, Nature **392**, 658 (1998).

[7] D. Goldhaber-Gordon, H. Shtrikman, D. Mahalu, D. Abusch-Magder, U. Meirav, and M. Kastner, Nature **391**, 156 (1998).

[8] A. C. Hewson, *The Kondo problem to heavy fermions*, Vol. 2 (Cambridge university press, 1997).

[9] A. O. Gogolin and A. Komnik, Phys. Rev. B **73**, 195301 (2006).

[10] G. D. Mahan, Phys. Rev. **163**, 612 (1967).

[11] P. Nozières and C. T. De Dominicis, Phys. Rev. **178**, 1097 (1969).

[12] K. A. Matveev and A. I. Larkin, Phys. Rev. B **46**, 15337 (1992).

[13] A. K. Geim, P. C. Main, N. La Scala, L. Eaves, T. J. Foster, P. H. Beton, J. W. Sakai, F. W. Sheard, M. Henini, G. Hill, and M. A. Pate, Phys. Rev. Lett. **72**, 2061 (1994).

[14] I. Hapke-Wurst, U. Zeitler, H. Frahm, A. G. M. Jansen, R. J. Haug, and K. Pierz, Phys. Rev. B **62**, 12621 (2000).

[15] D. A. Abanin and L. S. Levitov, Phys. Rev. Lett. **93**, 126802 (2004).

[16] P. W. Anderson, Phys. Rev. Lett. **18**, 1049 (1967).

[17] L. Levitov and G. Lesovik, JETP Lett. **58**, 230 (1993).

[18] L. S. Levitov, H. Lee, and G. B. Lesovik, J. Math. Phys. **37**, 4845 (1996).

[19] Y. V. Nazarov and M. Kindermann, Euro. Phys. J. B **35**, 413 (2003).

[20] J. P. Pekola, Nat. Phys. **11**, 118 (2015).

[21] M. Esposito, U. Harbola, and S. Mukamel, Rev. Mod. Phys. **81**, 1665 (2009).

[22] K. Saito and Y. Utsumi, Phys. Rev. B **78**, 115429 (2008).

[23] S. Nakamura, Y. Yamauchi, M. Hashisaka, K. Chida, K. Kobayashi, T. Ono, R. Leturcq, K. Ensslin, K. Saito, Y. Utsumi, and A. C. Gossard, Phys. Rev. Lett. **104**, 080602 (2010).

[24] S. Nakamura, Y. Yamauchi, M. Hashisaka, K. Chida, K. Kobayashi, T. Ono, R. Leturcq, K. Ensslin, K. Saito, Y. Utsumi, and A. C. Gossard, Phys. Rev. B **83**, 155431 (2011).

[25] B. Küng, C. Rössler, M. Beck, M. Marthaler, D. S. Golubev, Y. Utsumi, T. Ihn, and K. Ensslin, Phys. Rev. X **2**, 011001 (2012).

[26] O.-P. Saira, Y. Yoon, T. Tanttu, M. Möttönen, D. V. Averin, and J. P. Pekola, Phys. Rev. Lett. **109**, 180601 (2012).

[27] K. Kobayashi, Proc. the Jpn. Acad., Ser. B **92**, 204 (2016).

[28] G. Lesovik and R. Loosen, JETP Lett. **65**, 295 (1997).

[29] U. Gavish, Y. Levinson, and Y. Imry, Phys. Rev. B **62**, R10637 (2000).

[30] Y. Utsumi, D. S. Golubev, M. Marthaler, G. Schön, and K. Kobayashi, Phys. Rev. B **86**, 075420 (2012).

[31] M. Creux, A. Crépieux, and T. Martin, Phys. Rev. B **74**, 115323 (2006).

[32] A. Zazunov, M. Creux, E. Paladino, A. Crépieux, and T. Martin, Phys. Rev. Lett. **99**, 066601 (2007).

[33] D. Chevallier, T. Jonckheere, E. Paladino, G. Falci, and T. Martin, Phys. Rev. B **81**, 205411 (2010).

[34] R. Aguado and L. P. Kouwenhoven, Phys. Rev. Lett. **84**, 1986 (2000).

[35] E. Onac, F. Balestro, L. H. W. van Beveren, U. Hartmann, Y. V. Nazarov, and L. P. Kouwenhoven, Phys. Rev. Lett. **96**, 176601 (2006).

[36] S. Gustavsson, M. Studer, R. Leturcq, T. Ihn, K. Ensslin, D. C. Driscoll, and A. C. Gossard, Phys. Rev. Lett. **99**, 206804 (2007).

[37] M. Hashisaka, Y. Yamauchi, S. Nakamura, S. Kasai, T. Ono, and K. Kobayashi, Phys. Rev. B **78**, 241303 (2008).

[38] N. Ubbelohde, C. Fricke, C. Flindt, F. Hohls, and R. J. Haug, Nat. Commun. **3**, 612 (2012).

[39] Y. Jompol, P. Roulleau, T. Jullien, B. Roche, I. Farrer, D. Ritchie, and D. Glattli, Nat. Commun. **6** (2015).

[40] J. Tobiska and Y. V. Nazarov, Phys. Rev. Lett. **93**, 106801 (2004).

[41] J. P. Pekola, Phys. Rev. Lett. **93**, 206601 (2004).

[42] R. Deblock, E. Onac, L. Gurevich, and L. P. Kouwenhoven, Science **301**, 203 (2003).

[43] T. T. Heikkilä, P. Virtanen, G. Johansson, and F. K. Wilhelm, Phys. Rev. Lett. **93**, 247005 (2004).

[44] E. Onac, F. Balestro, B. Trauzettel, C. F. J. Lodewijk, and L. P. Kouwenhoven, Phys. Rev. Lett. **96**, 026803 (2006).

[45] P.-M. Billangeon, F. Pierre, H. Bouchiat, and R. Deblock, Phys. Rev. Lett. **96**, 136804 (2006).

[46] T. Fujisawa, T. Hayashi, R. Tomita, and Y. Hirayama, Science **312**, 1634 (2006).

[47] S. Gustavsson, R. Leturcq, B. Simovič, R. Schleser, T. Ihn, P. Studerus, K. Ensslin, D. C. Driscoll, and A. C. Gossard, Phys. Rev. Lett. **96**, 076605 (2006).

[48] B. Doyon, Phys. Rev. Lett. **99**, 076806 (2007).

[49] L. Borda, K. Vladár, and A. Zawadowski, Phys. Rev. B **75**, 125107 (2007).

[50] E. Boulat, H. Saleur, and P. Schmitteckert, Phys. Rev. Lett. **101**, 140601 (2008).

[51] C. Karrasch, M. Pletyukhov, L. Borda, and V. Meden, Phys. Rev. B **81**, 125122 (2010).

[52] C. Karrasch, S. Andergassen, M. Pletyukhov, D. Schuricht, L. Borda, V. Meden, and H. Schoeller, Europhys. Lett. **90**, 30003 (2010).

[53] S. Andergassen, M. Pletyukhov, D. Schuricht, H. Schoeller, and L. Borda, Phys. Rev. B **83**, 205103 (2011).

[54] A. Nishino, N. Hatano, and G. Ordonez, Phys. Rev. B **91**, 045140 (2015).

[55] A. Branschädel, E. Boulat, H. Saleur, and P. Schmitteckert, Phys. Rev. Lett. **105**, 146805 (2010).

[56] S. T. Carr, D. A. Bagrets, and P. Schmitteckert, Phys. Rev. Lett. **107**, 206801 (2011).

[57] S. T. Carr, P. Schmitteckert, and H. Saleur, Phys. Scr. **2015**, 014009 (2015).

[58] W. Metzner, M. Salmhofer, C. Honerkamp, V. Meden, and K. Schönhammer, Rev. Mod. Phys. **84**, 299 (2012).

[59] R. J. Glauber, Phys. Rev. **130**, 2529 (1963).

[60] Y. Nazarov, Ann. Phys. (Leipzig) **16**, 720 (2007).

[61] Y. V. Nazarov, Ann. Phys. (Leipzig) **8**, SI193 (1999).

[62] A. Shelankov and J. Rammer, Euro. Phys. Lett. **63**, 485 (2003).

[63] H. Lee, L. S. Levitov, and A. Y. Yakovets, Phys. Rev. B **51**, 4079 (1995).

[64] H. Saleur and U. Weiss, Phys. Rev. B **63**, 201302 (2001).

[65] S. Pilgram, A. N. Jordan, E. V. Sukhorukov, and M. Büttiker, Phys. Rev. Lett. **90**, 206801 (2003).

[66] D. A. Bagrets and Y. V. Nazarov, Phys. Rev. B **67**, 085316 (2003).

[67] S. T. Carr, D. A. Bagrets, and P. Schmitteckert, Phys. Rev. Lett. **107**, 206801 (2011).

[68] B. A. Muzykantskii and D. E. Khmelnitskii, Phys. Rev. B **50**, 3982 (1994).

[69] W. Belzig and Y. V. Nazarov, Phys. Rev. Lett. **87**, 197006 (2001).

[70] V. F. Maisi, D. Kambly, C. Flindt, and J. P. Pekola, Phys. Rev. Lett. **112**, 036801 (2014).

[71] D. A. Ivanov, H. W. Lee, and L. S. Levitov, Phys. Rev. B **56**, 6839 (1997).

[72] J. G. Skellam, J. R. Stat. Soc. **109**, 296 (1946).

[73] Y. Utsumi, D. S. Golubev, M. Marthaler, K. Saito, T. Fujisawa, and G. Schön, Phys. Rev. B **81**, 125331 (2010).

Chapter 2

Method for nonequilibrium fluctuation in open quantum systems

In this chapter, we develop a theoretical framework to investigate nonequilibrium fluctuation in mesoscopic conductors. We utilize the Keldysh formalism, which is one of the most successful theories to treat nonequilibrium quantum and classical systems. In particular, the path integral approach based on the Keldysh formalism provides a unified way to describe wide varieties of physics including nonequilibrium transport, many-body interaction, renormalization group structures, and the stochastic processes.

In section 2.1, we remark the general ideas in the Keldysh formalism and summarize the notation used in this thesis. In section 2.2, the path integral approach is developed based on the Keldysh formalism. In section 2.3, the nonequilibrium transport through open quantum systems is discussed by focusing on a generic noninteracting model. In section 2.4, a method for interacting systems is developed by using a functional renormalization group approach.

2.1 Keldysh formalism

The Keldysh formalism is one of the most powerful methods for nonequilibrium systems. The original idea was proposed by Schwinger [1], and later developed and elaborated by Keldysh [2]. It properly takes account of the effect of the dissipative environment as a boundary condition of the Green's function. There are some extensive textbooks and review papers on the subject [3–6].

In a field-theoretic formalism, a many-body perturbation theory is developed by adiabatically switching on the interaction from the noninteracting vacuum state [7, 8]. A core part of the equilibrium theory is the Gell-Mann and Low theorem, which relates the vacuum state of an interacting system to the corresponding noninteracting one up to a manageable phase factor [8, 9]. In nonequilibrium situations, the state is quite different from the initial one after asymptotically long times, and the Gell-Mann and Low theorem may not be applicable. A way out is to use the doubled contour, which is called the Keldysh contour (see Fig. 2.1) [1, 2]. With this, we do not need to pay attention to the infinite future. The complexity of the doubled contour brings great benefits, allowing unified understanding on nonequilibrium systems [4–6]. The techniques which have been developed in equilibrium systems can be straightforwardly generalized in the Keldysh formalism. In addition, it

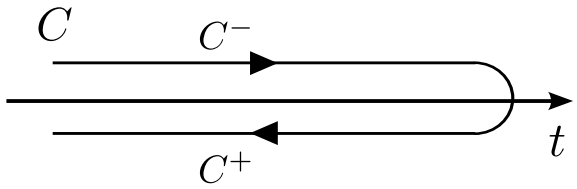

Fig. 2.1 The Keldysh contour C.

provides a clear reformulation of the full counting statistics [10, 11] and the stochastic processes [12]. Combined with the path integral approach, the renormalization structure [13] is transparently discussed.

Hereafter, we summarize the notation used in this thesis. The argument z defined on the Keldysh contour C is a combination of the real-time t and the Keldysh index $\rho = \mp$. The doubled degrees of freedom on the Keldysh contour C is conveniently described by a matrix structure. We introduce the Pauli matrices,

$$\tau_x \equiv \begin{pmatrix} 0 & 1 \\ 1 & 0 \end{pmatrix}, \quad \tau_y \equiv \begin{pmatrix} 0 & -i \\ i & 0 \end{pmatrix}, \quad \tau_z \equiv \begin{pmatrix} 1 & 0 \\ 0 & -1 \end{pmatrix}. \tag{2.1}$$

The integration of a function $f(z)$ over the Keldysh contour C is defined as

$$\int_C dz f(z) \equiv \int dt \left(f^-(t) - f^+(t) \right) \tag{2.2}$$

$$= \int dt \mathrm{Tr} \left[\tau_z \begin{pmatrix} f^-(t) & 0 \\ 0 & f^+(t) \end{pmatrix} \right], \tag{2.3}$$

where $f^\mp(t)$ is the function projected on the contour $C^\mp$ and Tr is the trace in the Keldysh space. The Dirac delta function on the Keldysh contour is defined as

$$\delta_{\mathrm{K}}(z,z') \equiv \tau_z \delta(t,t'), \tag{2.4}$$

with the Dirac delta function on the real-time axis $\delta(t,t')$. The integral of the product of the functions A and B defined on the Keldysh contour is abbreviated as $(AB)(z,z') \equiv \int dz_1 A(z,z_1)B(z_1,z')$. We use an analogous abbreviation for the functions with the arguments on the real time axis as $(AB)(t,t') \equiv \int dt_1 A(t,t_1)B(t_1,t')$.

It is useful to introduce the contour-ordering operator T_C along the Keldysh contour C. It is identical to the (anti-)time-ordering operator on the forward (backward) branch C^- (C^+). Any argument on the backward contour C^+ is considered to be later than all the arguments on the forward contour C^-.

2.2 Path integral approach

The path integral approach provides a systematic scheme to handle the seemingly over-complicated structure in the Keldysh formalism [6]. In order to compute the expectation value of observables, it is convenient to introduce the generating functional with a source term. Building blocks in the field theory, namely the Green's functions, are also defined on the Keldysh contour. The Green's functions defined on the Keldysh contour acquire

transparent physical meanings by employing a suitable basis. The basic computational tools developed in this section are utilized to discuss various nonequilibrium phenomena in later sections.

In subsection 2.2.1, basic ingredients for the functional representation of fermionic systems are introduced. In subsection 2.2.2, the Green's functions are defined as the derivatives of the generating functional. In subsection 2.2.3, the Green's functions of the noninteracting fermionic system are computed based on the functional approach.

2.2.1 Grassmann numbers and coherent states

Let us consider the path integral representation of fermionic annihilation and creation operators $\hat{f}$ and $\hat{f}^\dagger$. We introduce the Grassmann number ψ, which satisfies the relations

$$\psi\psi' = -\psi'\psi, \tag{2.5}$$

$$\psi^2 = 0, \tag{2.6}$$

$$\{\psi, \hat{f}\} = \{\psi, \hat{f}^\dagger\} = 0. \tag{2.7}$$

From this property, any functional of the Grassmann fields ψ is expressed as the first two terms of the Taylor expansion as $F[\psi] = f_0 + f_1\psi$. The functional differentiation of $F[\psi]$ is introduced in a natural way as

$$\frac{\delta}{\delta\psi}F[\psi] = f_1. \tag{2.8}$$

The functional derivatives with respect to the Grassmann fields ψ and ψ' are also mutually anti-commuting in order to be consistent with the commutation relations;

$$\left\{\frac{\delta}{\delta\psi}, \frac{\delta}{\delta\psi'}\right\} = 0. \tag{2.9}$$

We also define the integration over the Grassmann variables as

$$\int \mathcal{D}\psi 1 = 0, \tag{2.10}$$

$$\int \mathcal{D}\psi\psi = 1. \tag{2.11}$$

The coherent state is defined as a state associated with the Grassmann number ψ;

$$|\psi\rangle = \left(1 - \psi\hat{f}^\dagger\right)|0\rangle = e^{-\psi\hat{f}^\dagger}|0\rangle, \tag{2.12}$$

with the vacuum state $|0\rangle$. Then, the coherent state $|\psi\rangle$ is an eigenstate of the annihilation operator $\hat{f}$ with the Grassmann eigenvalue ψ, i.e. $\hat{f}|\psi\rangle = \psi|\psi\rangle$. We analogously define the Grassmann variable $\bar{\psi}$ and the left coherent state

$$\langle\psi| = \langle 0|\left(1 - \hat{f}\bar{\psi}\right) = \langle 0|e^{-\hat{f}\bar{\psi}}, \tag{2.13}$$

which satisfy the eigenequation $\langle\psi|\hat{f}^\dagger = \langle\psi|\bar{\psi}$. With the aid of the overlap of these coherent states

$$\langle\psi|\psi'\rangle = e^{\bar{\psi}\psi'}, \tag{2.14}$$

the matrix elements of an arbitrary normally ordered operator $F(\hat{f}^\dagger, \hat{f})$ take the form

$$\langle\psi|F(\hat{f}^\dagger, \hat{f})|\psi'\rangle = F(\bar{\psi}, \psi)e^{\bar{\psi}\psi'}. \tag{2.15}$$

Therefore, the path integral representation of the expectation value of an operator $\hat{\mathcal{O}}$ with the density matrix $\hat{\rho}$ is obtained as

$$\langle\hat{\mathcal{O}}\rangle \equiv \mathrm{Tr}(\hat{\mathcal{O}}\hat{\rho}) \tag{2.16}$$

$$= \int\int \mathcal{D}\bar{\psi}\mathcal{D}\psi e^{-\bar{\psi}\psi}\langle\psi|\hat{\mathcal{O}}\hat{\rho}|-\psi\rangle, \tag{2.17}$$

where the minus sign in $|-\psi\rangle$ is a consequence of the anticommuting property of the Grassman variable ψ. The identity operator $\hat{1}$ is represented in terms of the coherent states as

$$\hat{1} = \int\int \mathcal{D}\bar{\psi}\mathcal{D}\psi e^{-\bar{\psi}\psi}|\psi\rangle\langle\psi|. \tag{2.18}$$

The Gaussian integration is performed as

$$\int\int \prod_{i,j=1}^{N} \mathcal{D}\bar{\psi}_i\mathcal{D}\psi_j \exp\left[\sum_{i,j=1}^{N} \bar{\psi}_i M_{ij}\psi_j\right] = \det M, \tag{2.19}$$

for an $N \times N$ matrix M.

2.2.2 Generating functional

In order to systematically calculate various quantities, it is convenient to introduce the partition function with the fermionic source fields η and $\bar{\eta}$ as

$$Z[\eta, \bar{\eta}] \equiv \left\langle T_C \exp\left[\frac{i}{\hbar}\int_C dz \left[\bar{\eta}(z)\hat{f}(z) + \hat{f}^\dagger(z)\eta(z)\right]\right]\right\rangle. \tag{2.20}$$

The path integral representation of the partition function is

$$Z[\eta, \bar{\eta}] = \int \mathcal{D}\bar{\psi}\mathcal{D}\psi \exp\left(\frac{i}{\hbar}(S[\bar{\psi}, \psi] + S^s[\bar{\psi}, \psi; \eta, \bar{\eta}])\right), \tag{2.21}$$

where the density matrix is incorporated in the action $S[\bar{\psi}, \psi]$ [4]. The source term is

$$S^s[\bar{\psi}, \psi; \eta, \bar{\eta}] \equiv \int_C dz\,[\bar{\eta}(z)\psi(z) + \bar{\psi}(z)\eta(z)], \tag{2.22}$$

where the source fields $\eta(z)$ and $\bar{\eta}(z)$ are the Grassmann numbers and anticommute with the Grassmann fields of the fermions.

The generating functional of the connected Green's functions is defined as

$$W[\eta,\bar{\eta}] \equiv -i\ln Z[\eta,\bar{\eta}]. \tag{2.23}$$

The functional differentiation with respect to η and $\bar{\eta}$,

$$\frac{\delta}{\delta\eta(z)} \equiv \tau_z^\rho \frac{\delta}{\delta\eta^\rho(t)}, \tag{2.24}$$

$$\frac{\delta}{\delta\bar{\eta}(z)} \equiv \tau_z^\rho \frac{\delta}{\delta\bar{\eta}^\rho(t)}, \tag{2.25}$$

leads us to the equations

$$\frac{\delta W[\eta,\bar{\eta}]}{\delta\bar{\eta}(z)} = \langle\psi(z)\rangle^s, \tag{2.26}$$

$$\frac{\delta W[\eta,\bar{\eta}]}{\delta\eta(z)} = -\langle\bar{\psi}(z)\rangle^s, \tag{2.27}$$

where

$$\langle\mathcal{O}\rangle^s \equiv \frac{1}{Z[\eta,\bar{\eta}]}\int\int \mathcal{D}\bar{\psi}\mathcal{D}\psi\mathcal{O}\exp\left(\frac{i}{\hbar}(S[\bar{\psi},\psi]+S^s[\bar{\psi},\psi;\eta,\bar{\eta}])\right) \tag{2.28}$$

stands for the statistical average with the source term (2.22). These are reduced to the physical values when all the source fields are set to zero.

The connected two-point Green's function $G(z,z')$ on the Keldysh contour C is defined as a derivative of $W[\eta,\bar{\eta}]$ as

$$\begin{aligned} G(z,z') &\equiv -\left.\frac{\delta^2 W[\eta,\bar{\eta}]}{\delta\bar{\eta}(z)\delta\eta(z')}\right|_{\eta=\bar{\eta}=0} \\ &= -\frac{i}{\hbar}\left(\langle T_C\psi(z)\bar{\psi}(z')\rangle - \langle\psi(z)\rangle\langle\bar{\psi}(z')\rangle\right). \end{aligned} \tag{2.29}$$

The statistical average without the source fields is denoted by $\langle\mathcal{O}\rangle \equiv \langle\mathcal{O}\rangle^s|_{\eta=\bar{\eta}=0}$. The Green's function projected onto the real time axis by specifying the branches is denoted by $G^{\rho\rho'}(t,t') = G(z,z')$ for $z\in C^\rho$ and $z'\in C^{\rho'}$. From the definition of the contour-ordering operator, G^{--} (G^{++}) is the Green's function for the (anti-)time-ordering product. The remaining components G^{-+} and G^{+-} are called the lesser and the greater Green's functions, respectively.

It is often more convenient to introduce another representation of the Green's functions with a new pair of fields,

$$\psi^{\mathrm{p}} \equiv \frac{\psi^- + \psi^+}{2}, \tag{2.30}$$

$$\psi^{\mathrm{s}} \equiv \psi^- - \psi^+. \tag{2.31}$$

The subscripts "p" and "s" represent "physical" and "source", respectively. They are often called "classical" and "quantum" components [6]. The unitary matrix

$$Q \equiv \frac{1}{\sqrt{2}} \begin{pmatrix} 1 & -1 \\ 1 & 1 \end{pmatrix}, \tag{2.32}$$

transforms the original fields ψ^- and ψ^+ into the new basis as

$$\begin{pmatrix} \psi^{\mathrm{s}}/\sqrt{2} \\ \sqrt{2}\psi^{\mathrm{p}} \end{pmatrix} = Q \begin{pmatrix} \psi^- \\ \psi^+ \end{pmatrix}. \tag{2.33}$$

Accordingly, the Green's functions in the rotated basis are introduced as

$$\begin{pmatrix} G^{\tilde{\mathrm{K}}} & G^{\mathrm{a}} \\ G^{\mathrm{r}} & G^{\mathrm{K}} \end{pmatrix} \equiv Q \begin{pmatrix} G^{--} & G^{-+} \\ G^{+-} & G^{++} \end{pmatrix} Q^{\dagger} \tag{2.34}$$

$$= \frac{1}{2} \begin{pmatrix} G^{--} - G^{-+} - G^{+-} + G^{++} & G^{--} + G^{-+} - G^{+-} - G^{++} \\ G^{--} - G^{-+} + G^{+-} - G^{++} & G^{--} + G^{-+} + G^{+-} + G^{++} \end{pmatrix} \tag{2.35}$$

$$= \begin{pmatrix} -\frac{1}{2} \left. \dfrac{\delta^2 W[\eta,\bar{\eta}]}{\delta\bar{\eta}^{\mathrm{p}}(t)\delta\eta^{\mathrm{p}}(t')} \right|_{\eta=\bar{\eta}=0} & -\left. \dfrac{\delta^2 W[\eta,\bar{\eta}]}{\delta\bar{\eta}^{\mathrm{p}}(t)\delta\eta^{\mathrm{s}}(t')} \right|_{\eta=\bar{\eta}=0} \\ -\left. \dfrac{\delta^2 W[\eta,\bar{\eta}]}{\delta\bar{\eta}^{\mathrm{s}}(t)\delta\eta^{\mathrm{p}}(t')} \right|_{\eta=\bar{\eta}=0} & -2 \left. \dfrac{\delta^2 W[\eta,\bar{\eta}]}{\delta\bar{\eta}^{\mathrm{s}}(t)\delta\eta^{\mathrm{s}}(t')} \right|_{\eta=\bar{\eta}=0} \end{pmatrix}. \tag{2.36}$$

The components G^{r}, G^{a}, and G^{K} are called the retarded, advanced, and Keldysh Green's function, respectively. In the absence of the source component η^{s}, the forward and backward contributions in the partition function are canceled out [4, 6], and the partition function is constant, i.e. $Z[\eta,\bar{\eta}]|_{\eta^{\mathrm{s}}=0} = \mathrm{Tr}[\hat{\rho}]$. Hence, the p-p component of the Green's function vanishes,

$$G^{\tilde{\mathrm{K}}} = 0, \tag{2.37}$$

leading to the relations

$$G^{\mathrm{r}} = G^{--} - G^{-+} = G^{+-} - G^{++}, \tag{2.38}$$

$$G^{\mathrm{a}} = G^{--} - G^{+-} = G^{-+} - G^{++}, \tag{2.39}$$

$$G^{\mathrm{K}} = G^{-+} + G^{+-} = G^{--} + G^{++}. \tag{2.40}$$

The retarded and the advanced components are mutually Hermitian conjugate as

$$G^{\mathrm{a}}(t,t') = (G^{r}(t',t))^{*}. \tag{2.41}$$

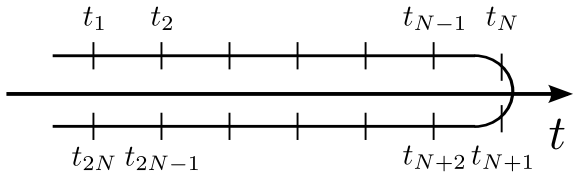

Fig. 2.2 Discretized Keldysh contour C.

The causality requires the retarded (advanced) Green's function lower (upper) triangular matrices in the time domain;

$$G^{\mathrm{r}}(t,t') = 0 \ \ (\text{for } \ t < t'), \tag{2.42}$$
$$G^{\mathrm{a}}(t,t') = 0 \ \ (\text{for } \ t > t'). \tag{2.43}$$

2.2.3 Noninteracting system

In order to demonstrate how the Green's functions are calculated based on the functional approach, we consider the simplest fermionic Hamiltonian

$$\hat{H}_0 = \varepsilon_f \hat{f}^\dagger \hat{f}, \tag{2.44}$$

with the fermionic creation (annihilation) operator $\hat{f}^\dagger$ ($\hat{f}$) and the energy level ε_f. The initial density matrix is chosen to be the equilibrium density matrix

$$\hat{\rho}_{\mathrm{eq}} = e^{-\beta(\hat{H}_0 - \mu\hat{N})}, \tag{2.45}$$

with the inverse temperature β, the chemical potential μ, and the particle number operator $\hat{N} = \hat{f}^\dagger \hat{f}$.

We divide the Keldysh contour C into $(2N-2)$ time intervals of small length δ_t such that $t_1 = t_{2N}$ and $t_N = t_{N+1}$ (Fig. 2.2), and insert the identity operator

$$\hat{1} = \int\int \mathcal{D}\bar{\psi}_i \mathcal{D}\psi_i e^{-\bar{\psi}_i \psi_i} |\psi_i\rangle\langle\psi_i|, \tag{2.46}$$

at $i = 1, 2, \cdots, 2N$. Then, the partition function (2.20) becomes

$$Z[\eta,\bar{\eta}] = \int \prod_{i=1}^{2N} \mathcal{D}\bar{\psi}_i \mathcal{D}\psi_i \exp\left[\frac{i}{\hbar}\sum_{i=1}^{2N}\delta_i\left(i\bar{\psi}_i\frac{\psi_i - \psi_{i-1}}{\delta_i} - \varepsilon_f\bar{\psi}_i\psi_{i-1} + \bar{\eta}_{i-1}\psi_{i-1} + \bar{\psi}_i\eta_i\right)\right] \times \langle\psi_1|\rho_{\mathrm{eq}}|-\psi_{2N}\rangle, \tag{2.47}$$

with $\delta_i \equiv t_i - t_{i-1}$. The last contribution is evaluated as

$$\langle\psi_1|\rho_{\mathrm{eq}}|-\psi_{2N}\rangle = \exp\left[-\bar{\psi}_1\psi_{2N}\rho_{\mathrm{eq}}(\varepsilon_f)\right], \tag{2.48}$$

with $\rho_{\rm eq}(\varepsilon_f) \equiv \exp\left[-\beta(\varepsilon_f-\mu)\right]$. Then, the partition function is rewritten as

$$Z[\eta,\bar{\eta}] = \int \prod_{i=1}^{2N} \mathcal{D}\bar{\psi}_i \mathcal{D}\psi_i \exp\left[\frac{i}{\hbar}\sum_{i,j=1}^{N} \bar{\psi}_i G_{ij}^{-1}\psi_j + \frac{i}{\hbar}\sum_{i=1}^{N}\delta_i\left(\bar{\eta}_{i-1}\psi_{i-1} + \bar{\psi}_i\eta_i\right)\right], \quad (2.49)$$

where the matrix is given by

$$iG_{ij}^{-1} = \begin{pmatrix} -1 & 0 & 0 & \dots & 0 & 0 & -\rho_{\rm eq}(\varepsilon_f) \\ h_2 & -1 & 0 & \dots & 0 & 0 & 0 \\ 0 & h_3 & -1 & \dots & 0 & 0 & 0 \\ \vdots & \vdots & \vdots & \ddots & \vdots & \vdots & \vdots \\ 0 & 0 & 0 & \dots & -1 & 0 & 0 \\ 0 & 0 & 0 & \dots & h_{2N-1} & -1 & 0 \\ 0 & 0 & 0 & \dots & 0 & h_{2N} & -1 \end{pmatrix}, \quad (2.50)$$

with $h_i = 1 - i\delta_i\varepsilon_f$.

The determinant of the matrix $-iG^{-1}$ is calculated as

$$\det\left(-iG^{-1}\right) = 1 + \rho_{\rm eq}(\varepsilon_f)\prod_{i=2}^{2N} h_i \to 1 + \rho_{\rm eq}(\varepsilon_f), \quad (2.51)$$

in the limit $\delta_t \to 0$. The (m,n) cofactor is similarly calculated as

$$(-1)^{n+m}\det\left[-iG^{-1}\right]_{mn} = \begin{cases} \displaystyle\prod_{k=m+1}^{n} h_k & (m<n) \\ 1 & (m=n) \\ \displaystyle -\rho_{\rm eq}(\varepsilon_f)\prod_{k=2}^{2N} h_k \Big/ \prod_{k=n+1}^{m} h_k & (m>n) \end{cases}. \quad (2.52)$$

Noting the relations $\prod_{k=2}^{2N} h_k = 1$ and $1/\prod_{k=n+1}^{m} h_k = \prod_{k=n+1}^{m} h_k^*$, we obtain the inverse matrix as

$$iG_{mn} = \frac{1}{1+\rho_{\rm eq}(\varepsilon_f)} \begin{cases} \displaystyle -\rho_{\rm eq}(\varepsilon_f)\prod_{k=m+1}^{n} h_k^*, & (m<n) \\ 1, & (m=n) \\ \displaystyle\prod_{k=n+1}^{m} h_k, & (n<m) \end{cases}. \quad (2.53)$$

Up to the first order in δ_t, the product of h_i is simplified as

$$\prod_{k=n+1}^{m} h_k = \begin{cases} e^{-i\varepsilon_f(t_m-t_n)}, & (z_n\in C^-,\ z_m\in C^-) \\ e^{-i\varepsilon_f(t_m-t_n)}, & (z_n\in C^-,\ z_m\in C^+) \\ e^{+i\varepsilon_f(t_m-t_n)}, & (z_n\in C^+,\ z_m\in C^+) \end{cases}. \quad (2.54)$$

where $z_{n(m)}$ is the variable on the Keldysh contour with the real time $t_{n(m)}$. If we introduce the Fermi-Dirac distribution

$$f(\omega) = \frac{\rho_{\rm eq}(\omega)}{\rho_{\rm eq}(\omega)+1} = \frac{1}{e^{\beta(\omega-\mu)}+1}, \tag{2.55}$$

the Green's function are obtained as

$$G^{--}(t,t') = -i\theta(t-t')(1-f(\varepsilon_f))e^{-i\varepsilon_f(t-t')} + i\theta(t'-t)f(\varepsilon_f)e^{-i\varepsilon_f(t-t')}, \tag{2.56}$$
$$G^{-+}(t,t') = if(\varepsilon_f)e^{-i\varepsilon_f(t-t')}, \tag{2.57}$$
$$G^{+-}(t,t') = -i(1-f(\varepsilon_f))e^{-i\varepsilon_f(t-t')}, \tag{2.58}$$
$$G^{++}(t,t') = -i\theta(t'-t)(1-f(\varepsilon_f))e^{-i\varepsilon_f(t-t')} + i\theta(t-t')f(\varepsilon_f)e^{-i\varepsilon_f(t-t')}, \tag{2.59}$$

in the continuous limit ($N \to \infty$) with the step function $\theta(t)$. The Fourier transforms of the Green's functions are

$$G^{--}(\omega) = \frac{1-f(\varepsilon_f)}{\omega-\varepsilon_f+i0^+} + \frac{f(\varepsilon_f)}{\omega-\varepsilon_f-i0^+}, \tag{2.60}$$
$$G^{-+}(\omega) = 2\pi i f(\varepsilon_f)\delta(\omega-\varepsilon_f), \tag{2.61}$$
$$G^{+-}(\omega) = -2\pi i(1-f(\varepsilon_f))\delta(\omega-\varepsilon_f), \tag{2.62}$$
$$G^{++}(\omega) = -\frac{1-f(\varepsilon_f)}{\omega-\varepsilon_f-i0^+} - \frac{f(\varepsilon_f)}{\omega-\varepsilon_f+i0^+}, \tag{2.63}$$

with the infinitesimal positive value 0^+. The Green's functions in the rotated basis are computed as

$$G^{\rm r}(t,t') = -i\theta(t-t')e^{-i\varepsilon_f(t-t')}, \tag{2.64}$$
$$G^{\rm a}(t,t') = i\theta(t'-t)e^{-i\varepsilon_f(t-t')}, \tag{2.65}$$
$$G^{\rm K}(t,t') = -i(1-2f(\varepsilon_f))e^{-i\varepsilon_f(t-t')}, \tag{2.66}$$

and, equivalently, their Fourier transforms are

$$G^{\rm r}(\omega) = \frac{1}{\omega-\varepsilon_f+i0^+}, \tag{2.67}$$
$$G^{\rm a}(\omega) = \frac{1}{\omega-\varepsilon_f-i0^+}, \tag{2.68}$$
$$G^{\rm K}(\omega) = -2\pi i(1-2f(\varepsilon_f))\delta(\omega-\varepsilon_f). \tag{2.69}$$

2.3 Nonequilibrium transport in open quantum systems

In this section, we provide a field-theoretic description of nonequilibrium transport through open quantum systems. One of the simplest examples of open quantum systems is the resonant level model, which is an archetypical and exactly solvable model. It is a very good starting point of the transport phenomena away from equilibrium. Moreover, it forms

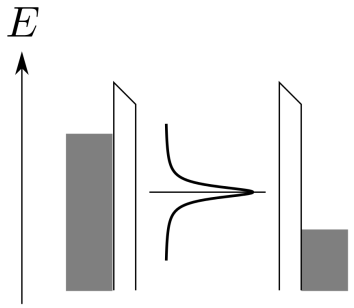

Fig. 2.3 Schematic energy diagram of the resonant level model.

a basis of interacting open quantum systems, which need further elaboration of theoretical treatment (see the next section). Though the present section is devoted to the analysis of the resonant level model, it is straightforward to generalize the discussions to other noninteracting systems, such as multiterminal systems and lattice systems.

In subsection 2.3.1, the resonant level model is introduced and solved by using the field-theoretic techniques. In subsection 2.3.2, the full counting statistics is revisited from a viewpoint of the Keldysh formalism. In subsection 2.3.3, useful expressions of the transport quantities through the open quantum systems are derived by utilizing the gauge structure of the system.

2.3.1 Resonant level model

In order to understand the nonequilibrium transport phenomena, we introduce the resonant level model with an applied bias voltage (see Fig. 2.3). The resonant level model consists of a single level which is coupled to fermionic reservoirs. Physically speaking, it describes a noninteracting electron residing in a quantum dot (QD) coupled with leads. The Hamiltonian of the resonant level model is written as

$$H_{\rm RLM} = \varepsilon_d \hat{d}^\dagger \hat{d} + \sum_{\alpha=L,R} \sum_{\boldsymbol{k}} (\varepsilon_{\alpha\boldsymbol{k}} - \mu_\alpha)\, \hat{c}^\dagger_{\alpha\boldsymbol{k}} \hat{c}_{\alpha\boldsymbol{k}} + \sum_{\alpha=L,R} \sum_{\boldsymbol{k}} (t_\alpha \hat{d}^\dagger \hat{c}_{\alpha\boldsymbol{k}} + \text{h.c.}), \tag{2.70}$$

where $\hat{d}^\dagger$ ($\hat{d}$) and $\hat{c}^\dagger_{\alpha\boldsymbol{k}}$ ($\hat{c}_{\alpha\boldsymbol{k}}$) are the creation (annihilation) operators of the electron in the QD and the conduction electron in the leads $\alpha = L,R$ with momentum $\boldsymbol{k}$ and dispersion relation $\varepsilon_{\alpha\boldsymbol{k}}$, respectively. For simplicity, we do not consider the spin degrees of freedom. The first term of the Hamiltonian describes an isolated QD with an energy level ε_d, whereas the second term represents noninteracting electron in the reservoirs with the chemical potentials $\mu_L = \varepsilon_F + eV/2$ and $\mu_R = \varepsilon_F - eV/2$. Here, ε_F and V are the Fermi energy and bias voltage, respectively. The third term describes electron tunneling between the QD and the leads with the hopping amplitudes t_α. The important assumption is that the both leads are always in equilibrium. This formally means that the correlation functions of the conduction electrons in the leads are given by the equilibrium ones.

The path integral representation of the resonant level model is given by the action

$$S_{\mathrm{RLM}}[\bar{d},d;\bar{c},c] = \int_C dz dz' \bar{d}(z) g_d^{-1}(z,z') d(z') + \int_C dz dz' \sum_{\alpha=L,R} \sum_{\boldsymbol{k}} \bar{c}_{\alpha\boldsymbol{k}}(z) g_{\alpha\boldsymbol{k}}^{-1}(z,z') c_{\alpha\boldsymbol{k}}(z') - \int_C dz \sum_{\alpha=L,R} \sum_{\boldsymbol{k}} (t_\alpha \bar{d}(z) c_{\alpha\boldsymbol{k}}(z) + \mathrm{h.c.}). \tag{2.71}$$

All the quantities in the action are defined on the Keldysh contour C shown in Fig. 2.1. The Grassmann fields of electrons in the QD are denoted by $\bar{d}$ (d) and $\bar{c}_{\alpha\boldsymbol{k}}$ ($c_{\alpha\boldsymbol{k}}$) represents the conduction electron in the leads $\alpha = L,R$ with momentum $\boldsymbol{k}$. The two-point Green's functions for the electrons in the isolated QD and those in the lead α with momentum $\boldsymbol{k}$ are defined as $g_d^{-1}(z,z') \equiv \delta(z-z')\left[i\frac{\partial}{\partial z'} - \varepsilon_d\right]$ and $g_{\alpha\boldsymbol{k}}^{-1}(z,z') \equiv \delta(z-z')\left[i\frac{\partial}{\partial z'} - \varepsilon_{\alpha\boldsymbol{k}}\right]$, respectively.

The Fourier transform of the Green's functions can be computed in the same manner as in subsection 2.2.3. The retarded and the lesser components of the isolated QD Green's function are given by

$$g_d^{\mathrm{r}}(\omega) = \frac{1}{\omega - \varepsilon_d + i0^+}, \tag{2.72}$$

$$g_d^{-+}(\omega) = 2\pi i n_d \delta(\omega - \varepsilon_d), \tag{2.73}$$

where n_d is the initial density of the QD. As we consider that the lead α is in equilibrium with the chemical potential μ_α and the inverse temperature β, the retarded and the lesser components of the isolated lead Green's function are

$$g_{\alpha\boldsymbol{k}}^{\mathrm{r}}(\omega) = \frac{1}{\omega - \varepsilon_{\alpha\boldsymbol{k}} + i0^+}, \tag{2.74}$$

$$g_{\alpha\boldsymbol{k}}^{-+}(\omega) = 2\pi i f_\alpha(\varepsilon_{\alpha\boldsymbol{k}}) \delta(\omega - \varepsilon_{\alpha\boldsymbol{k}}), \tag{2.75}$$

with the Fermi-Dirac distribution function for the lead α,

$$f_\alpha(\omega) = \frac{1}{e^{\beta(\omega-\mu_\alpha)}+1}. \tag{2.76}$$

The partition function Z_{RLM} is given by the functional integration over the fermionic degrees of freedom;

$$Z_{\mathrm{RLM}} \equiv \int \mathcal{D}[\bar{d}d]\mathcal{D}[\bar{c}c] \exp\left(\frac{i}{\hbar} S_{\mathrm{RLM}}[\bar{d},d;\bar{c},c]\right). \tag{2.77}$$

The fermionic environments consisting of the conduction electrons can be exactly traced out using the Gaussian integration. The hybridization between the QD and the lead α is expressed as the tunneling self-energy of the dot electron,

$$\Sigma_\alpha(z,z') = \sum_{\boldsymbol{k}} t_\alpha^2 g_{\alpha\boldsymbol{k}}(z,z'). \tag{2.78}$$

The retarded and the lesser components of the tunneling self-energy are

$$\begin{aligned}\Sigma_\alpha^{\mathrm{r}}(\omega) &= \sum_{\boldsymbol{k}} \frac{t_\alpha^2}{\omega - \varepsilon_{\alpha\boldsymbol{k}} + i0^+} \\ &= -\frac{i\Delta_\alpha(\omega)}{2}, \end{aligned} \tag{2.79}$$

$$\Sigma_\alpha^{-+}(\omega) = i\Delta_\alpha(\omega) f_\alpha(\omega). \tag{2.80}$$

where the real part of the Cauchy principal value is neglected in the second line of Eq. (2.79), and the linewidth is defined as $\Delta_\alpha(\omega) \equiv 2\pi t_\alpha^2 \rho_\alpha(\omega)$ with the density of states in the lead α denoted by $\rho_\alpha(\omega) \equiv \sum_{\boldsymbol{k}} \delta(\omega - \varepsilon_{\alpha\boldsymbol{k}})$. The matrix representation of the tunneling self-energy in the rotated basis is given by

$$\begin{pmatrix} \Sigma_\alpha^{\tilde{\mathrm{K}}}(\omega) & \Sigma_\alpha^{\mathrm{a}}(\omega) \\ \Sigma_\alpha^{\mathrm{r}}(\omega) & \Sigma_\alpha^{\mathrm{K}}(\omega) \end{pmatrix} = \begin{pmatrix} 0 & i\Delta_\alpha(\omega)/2 \\ -i\Delta_\alpha(\omega)/2 & i\Delta_\alpha(\omega)(2f_\alpha(\omega)-1) \end{pmatrix}. \tag{2.81}$$

After integrating out the conduction electrons, the partition function becomes

$$Z_{\mathrm{RLM}} = \int \mathcal{D}[\bar{d}d] \exp\left(\frac{i}{\hbar} S_{\mathrm{RLM}}[\bar{d}, d]\right), \tag{2.82}$$

up to an unimportant factor with the action

$$S_{\mathrm{RLM}}[\bar{d}, d] \equiv \int_C dz dz' \bar{d}(z) G_{0d}^{-1}(z, z') d(z'). \tag{2.83}$$

Here, the Green's function of the isolated QD is modified as

$$G_{0d}^{-1}(z, z') \equiv g_d^{-1}(z, z') - \Sigma_{\mathrm{res}}(z, z'), \tag{2.84}$$

with the tunneling self-energy $\Sigma_{\mathrm{res}}(z, z') \equiv \Sigma_L(z, z') + \Sigma_R(z, z')$. The index 0 means that the results are for noninteracting case. The Coulomb interaction term is considered in section 2.4. The retarded and the lesser components of the modified Green's function are

$$G_{0d}^{\mathrm{r}}(\omega) = \frac{1}{\omega + i\Delta(\omega)/2}, \tag{2.85}$$

$$G_{0d}^{-+}(\omega) = \sum_{\alpha=L,R} \frac{i\Delta_\alpha(\omega) f_\alpha(\varepsilon_{\alpha\boldsymbol{k}})}{\omega^2 + \Delta^2(\omega)/4}, \tag{2.86}$$

with the linewidth $\Delta(\omega) \equiv \Delta_L(\omega) + \Delta_R(\omega)$. We note that the lesser component (2.86) is no longer dependent on the initial QD density n_d described by the lesser component of the isolated Green's function $g_d^{-+}(\omega)$. It also holds for the greater component. Hence, the lesser and the greater components of the isolated QD Green's function can be set to zero, i.e. $g_d^{-+}(\omega) = g_d^{+-}(\omega) = 0$ as far as we are concerned with the steady-state of the QD-reservoir coupled system;

$$\begin{pmatrix} g_d^{\tilde{\mathrm{K}}}(\omega) & g_d^{\mathrm{a}}(\omega) \\ g_d^{\mathrm{r}}(\omega) & g_d^{\mathrm{K}}(\omega) \end{pmatrix} = \begin{pmatrix} 0 & 1/(\omega - \varepsilon_d - i0^+) \\ 1/(\omega - \varepsilon_d + i0^+) & 0 \end{pmatrix}. \tag{2.87}$$

2.3.2 Full counting statistics revisited

The full counting statistics [14, 15] is elegantly incorporated in the Keldysh formalism [10, 11]. In order to trace the hopping process of the electrons in the time interval $[0,\tau]$, we introduce the auxiliary phase $\gamma(z) = -(\rho\lambda/2)\theta(t)\theta(\tau-t)$ for $z \in C^{\rho}$ so that the transmission amplitude t_R acquires the phase as $t_R e^{i\gamma(z)}$. The introduced parameter serves as a "non-demolishing marker" because it can detect the electron hopping without disturbing its dynamics. As a consequence of the additional phase, the tunneling self-energy (2.78) associated with the right reservoir is transformed as

$$\Sigma_{R\gamma}(z,z') = t_R^2 \sum_{\boldsymbol{k}} e^{-i\gamma(z)} g_{R\boldsymbol{k}}(z,z') e^{i\gamma(z')}, \tag{2.88}$$

which is equivalent to the matrix

$$\begin{pmatrix} \Sigma_{R\gamma}^{--}(t,t') & \Sigma_{R\gamma}^{-+}(t,t') \\ \Sigma_{R\gamma}^{+-}(t,t') & \Sigma_{R\gamma}^{++}(t,t') \end{pmatrix} = \begin{pmatrix} e^{-i(\gamma^-(t)-\gamma^-(t'))}\Sigma_R^{--}(t,t') & e^{-i(\gamma^-(t)-\gamma^+(t'))}\Sigma_R^{-+}(t,t') \\ e^{-i(\gamma^+(t)-\gamma^-(t'))}\Sigma_R^{+-}(t,t') & e^{-i(\gamma^+(t)-\gamma^+(t'))}\Sigma_R^{++}(t,t') \end{pmatrix}. \tag{2.89}$$

The partition function is modified as

$$Z_{\mathrm{RLM}}(\gamma) = \int \mathcal{D}[\bar{d}d] \exp\left(i \int_C dz dz' \bar{d}(z) G_{0d\gamma}^{-1}(z,z') d(z') \right), \tag{2.90}$$

with the gauge-transformed tunneling self-energy $\Sigma_{\mathrm{res}\gamma} \equiv \Sigma_L + \Sigma_{R\gamma}$ and the Green's function

$$G_{0d\gamma}^{-1}(z,z') = g_d^{-1}(z,z') - \Sigma_{\mathrm{res}\gamma}(z,z'). \tag{2.91}$$

Since the action is quadratic with respect to the fermionic Grassmann fields, the Gaussian integration is formally performed as

$$Z_{\mathrm{RLM}}(\gamma) = \det\left(i G_{0d\gamma}^{-1} \right). \tag{2.92}$$

If we multiply the above equation by the constant $\det(-ig_d)$ and redefine the partition function, its logarithm is obtained as

$$\begin{aligned} \ln Z_{\mathrm{RLM}}(\gamma) &= \ln\left[\det\left(1 - g_d \Sigma_{\mathrm{res}\gamma}\right) \right] \\ &= \mathrm{Tr}\left[\ln\left(1 - g_d \Sigma_{\mathrm{res}\gamma}\right) \right] \\ &= -\sum_{k=1}^{\infty} \mathrm{Tr}\left[\left(g_d \Sigma_{\mathrm{res}\gamma}\right)^k \right] \\ &= -\sum_{k=1}^{\infty} \int_0^{\tau} dt \mathrm{Tr}\left[\left(\boldsymbol{g}_d \tau_x \boldsymbol{\Sigma}_{\mathrm{res}\gamma} \tau_x\right)^k \right](t,t). \end{aligned} \tag{2.93}$$

The bold letters represent the matrix of the Green's function and the self-energy in the rotated Keldysh basis.

Here, we assume that the observation time τ is so large that the gauge phase is approximated as

$$\gamma(z) = -\frac{\rho\lambda}{2}, \tag{2.94}$$

for $z \in C^{\rho}$. It is possible to justify this assumption by noting that the sub-leading contribution is just logarithmic in τ [16]. Then, the logarithm of the partition function is further calculated as

$$\begin{aligned}\lim_{\tau\to\infty}\frac{1}{\tau}\ln Z_{\mathrm{RLM}}(\lambda) &= -\sum_{k=1}^{\infty}\int\frac{d\omega}{2\pi}\mathrm{Tr}\left[\left(\boldsymbol{g}_d(\omega)\tau_x\boldsymbol{\Sigma}_{\mathrm{res}\lambda}(\omega)\tau_x\right)^k\right] \\ &= \int\frac{d\omega}{2\pi}\mathrm{Tr}\left[\ln\left(1-\boldsymbol{g}_d(\omega)\tau_x\boldsymbol{\Sigma}_{\mathrm{res}\lambda}(\omega)\tau_x\right)\right] \\ &= \int\frac{d\omega}{2\pi}\ln\left[\det\left(1-\boldsymbol{g}_d(\omega)\tau_x\boldsymbol{\Sigma}_{\mathrm{res}\lambda}(\omega)\tau_x\right)\right]. \end{aligned} \tag{2.95}$$

The tunneling self-energy is Fourier transformed as

$$\begin{pmatrix} \Sigma^{--}_{R\lambda}(\omega) & \Sigma^{-+}_{R\lambda}(\omega) \\ \Sigma^{+-}_{R\lambda}(\omega) & \Sigma^{++}_{R\lambda}(\omega) \end{pmatrix} = \begin{pmatrix} \Sigma^{--}_{R}(\omega) & e^{-i\lambda}\Sigma^{-+}_{R}(\omega) \\ e^{i\lambda}\Sigma^{+-}_{R}(\omega) & \Sigma^{++}_{R}(\omega) \end{pmatrix}. \tag{2.96}$$

In the rotated basis, the tunneling self-energy is given by

$$\begin{pmatrix} \Sigma^{\tilde{\mathrm{K}}}_{R\lambda} & \Sigma^{\mathrm{a}}_{R\lambda} \\ \Sigma^{\mathrm{r}}_{R\lambda} & \Sigma^{\mathrm{K}}_{R\lambda} \end{pmatrix} = \frac{i\Delta_R(\omega)}{2}\begin{pmatrix} (1-e^{-i\lambda})f_R-(1-e^{i\lambda})\bar{f}_R & e^{-i\lambda}f_R+e^{i\lambda}\bar{f}_R \\ -e^{-i\lambda}f_R-e^{i\lambda}\bar{f}_R & (1+e^{-i\lambda})f_R-(1+e^{i\lambda})\bar{f}_R \end{pmatrix}, \tag{2.97}$$

with $\bar{f}_\alpha(\omega) \equiv 1-f_\alpha(\omega)$. With the aid of the formal expression of the partition function (2.95), we obtain the result

$$\begin{aligned}\lim_{\tau\to\infty}\frac{1}{\tau}\ln Z_{\mathrm{RLM}}(\lambda) = \int\frac{d\omega}{2\pi}\ln\Big[1+T_{LR}(\omega)\Big[&f_L(\omega)(1-f_R(\omega))(e^{i\lambda}-1) \\ &+f_R(\omega)(1-f_L(\omega))(e^{-i\lambda}-1)\Big]\Big], \end{aligned} \tag{2.98}$$

with the transmission coefficient

$$T_{LR}(\omega) = \frac{1}{4}\frac{\Delta_L(\omega)\Delta_R(\omega)}{(\omega-\varepsilon_d)^2+(\Delta_L(\omega)+\Delta_R(\omega))^2/4}. \tag{2.99}$$

This is the Levitov-Lesovik formula (1.9) for the transport through the single resonant level. We note that the general procedures of the full counting statistics outlined in this subsection can be generalized to interacting electronic systems such as the QD in the Kondo regime [17] and the charge-fluctuating regime [18].

2.3.3 Field-theoretic description of transport quantities

The full counting statistics combined with the two-point measurement scheme is well suited to describe the time-averaged transport quantity in a long time interval. However, the formulation is of limited use to describe time-dependent problems such as the photon-assisted transport. Moreover, it is more transparent to formulate the problem from a general point of view by separating it from the specific realization of the measurement protocol. A key observation to generalize the full counting statistics is that the structure of the counting field is the same as the gauge field defined on the Keldysh contour. We explicitly investigate the gauge structure of the Lagrangian of the resonant level model, and show that the full counting statistics is naturally built in the Keldysh formalism. The result of the two-point measurement is recovered in a certain limit of the theory.

The action of the resonant level model with the gauge fields is written as

$$\begin{aligned} S_{\mathrm{RLM}}[\bar{d},d;\bar{c},c;A] = &\int_C dz\bar{d}(z)\left(i\frac{\partial}{\partial z}-\varepsilon_d-eA_0(z)\right)d(z) \\ &+\int_C dz\sum_{\alpha\boldsymbol{k}}\bar{c}_{\alpha\boldsymbol{k}}(z)\left(i\frac{\partial}{\partial z}-\varepsilon_{\alpha\boldsymbol{k}}-ev_\alpha(z)\right)c_{\alpha\boldsymbol{k}}(z) \\ &-\int_C dz\sum_{\alpha\boldsymbol{k}}\left(t_\alpha e^{ieA_\alpha(z)}\bar{c}_{\alpha\boldsymbol{k}}(z)d(z)+\mathrm{h.c.}\right). \end{aligned} \tag{2.100}$$

All the quantities in the action including the gauge fields are defined on the Keldysh contour C shown in Fig. 2.1. Scalar potentials in the QD and the lead α are written as A_0 and v_α, respectively. The vector potentials A_α are incorporated using the Peierls substitution: The hopping parameters t_α are modified as $t_\alpha e^{ie\int_\alpha d\boldsymbol{r}\cdot\boldsymbol{A}}$ where $\int_\alpha d\boldsymbol{r}\cdot\boldsymbol{A}$ are the integral of the vector potentials along the paths from the QD to the lead α. Here, we assume that these integrals can be averaged over the path, whose length is set to one. The gauge invariance of the action can be readily confirmed as shown in Appendix 2.A. By using the gauge transformation, it is always possible to consider the gauge-fixing condition $A_0(z)=v_\alpha(z)=0$. Hence, we do not consider the scalar potentials A_0 and v_α in the subsequent discussions.

The action (2.100) with the gauge-fixing condition is solved in the same way as the previous case. The dependence on A_α is incorporated in the tunneling self-energy as

$$\Sigma_\alpha(z,z') = \sum_{\boldsymbol{k}} t_\alpha^2 e^{-ieA_\alpha(z)} g_{\alpha\boldsymbol{k}}(z,z') e^{ieA_\alpha(z')}. \tag{2.101}$$

From this expression, it is clear that the tunneling self-energy with the counting field (2.88) is expressed by setting the gauge field $A_\alpha(z)$ in a specific way.

By doubling the degrees of freedom of the external gauge fields as $A_\alpha^{\mp}(t)$, we can describe both the time-evolution and the statistical correlation. The functional differentiation with respect to the gauge potentials on the Keldysh contour is represented in the Keldysh

space as

$$\frac{\delta}{\delta A_\alpha(z)} = \begin{pmatrix} \dfrac{\delta}{\delta A^-_\alpha(t)} & 0 \\ 0 & -\dfrac{\delta}{\delta A^+_\alpha(t)} \end{pmatrix}. \tag{2.102}$$

The expectation value of the current and its higher-order cumulants are obtained by differentiating the generating functional with respect to the gauge field.

We define physical fields and source fields as

$$A^p_\alpha(t) \equiv \frac{1}{2}\left(A^-_\alpha(t) + A^+_\alpha(t)\right), \tag{2.103}$$

$$A^s_\alpha(t) \equiv A^-_\alpha(t) - A^+_\alpha(t). \tag{2.104}$$

In order to preserve the normalization and the causality structure of the partition function, the gauge fields should satisfy the condition $A^-_\alpha(t) = A^+_\alpha(t) = A^p_\alpha(t)$ in the end of the calculation. Hence, the source field $A^s_\alpha(t)$ must be set to zero in the last step of calculations. On the other hand, the physical components $A^p_\alpha(t)$ can be left finite to describe an external driving field. Noting the relation $\langle j^-_\alpha(t)\rangle = \langle j^+_\alpha(t)\rangle$ with the current operator $j_\alpha(z)$, the expectation value of the current can be obtained on the real time axis as

$$\langle j_\alpha(t)\rangle = \left.\frac{\delta W[\eta,\bar\eta;A]}{\delta A^s_\alpha(t)}\right|_{\eta=\bar\eta=A^s=0}. \tag{2.105}$$

The source component of the vector potential $A^s_\alpha(t)$ is closely related to the counting field which is introduced in the full counting statistics. The important difference is that the counting field is designed to describe the time-averaged current while the vector potential is applicable to arbitrary time-dependent transport.

The current-current correlation function is defined as the second derivative of the generating functional

$$D_{\alpha_1\alpha_2}(z_1'', z_2'') \equiv -i\frac{\delta^2 W[\eta,\bar\eta;A]}{\delta A_{\alpha_1}(z_1'')\delta A_{\alpha_2}(z_2'')}. \tag{2.106}$$

Its real-time representation is given as

$$D_{\alpha\alpha'}(t,t') = \begin{pmatrix} -i\left.\dfrac{\delta^2 W[\eta,\bar\eta;A]}{\delta A^-_\alpha(t)\delta A^-_{\alpha'}(t')}\right|_{\eta=\bar\eta=A^s=0} & i\left.\dfrac{\delta^2 W[\eta,\bar\eta;A]}{\delta A^-_\alpha(t)\delta A^+_{\alpha'}(t')}\right|_{\eta=\bar\eta=A^s=0} \\ i\left.\dfrac{\delta^2 W[\eta,\bar\eta;A]}{\delta A^+_\alpha(t)\delta A^-_{\alpha'}(t')}\right|_{\eta=\bar\eta=A^s=0} & -i\left.\dfrac{\delta^2 W[\eta,\bar\eta;A]}{\delta A^+_\alpha(t)\delta A^+_{\alpha'}(t')}\right|_{\eta=\bar\eta=A^s=0} \end{pmatrix}, \tag{2.107}$$

where the minus signs of the lesser and the greater components come from the signs in Eq. (2.102). The current noise is given as

$$S_{\alpha\alpha'}(t,t') \equiv -2i \left. \frac{\delta^2 W[\eta,\bar{\eta};A]}{\delta A^s_\alpha(t)\delta A^s_{\alpha'}(t')} \right|_{\eta=\bar{\eta}=A^s=0} = D^{-+}_{\alpha\alpha'}(t,t') + D^{+-}_{\alpha\alpha'}(t,t'). \tag{2.108}$$

The current-current correlation function defined in this way is Hermite, and relevant in experiments as far as we focus on the time-averaged value.

2.4 Method for interacting nonequilibrium systems

In this section, we establish a theoretical method for nonequilibrium fluctuation in interacting quantum systems. Based on the path integral formalism, we introduce the effective action and vertex functions, which are convenient to express the transport quantities. Though the derivation is rather formal, the resulting expressions provide a good starting point to further elaborate the theoretical scheme. In particular, the problem is reduced to how the vertex functions are calculated in various interacting systems. The functional renormalization group approach, which is mainly used in chapter 5, is such a formalism to calculate the vertex functions.

In subsection 2.4.1, we define the effective action and the vertex functions. In subsection 2.4.2, we provide formal expressions of the transport quantities in a generic interacting system in terms of the vertex functions. In subsection 2.4.3, the expressions are applied to the interacting quantum dot system. In subsection 2.4.4, the functional renormalization group approach is developed.

2.4.1 Effective action and vertex functions

The effective action is a quantum analog of the classical action [7]. The quantum field theory can be reformulated in terms of variational problems of the effective action. This advantage of the effective action has been utilized for analyzing quantum many-body problems. In the quantum field theory, various quantities are conveniently described by the vertex functions. They are diagrammatically obtained by removing the external propagators included in connected correlation functions, and belong to the class of one-particle-irreducible (1PI) diagrams. The effective action is proved to be a generating functional of the 1PI vertex functions. This is the second reason why the effective action is an important object in the quantum field theory.

Let us consider an interacting fermionic system;

$$S[\bar{\psi},\psi;A] = S_0[\bar{\psi},\psi;A] + S_{\rm int}[\bar{\psi},\psi], \tag{2.109}$$

where the S_0 and $S_{\rm int}$ are the actions for the bare part and the interaction part, respectively. The bare action is written as

$$S_0[\bar{\psi},\psi;A] = \int_C dz dz' \bar{\psi}_i(z) G^{-1}_{0ij}[A](z,z')\psi_j(z'), \tag{2.110}$$

where the repeated indices are summed over. We assume that the external gauge field A can be solely incorporated in the noninteracting Green's function $G_0[A]$. This is true for various important examples including the resonant level model, the single-impurity Anderson model, and the interacting resonant level model. The generating functional for the connected Green's functions is given by

$$W[\eta,\bar{\eta};A] = -i\ln\int \mathcal{D}\bar{\psi}\mathcal{D}\psi \exp\left(\frac{i}{\hbar}(S[\bar{\psi},\psi;A]+S^s[\bar{\psi},\psi;\eta,\bar{\eta}])\right), \tag{2.111}$$

with the the source term

$$S^s[\bar{\psi},\psi;\eta,\bar{\eta}] = \int_C dz\,[\bar{\eta}_i(z)\psi_i(z)+\bar{\psi}_i(z)\eta_i(z)]\,. \tag{2.112}$$

The effective action $\Gamma[\langle\bar{\psi}\rangle^s,\langle\psi\rangle^s;A]$ is defined as the Legendre transform of $W[\eta,\bar{\eta};A]$,

$$\Gamma[\langle\bar{\psi}\rangle^s,\langle\psi\rangle^s;A] \equiv W[\eta,\bar{\eta};A] - \int_C dz\,[\bar{\eta}_i(z)\langle\psi_i(z)\rangle^s+\langle\bar{\psi}_i(z)\rangle^s\eta_i(z)]\,. \tag{2.113}$$

By using $\frac{\delta W[\eta,\bar{\eta};A]}{\delta\bar{\eta}_i(z)} = \langle\psi_i(z)\rangle^s$ and $\frac{\delta W[\eta,\bar{\eta};A]}{\delta\eta_i(z)} = -\langle\bar{\psi}_i(z)\rangle^s$ [see Eqs. (2.26) and (2.27)] and the chain rule, we can obtain the important relations to determine η and $\bar{\eta}$;

$$\frac{\delta\Gamma[\langle\bar{\psi}\rangle^s,\langle\psi\rangle^s;A]}{\delta\langle\psi_i(z)\rangle^s} = \bar{\eta}_i(z), \tag{2.114}$$

$$\frac{\delta\Gamma[\langle\bar{\psi}\rangle^s,\langle\psi\rangle^s;A]}{\delta\langle\bar{\psi}_i(z)\rangle^s} = -\eta_i(z). \tag{2.115}$$

Equations (2.114) and (2.115) provide a variational problem because the physical state can be realized in the limit of $\eta,\bar{\eta}\to 0$. The effective action is identical to the action in the tree approximation [7], where the optimal-path solution corresponds to the classical Euler-Lagrange equations. The full quantum effect can be incorporated in a perturbative manner. This is the reason why $\Gamma[\langle\bar{\psi}\rangle^s,\langle\psi\rangle^s;A]$ is called the effective action.

By using Eqs. (2.27), (2.29), and $\left.\frac{\delta^2 W[\eta,\bar{\eta};A]}{\delta\bar{\eta}_{i'}(z')\bar{\eta}_{i''}(z'')}\right|_{\eta=\bar{\eta}=0} = 0$, the chain rule for the arbitrary functional $f[\bar{\psi},\psi]$ is written as

$$\left.\frac{\delta f[\bar{\psi},\psi]}{\delta\bar{\eta}_i(z)}\right|_{\eta=\bar{\eta}=A^s=0} = \int_C dz' G_{ii'}(z,z')\left.\frac{\delta f[\bar{\psi},\psi]}{\delta\langle\bar{\psi}_{i'}(z')\rangle^s}\right|_{\eta=\bar{\eta}=A^s=0}. \tag{2.116}$$

The functional differentiation of Eq. (2.114) with respect to $\bar{\eta}_i$ can be performed by substituting $\frac{\delta\Gamma[\langle\bar{\psi}\rangle^s,\langle\psi\rangle^s;A]}{\delta\langle\psi_i(z)\rangle^s}$ for f in Eq. (2.116). This leads us to the equation

$$\delta(z,z')\delta_{ii'} = \int_C dz'' G_{ii''}(z,z'')\left.\frac{\delta^2\Gamma[\langle\bar{\psi}\rangle^s,\langle\psi\rangle^s;A]}{\delta\langle\bar{\psi}_{i''}(z'')\rangle^s\delta\langle\psi_{i'}(z')\rangle^s}\right|_{\eta=\bar{\eta}=A^s=0}. \tag{2.117}$$

This expression indicates that the second functional dervative of the effective action is the inverse propagator

$$\left.\frac{\delta^2\Gamma[\langle\bar{\psi}\rangle^s,\langle\psi\rangle^s;A]}{\delta\langle\bar{\psi}_i(z)\rangle^s\delta\langle\psi_{i'}(z')\rangle^s}\right|_{\eta=\bar{\eta}=A^s=0}=G^{-1}_{ii'}(z,z'). \tag{2.118}$$

If we define the self-energy as

$$\Sigma_{ii'}(z,z')\equiv G^{-1}_{0ii'}(z,z')-\left.\frac{\delta^2\Gamma[\langle\bar{\psi}\rangle^s,\langle\psi\rangle^s;A]}{\delta\langle\bar{\psi}_i(z)\rangle^s\delta\langle\psi_{i'}(z')\rangle^s}\right|_{\eta=\bar{\eta}=A^s=0}, \tag{2.119}$$

with the noninteracting Green's function G_0, Eq. (2.118) becomes the Dyson equation of the two-point connected Green's function.

The effective action is the generating functional for the 1PI vertex functions [7]. The 1PI vertex functions can be diagrammatically obtained by truncating the external legs of connected correlation functions. The vertex expansion of the effective action is given as

$$\begin{aligned}
&\Gamma[\langle\psi\rangle^{\rm s},\langle\bar{\psi}\rangle^{\rm s},A]\\
&=\sum_{m,n=0}^{\infty}\frac{(-1)^m}{(m!)^2n!}\prod_{j,k=0}^{m}\prod_{l=0}^{n}\int_C dz_j dz'_k dz''_l\,\gamma^{(2m,n)}_{i'_1\cdots i'_m;i_1\cdots i_m;\alpha_1\cdots\alpha_n}(z'_1,\cdots,z'_m;z_1,\cdots,z_m;z''_1,\cdots,z''_n)\\
&\qquad\times\langle\bar{\psi}_{i'_1}\rangle^{\rm s}(z'_1)\cdots\langle\bar{\psi}_{i'_m}\rangle^{\rm s}(z'_m)\langle\psi_{i_1}\rangle^{\rm s}(z_1)\cdots\langle\psi_{i_m}\rangle^{\rm s}(z_m)A_{\alpha_1}(z''_1)\cdots A_{\alpha_n}(z''_n).
\end{aligned} \tag{2.120}$$

We note that the auxiliary vector potential $A_\alpha(z)$ is also defined on the Keldysh contour, i.e. it has the two components $A^-_\alpha(t)$ and $A^+_\alpha(t)$. Hence, there are in total 2^{2m+n} components for the current-vertex function $\gamma^{(2m,n)}$.

Arbitrary vertex functions can be generated by functionally differentiating the effective action with respect to $\langle\bar{\psi}\rangle^s$, $\langle\psi\rangle^s$, and A. In particular, the functional differentiation of Eq. (2.118) with respect to the gauge fields generates the three-point 1PI vertex functions with two external electron lines and one external photon line. With the aid of the Dyson equation $G^{-1}=G_0^{-1}-\Sigma$, the three-point 1PI vertex function is divided into the noninteracting part and the interaction-induced part as

$$\begin{aligned}
\gamma^{(2,1)}_{i';i;\alpha}(z';z;z'')&=-\left.\frac{\delta^3\Gamma[\langle\bar{\psi}\rangle^s,\langle\psi\rangle^s;A]}{\delta\langle\bar{\psi}_{i'}(z')\rangle^s\delta\langle\psi_i(z)\rangle^s\delta A_\alpha(z'')}\right|_{\eta=\bar{\eta}=A^s=0}\\
&=\gamma^{(2,1)}_{0i';i;\alpha}(z';z;z'')+\bar{\gamma}^{(2,1)}_{i';i;\alpha}(z';z;z''),
\end{aligned} \tag{2.121}$$

$$\gamma^{(2,1)}_{0i';i;\alpha}(z';z;z'')\equiv-\frac{\delta G^{-1}_{0i'i}(z',z)}{\delta A_\alpha(z'')}, \tag{2.122}$$

$$\bar{\gamma}^{(2,1)}_{i';i;\alpha}(z',z;z'')\equiv\frac{\delta\Sigma_{i'i}(z',z)}{\delta A_\alpha(z'')}. \tag{2.123}$$

Here, $\gamma^{(2,1)}_{0i';i;\alpha}$ and $\bar{\gamma}^{(2,1)}_{i';i;\alpha}$ are called the bare vertex function and the dressed vertex function, respectively. The vertex functions are straightforwardly generalized to the higher-order

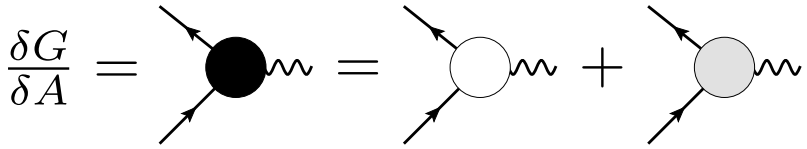

Fig. 2.4 Diagrammatic representation of Eq. (2.126) relating the three-point correlation function and the three-point vertex function. The black filled circle with the two fermion lines and one wavy line represents the three-point current vertex function. The wavy line denotes the external gauge field which couples to the electron system. The open and gray circles represent the bare and the dressed three-point current vertex function, respectively.

terms. For example, the bare and dressed four-point current vertex functions are defined as

$$\gamma^{(2,2)}_{0i';i;\alpha_1\alpha_2}(z';z;z_1'',z_2'') \equiv -\frac{\delta G^{-1}_{0i'i}(z',z)}{\delta A_{\alpha_1}(z_1'')\delta A_{\alpha_2}(z_2'')}, \tag{2.124}$$

$$\bar{\gamma}^{(2,2)}_{i';i;\alpha_1\alpha_2}(z',z;z_1'',z_2'') \equiv \frac{\delta \Sigma_{i'i}(z',z)}{\delta A_{\alpha_1}(z_1'')\delta A_{\alpha_2}(z_2'')}, \tag{2.125}$$

respectively.

The three-point connected correlation function is related to the vertex function as

$$\frac{\delta G_{i'i}(z',z)}{\delta A_\alpha(z'')} = \int_C dz_1 dz_1' G_{i'i_1'}(z',z_1')\gamma^{(2,1)}_{i_1';i_1;\alpha}(z_1';z_1;z'')G_{i_1 i}(z_1,z), \tag{2.126}$$

which can be confirmed by differentiating the identity (2.117) with respect to the vector potential. The diagrammatic representation is shown in Fig. 2.4. Repeating the same argument for the noninteracting Green's function, we obtain an analogous equation for the bare part as

$$\frac{\delta G_{0i'i}(z',z)}{\delta A_\alpha(z'')} = \int_C dz_1 dz_1' G_{0i'i_1'}(z',z_1')\gamma^{(2,1)}_{0i_1';i_1;\alpha}(z_1';z_1;z'')G_{0i_1 i}(z_1,z). \tag{2.127}$$

The equation can be diagrammatically interpreted that the functional derivative of the noninteracting propagator with respect to the gauge field A_α corresponds to the insertion of the bare vertex function. This interpretation is useful to determine the diagrams of the dressed vertex functions (2.123): They can be given by inserting a bare current vertex function at every internal noninteracting propagator of the self-energy.

2.4.2 Formal expression of current fluctuation

In this subsection, we derive formal expressions of the current and the current fluctuation in terms of the vertex functions. As was discussed in section 2.3.3, the expectation values of the transport quantities are obtained as the functional derivatives of the generating

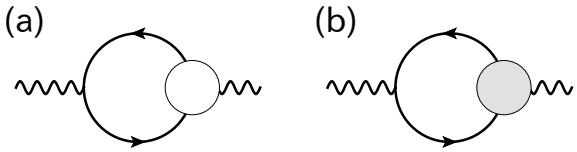

Fig. 2.5 Diagrammatic representation of (a) the bare part S_0 and (b) the vertex correction $\bar{S}$ of the current noise.

functional $W[\eta,\bar{\eta};A]$. The current is obtained as

$$\begin{aligned}\frac{\delta W[\eta,\bar{\eta};A]}{\delta A_\alpha(z)} &= -i\int_C dzdz' \frac{\delta G^{-1}_{0i'i}[A](z',z)}{\delta A_\alpha(z'')} G_{ii'}(z,z'),\\ &= i\int_C dzdz' \gamma^{(2,1)}_{0i';i;\alpha}(z';z;z'')G_{ii'}(z,z'). \end{aligned} \tag{2.128}$$

The higher-order transport quantities can be obtained by further functional differentiating the generating functional. With the aid of the four-point current vertex function (2.124) and the identity for the three-point connected Green's function (2.126), the current-current correlation function (2.106) is also divided into two parts as

$$D_{\alpha_1\alpha_2}(z_1'',z_2'') = D_{0\alpha_1\alpha_2}(z_1'',z_2'') + \bar{D}_{\alpha_1\alpha_2}(z_1'',z_2''), \tag{2.129}$$

with the bare term of the correlation function

$$\begin{aligned} D_{0\alpha_1\alpha_2}(z_1'',z_2'') \equiv &\int_C dz_1 dz_1' \gamma^{(2,2)}_{0i_1';i_1;\alpha_1\alpha_2}(z_1';z_1;z_1'',z_2'')G_{i_1i_1'}(z_1,z_1')\\ &+\int_C dz_1dz_1'dz_2dz_2'\gamma^{(2,1)}_{0i_1';i_1;\alpha_1}(z_1';z_1;z_1'')G_{i_1i_2'}(z_1,z_2')\\ &\times\gamma^{(2,1)}_{0i_2';i_2;\alpha_2}(z_2';z_2;z_2'')G_{i_2i_1'}(z_2,z_1'), \end{aligned} \tag{2.130}$$

and the vertex correction term

$$\begin{aligned} \bar{D}_{\alpha_1\alpha_2}(z_1'',z_2'') \equiv &\int_C dz_1dz_1'dz_2dz_2'\gamma^{(2,1)}_{0i_1';i_1;\alpha_1}(z_1';z_1;z_1'')G_{i_1i_2'}(z_1,z_2')\\ &\times\bar{\gamma}^{(2,1)}_{i_2';i_2;\alpha_2}(z_2';z_2;z_2'')G_{i_2i_1'}(z_2,z_1'). \end{aligned} \tag{2.131}$$

The same formulas have been obtained by G. H. Ding and B. Dong [19] using the full counting statistics. The symmetrized current noise (2.108) is divided into the bare part and the vertex correction as

$$S_{\alpha\alpha'}(t,t') = S_{0\alpha\alpha'}(t,t') + \bar{S}_{\alpha\alpha'}(t,t'), \tag{2.132}$$

$$S_{0\alpha\alpha'}(t,t') \equiv D^{-+}_{0\alpha\alpha'}(t,t') + D^{+-}_{0\alpha\alpha'}(t,t'), \tag{2.133}$$

$$\bar{S}_{\alpha\alpha'}(t,t') \equiv \bar{D}^{-+}_{\alpha\alpha'}(t,t') + \bar{D}^{+-}_{\alpha\alpha'}(t,t'). \tag{2.134}$$

The diagrammatic representation is shown in Fig. 2.5.

2.4.3 Application to interacting quantum dot systems

The noninteracting part of quantum dot system is often given by the resonant level model (2.100). The bare current vertex functions Eqs. (2.122) and (2.124) are calculated by differentiating the tunneling self-energy (2.101) as

$$\gamma_{0\alpha}^{(2,1)}(z';z;z'') = ie\left[\delta(z'',z) - \delta(z',z'')\right]\Sigma_\alpha(z',z), \tag{2.135}$$

$$\gamma_{0\alpha_1\alpha_2}^{(2,2)}(z';z;z_1'',z_2'') = (ie)^2\delta_{\alpha_1\alpha_2}\left[\delta(z_1'',z) - \delta(z',z_1'')\right]\left[\delta(z_2'',z) - \delta(z',z_2'')\right]\Sigma_\alpha(z',z). \tag{2.136}$$

These equations are used to express various quantities in terms of the Green's functions and the tunneling self-energy.

With the aid of Eq. (2.135), the formal expression of the current (2.128) leads to

$$\langle j_\alpha(z)\rangle = e\left[(\Sigma_\alpha G)(z,z) - (G\Sigma_\alpha)(z,z)\right], \tag{2.137}$$

where $(AB)(z,z') \equiv \int dz_1 A(z,z_1)B(z_1,z')$. By using Langreth's theorem [5], the above equation is projected onto the real-time axis as

$$\frac{1}{e}\langle j_\alpha(t)\rangle = \left(\Sigma_\alpha^r G^{-+}\right)(t,t) + \left(\Sigma_\alpha^{-+} G^a\right)(t,t) - \left(G^r\Sigma_\alpha^{-+}\right)(t,t) - \left(G^{-+}\Sigma_\alpha^a\right)(t,t), \tag{2.138}$$

where $(AB)(t,t') \equiv \int dt_1 A(t,t_1)B(t_1,t')$. Hence, the problem of calculating the current is reduced to the evaluation of the Green's functions in the QD. In the stationary system, the tunneling self-energy is given by Eqs. (2.79) and (2.80). Then, the expectation value of the current $\langle j\rangle = \langle j_R(t)\rangle = -\langle j_L(t)\rangle$ is simplified as

$$\langle j\rangle = e\int d\omega \frac{\Delta_L(\omega)\Delta_R(\omega)}{\Delta_L(\omega)+\Delta_R(\omega)} A(\omega)\left(f_L(\omega) - f_R(\omega)\right), \tag{2.139}$$

with the spectral function

$$A(\omega) \equiv -\frac{1}{\pi}\mathrm{Im}G^r(\omega). \tag{2.140}$$

Equation (2.139) is equivalent to the Meir-Wingreen formula [20].

The formal expressions of the current fluctuation [see Eqs. (2.130) and (2.131)] require rather laborious calculations. The important difference between the current and its fluctuation is the existence of the vertex correction term, which cannot be expressed solely in terms of the self-energy. We need to develop suitable schemes to determine the three-point dressed vertex function (2.123). One way is to straightforwardly evaluate the diagrams in the perturbation theory. Another promising way is to utilize the functional renormalization group, which is discussed in subsection 2.4.4.

2.4.4 Functional renormalization group approach

We develop a functional renormalization group (FRG) method [13, 21–23] for the nonequilibrium transport of correlated fermions. The FRG is an implementation of Wilson's idea of the renormalization group, where the high-energy degrees of freedom are successively

incorporated to reach the emerging low-energy physics. While deep philosophy of the renormalization group theory is inherited in the FRG scheme, it is also useful to invent efficient approximation schemes. This method has contributed to deepen our understanding of the nonequilibrium transport through interacting quantum dot systems [24–27].

In setting up the FRG scheme, we have to (i) introduce a flow parameter Λ and a regulator function R_Λ, (ii) derive flow equations for a Λ-dependent effective action Γ_Λ, (iii) use an appropriate initial condition of Γ_Λ at $\Lambda_{\rm init}$, (iv) truncate the flow equations into a finite set of ordinary differential equations, and (v) numerically or analytically solve the equations. We outline the procedure in the following.

Regulator function

The first step in the FRG approach is to introduce a regulator function R_Λ, which suppresses the low-energy degrees of freedom. The parameter Λ is called the flow parameter. In the following, we choose the regulator function by replacing the unperturbed propagator G_0^{-1} with a Λ-dependent propagator $G_{0\Lambda}^{-1} \equiv G_0^{-1} + R_\Lambda$. This is equivalent to introduce the additional action

$$\Delta S_\Lambda[\bar\psi,\psi] \equiv \int_C dz dz' \bar\psi_i(z) R_{\Lambda ij}(z,z') \psi_j(z'). \tag{2.141}$$

In contrast to the usual renormalization group procedure where the original action S is described by a set of parameters at different scales Λ, the model itself is modified as $S+\Delta S_\Lambda$ in the FRG approach. In order to recover the original problem in the limit $\Lambda \to 0$, the regulator function R_Λ must be chosen to satisfy the condition $R_{\Lambda\to 0} = 0$

We define the Λ-dependent generating functional

$$W_\Lambda[\eta,\bar\eta;A] = -i \ln \int \mathcal{D}\bar\psi \mathcal{D}\psi \exp\left(\frac{i}{\hbar}(S[\bar\psi,\psi] + \Delta S_\Lambda[\bar\psi,\psi] + S^s[\bar\psi,\psi;\eta,\bar\eta])\right), \tag{2.142}$$

and the Λ-dependent effective action

$$\begin{aligned}&\Gamma_\Lambda[\langle\bar\psi\rangle^s, \langle\psi\rangle^s; A] \\ &\equiv W_\Lambda[\eta_\Lambda,\bar\eta_\Lambda;A] - \int_C dz\, [\bar\eta_{\Lambda i}(z)\langle\psi_i(z)\rangle^s + \langle\bar\psi_i(z)\rangle^s \eta_{\Lambda i}(z)] - \Delta S_\Lambda[\langle\bar\psi\rangle^s, \langle\psi\rangle^s].\end{aligned} \tag{2.143}$$

Here, $\bar\eta_{\Lambda i}$ and $\eta_{\Lambda i}$ are determined by solving the following equations

$$\frac{\delta\Gamma_\Lambda[\langle\bar\psi\rangle^s, \langle\psi\rangle^s; A]}{\delta\langle\psi_i(z)\rangle^s} = \bar\eta_{\Lambda i}(z) + \langle\bar\psi_{i'}\rangle^s R_{\Lambda i' i}, \tag{2.144}$$

$$\frac{\delta\Gamma_\Lambda[\langle\bar\psi\rangle^s, \langle\psi\rangle^s; A]}{\delta\langle\bar\psi_i(z)\rangle^s} = -\eta_{\Lambda i}(z) - R_{\Lambda i i'}\langle\psi_{i'}\rangle^s. \tag{2.145}$$

Flow equation

The Λ-dependent effective action satisfies the equation

$$\frac{d\Gamma_\Lambda[\langle\bar{\psi}\rangle^s,\langle\psi\rangle^s;A]}{d\Lambda} = -i\int_C dz dz' \frac{dR_{\Lambda ii'}(z,z')}{dk}\frac{\delta^2 W_\Lambda[\eta_\Lambda,\bar{\eta}_\Lambda;A]}{\delta\bar{\eta}_{\Lambda i'}(z')\delta\eta_{\Lambda i}(z)}, \tag{2.146}$$

whose derivation is given in Appendix 2.B. In the following, we simplify Eq. (2.146) by introducing auxiliary matrices for the Λ-dependent Green's function

$$\boldsymbol{G}^{(2)}_{\Lambda ii'}[\eta_\Lambda,\bar{\eta}_\Lambda;A](z,z') \equiv \begin{pmatrix} \dfrac{\delta^2 W_\Lambda[\eta_\Lambda,\bar{\eta}_\Lambda;A]}{\delta\bar{\eta}_{\Lambda i}(z)\delta\eta_{\Lambda i'}(z')} & -\dfrac{\delta^2 W_\Lambda[\eta_\Lambda,\bar{\eta}_\Lambda;A]}{\delta\bar{\eta}_{\Lambda i}(z)\delta\bar{\eta}_{\Lambda i'}(z')} \\ -\dfrac{\delta^2 W_\Lambda[\eta_\Lambda,\bar{\eta}_\Lambda;A]}{\delta\eta_{\Lambda i}(z)\delta\eta_{\Lambda i'}(z')} & \dfrac{\delta^2 W_\Lambda[\eta_\Lambda,\bar{\eta}_\Lambda;A]}{\delta\eta_{\Lambda i}(z)\delta\bar{\eta}_{\Lambda i'}(z')} \end{pmatrix}, \tag{2.147}$$

and for the regulator function

$$\boldsymbol{R}_{\Lambda ii'}(z,z') \equiv \begin{pmatrix} R_{\Lambda ii'}(z,z') & 0 \\ 0 & -R_{\Lambda i'i}(z',z) \end{pmatrix}. \tag{2.148}$$

We note that the off-diagonal components of the Green's function can be finite in the presence of the source fields η and $\bar{\eta}$. With the auxiliary matrices, Eq. (2.146) is written as

$$\frac{d\Gamma_\Lambda[\langle\bar{\psi}\rangle^s,\langle\psi\rangle^s;A]}{d\Lambda} = \frac{-i}{2}\mathrm{Tr}\left(\frac{d\boldsymbol{R}_\Lambda}{dk}\boldsymbol{G}^{(2)}_\Lambda[\eta_\Lambda,\bar{\eta}_\Lambda;A]\right), \tag{2.149}$$

where the trace involves integration over all the internal indices. The auxiliary vertex function

$$\boldsymbol{\Gamma}^{(2)}_{\Lambda ii'}[\langle\bar{\psi}\rangle^s,\langle\psi\rangle^s;A](z,z') \equiv \begin{pmatrix} \dfrac{\delta^2\Gamma_\Lambda[\langle\bar{\psi}\rangle^s,\langle\psi\rangle^s;A]}{\delta\langle\bar{\psi}_i\rangle^s(z)\delta\langle\psi_{i'}\rangle^s(z')} & -\dfrac{\delta^2\Gamma_\Lambda[\langle\bar{\psi}\rangle^s,\langle\psi\rangle^s;A]}{\delta\langle\bar{\psi}_i\rangle^s(z)\delta\langle\bar{\psi}_{i'}\rangle^s(z')} \\ -\dfrac{\delta^2\Gamma_\Lambda[\langle\bar{\psi}\rangle^s,\langle\psi\rangle^s;A]}{\delta\langle\psi_i\rangle^s(z)\delta\langle\bar{\psi}_{i'}\rangle^s(z')} & \dfrac{\delta^2\Gamma_\Lambda[\langle\bar{\psi}\rangle^s,\langle\psi\rangle^s;A]}{\delta\langle\psi_i\rangle^s(z)\delta\langle\bar{\psi}_{i'}\rangle^s(z')} \end{pmatrix} \tag{2.150}$$

can be proven to be related to the Λ-dependent Green's function as

$$\boldsymbol{G}^{(2)}_\Lambda[\eta_\Lambda,\bar{\eta}_\Lambda;A] = \left(\boldsymbol{\Gamma}^{(2)}_\Lambda[\langle\bar{\psi}\rangle^s,\langle\psi\rangle^s;A] + \boldsymbol{R}_\Lambda\right)^{-1}. \tag{2.151}$$

Using this relation in Eq. (2.149), we obtain the exact functional differential equation for the Λ-dependent effective action;

$$\frac{d\Gamma_\Lambda[\langle\bar{\psi}\rangle^s,\langle\psi\rangle^s;A]}{d\Lambda} = \frac{-i}{2}\mathrm{Tr}\left(\frac{d\boldsymbol{R}_\Lambda}{dk}\left(\boldsymbol{\Gamma}^{(2)}_\Lambda[\langle\bar{\psi}\rangle^s,\langle\psi\rangle^s;A] + \boldsymbol{R}_\Lambda\right)^{-1}\right), \tag{2.152}$$

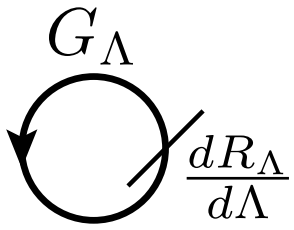

Fig. 2.6 Diagrammatic representation of the flow equation (2.152). The slash line represents the insertion of the derivative of the regulator function $\frac{d\boldsymbol{R}_\Lambda}{d\Lambda}$.

which is called the flow equation. This is the central tool of the FRG approach. Though it has a simple one-loop structure (Fig. 2.6), it describes the evolution of arbitrary vertex functions under the change of the flow parameter Λ.

Initial condition

The flow equation must be supplemented with an appropriate initial condition, which depends on the choice of the regulator function R_Λ. Usually, the regulator function at initial value $\Lambda_{\rm init}$ is chosen as $R_{\Lambda_{\rm init}} \to \infty$ for $\Lambda_{\rm init} \to \infty$ so that all the fluctuation can be suppressed at $\Lambda_{\rm init}$. As the lowest-order term of the effective action is the bare action, the initial condition of the effective action is given by $\Gamma_{\Lambda_{\rm init}} = S$. The Λ-dependent effective action (2.143) connects the classical action S with the effective action Γ. Although the trajectory is dependent on the detail of the regulator function R_Λ, it reaches the unique original effective action at the end of the flow ($\Lambda = 0$) irrespective of the choice of R_Λ.

Infinite hierarchy

One systematic way to analyze the flow equation (2.152) is to expand it in terms of the fields $\langle\bar{\psi}\rangle^s$ and $\langle\bar{\psi}\rangle^s$. In order to isolate the term depending on $\langle\bar{\psi}\rangle^s$ and $\langle\psi\rangle^s$, we define the self-energy and the Green's function as

$$\tilde{\boldsymbol{\Sigma}}_\Lambda \equiv -\boldsymbol{\Gamma}^{(2)}_\Lambda + \boldsymbol{\Gamma}^{(2)}_\Lambda\Big|_{\langle\bar{\psi}\rangle^s=\langle\psi\rangle^s=0} \tag{2.153}$$

$$\boldsymbol{G}^{-1}_\Lambda = \boldsymbol{\Gamma}^{(2)}_\Lambda\Big|_{\langle\bar{\psi}\rangle^s=\langle\psi\rangle^s=0} + \boldsymbol{R}_\Lambda. \tag{2.154}$$

Then, the flow equation becomes

$$\begin{aligned}
\frac{d\Gamma_\Lambda}{d\Lambda} &= \frac{-i}{2}\mathrm{Tr}\left(\frac{d\boldsymbol{R}_\Lambda}{dk}\left(\boldsymbol{G}^{-1}_\Lambda - \tilde{\boldsymbol{\Sigma}}_\Lambda\right)^{-1}\right) \\
&= \frac{-i}{2}\mathrm{Tr}\left(\frac{d\boldsymbol{R}_\Lambda}{dk}\boldsymbol{G}_\Lambda + \frac{d\boldsymbol{R}_\Lambda}{dk}\boldsymbol{G}_\Lambda\tilde{\boldsymbol{\Sigma}}_\Lambda\boldsymbol{G}_\Lambda + \frac{d\boldsymbol{R}_\Lambda}{dk}\boldsymbol{G}_\Lambda\tilde{\boldsymbol{\Sigma}}_\Lambda\boldsymbol{G}_\Lambda\tilde{\boldsymbol{\Sigma}}_\Lambda\boldsymbol{G}_\Lambda\right) + \cdots \\
&= \frac{i}{2}\mathrm{Tr}\left(\boldsymbol{G}^{-1}_\Lambda\boldsymbol{S}_\Lambda + \boldsymbol{S}_\Lambda\tilde{\boldsymbol{\Sigma}}_\Lambda + \boldsymbol{S}_\Lambda\tilde{\boldsymbol{\Sigma}}_\Lambda\boldsymbol{G}_\Lambda\tilde{\boldsymbol{\Sigma}}_\Lambda\right) + \cdots,
\end{aligned} \tag{2.155}$$

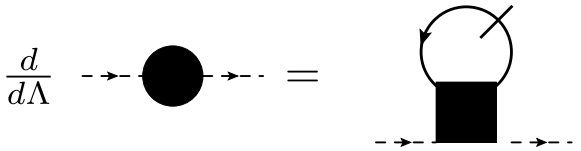

Fig. 2.7 Diagrammatic representation of the flow equation of the self-energy (2.157). The black filled circle (square) with two (four) fermion lines is the self-energy (four-point vertex function. The slashed inner propagator represents the scale-dependent propagator $\boldsymbol{S}_\Lambda$ defined in Eq. (2.156).

with the scale-dependent propagator

$$\boldsymbol{S}_\Lambda = -\boldsymbol{G}_\Lambda \frac{d\boldsymbol{R}_\Lambda}{dk} \boldsymbol{G}_\Lambda. \tag{2.156}$$

If we expand the flow equation (2.155) in terms of $\langle\bar{\psi}\rangle^s$ and $\langle\psi\rangle^s$, each term of the expansion is expressed in terms of the vertex functions with the aid of the vertex expansion (2.120). By comparing the coefficients of the corresponding terms in the left and right hand side of Eq. (2.155), we obtain the flow equation of the vertex functions.

The flow equation of the two-point vertex function, which is related to the self-energy (2.119), is

$$\frac{d\gamma_\Lambda^{(2,0)}(z_1';z_1;)}{d\Lambda} = i\mathrm{Tr}\left(\boldsymbol{S}_\Lambda \gamma_\Lambda^{(4,0)}(\cdot,z_1';\cdot,z_1;)\right). \tag{2.157}$$

The diagrammatic representation of the flow equation is given in Fig. 2.7. It is found that we need to determine the four-point vertex function $\gamma_\Lambda^{(4,0)}$, whose flow equation is obtained as

$$\begin{aligned}
&\frac{d\gamma_\Lambda^{(4,0)}(z_1',z_2',z_1,z_2;)}{d\Lambda} \\
&= i\mathrm{Tr}\Big(\boldsymbol{S}_\Lambda \gamma_\Lambda^{(4,0)}(\cdot,z_1';\cdot,z_1;)\boldsymbol{G}_\Lambda \gamma_\Lambda^{(4,0)}(\cdot,z_2';\cdot,z_2;) + \boldsymbol{G}_\Lambda \gamma_\Lambda^{(4,0)}(\cdot,z_1';\cdot,z_1;)\boldsymbol{S}_\Lambda \gamma_\Lambda^{(4,0)}(\cdot,z_2';\cdot,z_2;) \\
&\quad - \boldsymbol{S}_\Lambda \gamma_\Lambda^{(4,0)}(\cdot,z_1';\cdot,z_2;)\boldsymbol{G}_\Lambda \gamma_\Lambda^{(4,0)}(\cdot,z_2';\cdot,z_1;) - \boldsymbol{G}_\Lambda \gamma_\Lambda^{(4,0)}(\cdot,z_1';\cdot,z_2;)\boldsymbol{S}_\Lambda \gamma_\Lambda^{(4,0)}(\cdot,z_2';\cdot,z_1;) \\
&\quad + \boldsymbol{S}_\Lambda \gamma_\Lambda^{(4,0)}(\cdot,\cdot;z_1,z_2;)\boldsymbol{G}_\Lambda^{\mathrm{t}} \gamma_\Lambda^{(4,0)}(z_1',z_2';\cdot,\cdot;) + \boldsymbol{S}_\Lambda \gamma_\Lambda^{(6,0)}(\cdot,z_1',z_2';\cdot,z_1,z_2;)\Big).
\end{aligned} \tag{2.158}$$

Then, we need to determine the six-point vertex functions to solve the flow equation. This procedure is endless, forming an infinite hierarchy of the flow equations.

We need to calculate the three-point current vertex function $\gamma_\Lambda^{(2,1)}$ to determine the vertex correction of the current noise (2.131). The flow equation of the current vertex

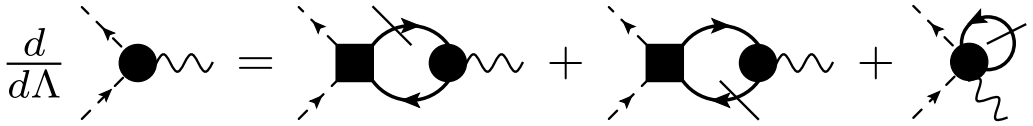

Fig. 2.8 Diagrammatic representation of the flow equation of the three-point vertex function (2.159). The black filled circle with the four fermion lines and one wavy line represents the five-point current vertex function.

functions are obtained in the same way as the self-energy as

$$\begin{aligned}\frac{d\gamma_\Lambda^{(2,1)}(z';z;z'')}{d\Lambda} = i\mathrm{Tr}\Big(&\boldsymbol{S}_\Lambda\gamma_\Lambda^{(4,0)}(\cdot,z';\cdot,z;)\boldsymbol{G}_\Lambda\gamma_\Lambda^{(2,1)}(\cdot;\cdot;z'')\\ &+\boldsymbol{G}_\Lambda\gamma_\Lambda^{(4,0)}(\cdot,z';\cdot,z;)\boldsymbol{S}_\Lambda\gamma_\Lambda^{(2,1)}(\cdot;\cdot;z'')\\ &+\boldsymbol{S}_\Lambda\gamma_\Lambda^{(4,1)}(\cdot,z';\cdot,z;z'')\Big),\end{aligned} \tag{2.159}$$

whose diagrammatic representation is shown in Fig. 2.8.

The flow equations of $\gamma_{\Lambda\alpha}^{(0,1)}(;z'')$ and $\gamma_\Lambda^{(0,2)}(;z_1'',z_2'')$ are obtained, respectively, as

$$\frac{d\gamma_\Lambda^{(0,1)}(;z'')}{d\Lambda} = i\mathrm{Tr}\Big(\boldsymbol{S}_\Lambda\gamma_\Lambda^{(2,1)}(\cdot;\cdot;z'')\Big), \tag{2.160}$$

$$\begin{aligned}\frac{d\gamma_\Lambda^{(0,2)}(;z_1'',z_2'')}{d\Lambda} = i\mathrm{Tr}\Big(&\boldsymbol{S}_\Lambda\gamma_\Lambda^{(2,1)}(\cdot;\cdot;z_1'')\boldsymbol{G}_\Lambda\gamma_\Lambda^{(2,1)}(\cdot;\cdot;z_2'')+\boldsymbol{G}_\Lambda\gamma_\Lambda^{(2,1)}(\cdot;\cdot;z_1'')\boldsymbol{S}_\Lambda\gamma_\Lambda^{(2,1)}(\cdot;\cdot;z_2'')\\ &+\boldsymbol{S}_\Lambda(\cdot,\cdot)\gamma_\Lambda^{(2,2)}(\cdot;\cdot;z_1'',z_2'')\Big).\end{aligned} \tag{2.161}$$

Noting that the first (second) derivative of the effective action in terms of the gauge field is directly related to the current (noise), Eq. (2.160) (Eq. (2.161)) provides a way to determine the transport quantities within the FRG scheme.

Truncation

In spite of its appealingly simple structure, the flow equation of the effective action (2.152) cannot be solved exactly due to the infinite hierarchy of the flow equations of the vertex functions. Hence, we have to devise an approximation scheme to handle the problem. The simplest way is to truncate the hierarchy by neglecting the higher-order vertices. In chapter 5, we use the lowest-order approximation to determine the vertex functions.

Appendix 2.A Gauge transformation

Let χ_α and χ_d be arbitary functions whose supports are the lead α and the QD, respectively. Then, the gauge transformation on the Keldysh contour is expressed as

$$\begin{aligned} c'_{\alpha\boldsymbol{k}}(z) &= c_{\alpha\boldsymbol{k}}(z)e^{ie\chi_\alpha(z)}, \\ \bar{c}'_{\alpha\boldsymbol{k}}(z) &= \bar{c}_{\alpha\boldsymbol{k}}(z)e^{-ie\chi_\alpha(z)}, \\ d'(z) &= d(z)e^{ie\chi_d(z)}, \\ \bar{d}'(z) &= \bar{d}(z)e^{-ie\chi_d(z)}, \end{aligned} \tag{2.162}$$

and

$$v'_\alpha(z) = v_\alpha(z) - \partial_z\chi_\alpha(z), \tag{2.163}$$
$$A'_0(z) = A_0(z) - \partial_z\chi_d(z), \tag{2.164}$$
$$A'_\alpha(z) = A_\alpha(z) + (\chi_\alpha(z) - \chi_d(z)). \tag{2.165}$$

The gauge invariance of the tunneling part of the action (2.100) is confirmed by calculation such as

$$\begin{aligned} e^{ieA'_\alpha}\bar{c}'_{\alpha\boldsymbol{k}}d' &= e^{ie(A_\alpha+\chi_\alpha-\chi_d)}e^{-ie\chi_\alpha}\bar{c}_{\alpha\boldsymbol{k}}e^{ie\chi_d}d \\ &= e^{ieA_\alpha}\bar{c}_{\alpha\boldsymbol{k}}d. \end{aligned} \tag{2.166}$$

Appendix 2.B Derivation of the flow equation (2.146)

In this appendix, we derive the flow equation of the Λ-dependent effective action Γ_Λ. Straightforwardly differentiating the definition (2.143) of Γ_Λ with respect to Λ, we obtain

$$\begin{aligned} \frac{d}{d\Lambda}\Gamma_\Lambda[\langle\bar{\psi}\rangle^s, \langle\psi\rangle^s; A] = \frac{d}{d\Lambda}W_\Lambda[\eta_\Lambda, \bar{\eta}_\Lambda; A] - \frac{d}{d\Lambda}\Delta S_\Lambda[\langle\bar{\psi}\rangle^s, \langle\psi\rangle^s] \\ - \int_C dz \left[\frac{d\bar{\eta}_{\Lambda i}(z)}{d\Lambda}\langle\psi_i(z)\rangle^s + \langle\bar{\psi}_i(z)\rangle^s\frac{d\eta_{\Lambda i}(z)}{d\Lambda}\right]. \end{aligned} \tag{2.167}$$

By noting that the source fields $\eta_{\Lambda i}$ and $\bar{\eta}_{\Lambda i}$ are dependent on Λ, the derivative of the generating functional W_Λ with respect to Λ leads to the equation

$$\begin{aligned} &\frac{d}{d\Lambda}W_\Lambda[\eta_\Lambda, \bar{\eta}_\Lambda; A] - \left.\frac{d}{d\Lambda}\right|_{\eta_\Lambda, \bar{\eta}_\Lambda} W_\Lambda[\eta_\Lambda, \bar{\eta}_\Lambda; A] \\ &= \int_C dz \left[\frac{d\bar{\eta}_{\Lambda i}(z)}{d\Lambda}\frac{\delta W_\Lambda[\eta_\Lambda, \bar{\eta}_\Lambda; A]}{\delta\bar{\eta}_{\Lambda i}(z)} + \frac{\delta W_\Lambda[\eta_\Lambda, \bar{\eta}_\Lambda; A]}{\delta\eta_{\Lambda i}(z)}\frac{d\eta_{\Lambda i}(z)}{d\Lambda}\right] \\ &= \int_C dz \left[\frac{d\bar{\eta}_{\Lambda i}(z)}{d\Lambda}\langle\psi_i(z)\rangle^s + \langle\bar{\psi}_i(z)\rangle^s\frac{d\eta_{\Lambda i}(z)}{d\Lambda}\right]. \end{aligned} \tag{2.168}$$

Hence, the right-hand side of this equation are canceled with the last two terms in Eq. (2.167). Keeping the source fields $\eta_{\Lambda i}$ and $\bar{\eta}_{\Lambda i}$ fixed, the second term of the left-

hand side of the above equation is

$$\begin{aligned}
&\frac{d}{d\Lambda}\bigg|_{\eta_\Lambda,\bar{\eta}_\Lambda} W_\Lambda[\eta_\Lambda,\bar{\eta}_\Lambda;A] \\
&= \frac{1}{Z_\Lambda}\int \mathcal{D}\bar{\psi}\mathcal{D}\psi\, \frac{1}{\hbar}\frac{d}{d\Lambda}\Delta S_\Lambda[\bar{\psi},\psi]\exp\left(\frac{i}{\hbar}(S[\bar{\psi},\psi;A]+\Delta S_\Lambda[\bar{\psi},\psi]+S^s[\bar{\psi},\psi;\eta,\bar{\eta}])\right), \\
&= \frac{1}{\hbar}\int_C dz dz' \frac{d}{d\Lambda}R_{\Lambda ij}(z,z')\langle\bar{\psi}_i(z)\psi_j(z')\rangle \\
&= -i\int_C dz dz' \frac{dR_{\Lambda ii'}(z,z')}{dk}\frac{\delta^2 W_\Lambda[\eta_\Lambda,\bar{\eta}_\Lambda;A]}{\delta\bar{\eta}_{\Lambda i'}(z')\delta\eta_{\Lambda i}(z)}.
\end{aligned} \tag{2.169}$$

Collecting Eqs. (2.167), (2.168), and (2.169), we can prove the flow equation (2.146).

References

[1] J. Schwinger, J. Math. Phys. **2**, 407 (1961).

[2] L. V. Keldysh, Sov. Phys. JETP **20**, 1018 (1965).

[3] L. P. Kadanoff and G. A. Baym, *Quantum statistical mechanics* (Benjamin, 1962).

[4] K. Chou, Z. Su, B. Hao, and L. Yu, Phys. Rep. **118**, 1 (1985).

[5] H. Haug and A.-P. Jauho, *Quantum kinetics in transport and optics of semiconductors* (Springer, 2008).

[6] A. Kamenev, *Field theory of non-equilibrium systems* (Cambridge University Press Cambridge, 2011).

[7] M. E. Peskin and D. V. Schroeder, *An Introduction to Quantum Field Theory* (Perseus Books, Cambridge, Massachusetts, 1995).

[8] A. L. Fetter and J. D. Walecka, *Quantum theory of many-particle systems* (Courier Corporation, 2003).

[9] M. Gell-Mann and F. Low, Phys. Rev. **84**, 350 (1951).

[10] Y. V. Nazarov, Ann. Phys. (Leipzig) **8**, SI193 (1999).

[11] Y. Nazarov, Ann. Phys. (Leipzig) **16**, 720 (2007).

[12] P. C. Martin, E. D. Siggia, and H. A. Rose, Phys. Rev. A **8**, 423 (1973).

[13] W. Metzner, M. Salmhofer, C. Honerkamp, V. Meden, and K. Schönhammer, Rev. Mod. Phys. **84**, 299 (2012).

[14] L. Levitov and G. Lesovik, JETP Lett. **58**, 230 (1993).

[15] L. S. Levitov, H. Lee, and G. B. Lesovik, J. Math. Phys. **37**, 4845 (1996).

[16] B. A. Muzykantskii and Y. Adamov, Phys. Rev. B **68**, 155304 (2003).

[17] A. O. Gogolin and A. Komnik, Phys. Rev. B **73**, 195301 (2006).

[18] S. T. Carr, D. A. Bagrets, and P. Schmitteckert, Phys. Rev. Lett. **107**, 206801 (2011).

[19] G. H. Ding and B. Dong, Phys. Rev. B **87**, 235303 (2013).

[20] Y. Meir and N. S. Wingreen, Phys. Rev. Lett. **68**, 2512 (1992).

[21] J. Berges, N. Tetradis, and C. Wetterich, Physics Reports **363**, 223 (2002), renormalization group theory in the new millennium. {IV}.

[22] H. Gies, Lect. Notes Phys. **852**, 287 (2012).

[23] P. Kopietz, L. Bartosch, and F. Schütz, *Introduction to the functional renormalization group*, Vol. 798 (Springer, 2010).

[24] C. Karrasch, S. Andergassen, M. Pletyukhov, D. Schuricht, L. Borda, V. Meden, and H. Schoeller, Europhys. Lett. **90**, 30003 (2010).

[25] C. Karrasch, M. Pletyukhov, L. Borda, and V. Meden, Phys. Rev. B **81**, 125122 (2010).

[26] S. G. Jakobs, M. Pletyukhov, and H. Schoeller, Phys. Rev. B **81**, 195109 (2010).

[27] S. G. Jakobs, M. Pletyukhov, and H. Schoeller, J. Phys. A: Math. Theor. **43**, 103001 (2010).

Chapter 3

Particle coupled to environments

In mesoscopic systems, we frequently encounter a situation where a few degrees of freedom are considered to be coupled to one or more environments. The degrees of freedom are not only microscopic coordinates, such as the positions of particles, but also macroscopic variables, such as the flux through a simple LC circuit [1]. The environment causes dissipation and fluctuation of the "particles", invoking stochastic description of the dynamics. Microscopic description of the damped harmonic oscillator is given by the Caldeira-Leggett model [2]. In the path integral approach, the dissipative equation of motion is recovered as the optimal path of the action, and the fluctuation is systematically incorporated around the path. Remarkably, the path integral approach can even describe non-Gaussian stochastic processes [3].

A particle coupled to an environment is often viewed from a reversed perspective: The characteristic nature of a specific environment is probed by introducing a tracer particle. The inverse problem to detect the full counting statistics through a mesoscopic conductor was put forward in Ref. [4] by using a detector LC circuit, whose variance was perturbatively evaluated to extract the information on the current noise. Later, quantum mechanical treatment of the detector circuit was discussed to consistently assess the current fluctuation in various setups [5–9].

The difficulty of detecting the current distribution originates from the fact that the non-Gaussianity is characterized by rare events with exponentially small probability. A physical intuition of the dominance of the Gaussian fluctuation can be substantiated by the theory of Van Kampen [10]. On the other hand, new insights on non-Gaussian noise in classical systems have been presented lately by Kanazawa *et al.* [11, 12]. They clarified that a non-Gaussian Langevin equation universally appears in a classical stochastic system which is composed of multiple environments. They have also derived an inverse formula to infer the statistics of the non-Gaussian noise from the tracer particle. These achievements are crucial in the context of detecting the full counting statistics.

In section 3.1, the Caldeira-Leggett model is introduced and its deterministic motion is derived using the optimal path approximation. In section 3.2, the classical fluctuation of the particle is systematically incorporated and analyzed based on stochastic methods. In section 3.3, the path integral representation of stochastic processes are derived by utilizing characteristic functionals. In section 3.4, the universality of non-Gaussian noise is discussed.

3.1 Caldeira-Leggett model

Let us consider damping motion of a particle of mass M moving in a potential U. The classical dynamics of the coordinate variable X is given by the damped equation of motion

$$M\ddot{X} + \gamma\dot{X} + \frac{\partial U(X)}{\partial X} = 0, \tag{3.1}$$

with the friction coefficient γ. The coordinate X in the damped equation of motion (3.1) can represent not only the position of a point particle but also a collective motion of macroscopic numbers of small constituents. For example, it is known that the magnetic flux Φ threading a superconducting interference device (SQUID) is phenomenologically described by the same equation with the replacement $X \to \Phi$, $U(X) \to U(\Phi)$, $M \to C$, and $\gamma \to 1/R$ [1]. Here, C and R represent the capacitance and the resistance, respectively. This is a typical example of macroscopic quantum phenomena; collective behavior of macroscopic numbers of coherent quantum particles. If we consider the harmonic potential $U(\Phi) = \Phi^2/2L$ with the inductance L, Eq. (3.1) is equivalent to the circuit equation for the RLC circuit.

What kind of quantum dissipative dynamics is expected in a system whose classical dynamics obeys the damped equation of motion (3.1)? This question was featured by Caldeira and Leggett [2]. They ascribed the physical mechanism of the dissipation to a large external environment surrounding the system. The crucial assumption is that the equilibrium state of the environment is just weakly perturbed by the motion of the system. This allows the environment to be represented as a collection of infinitely large numbers of harmonic oscillators which are linearly coupled to the system. Moreover, if the classical dynamics is given by Eq. (3.1), the coupling between the system and the environment is assumed to be bilinear in the system and bath coordinates. Another important point is the introduction of the counter term, which compensates the frequency-dependent shift of the potential under a physical assumption that the coupling between the system and the environment should not modify the potential. Further considerations are given in the main text and Appendix C in the paper by Caldeira and Leggett [2].

Keldysh action of the Caldeira-Leggett model

The action of the Caldeira-Leggett model on the Keldysh contour is given by

$$S_{\rm CL}[X;\{x_\alpha\}] = S_{\rm sys}[X;\{x_\alpha\}] + S_{\rm env}[\{x_\alpha\}] + S_{\rm int}[X;\{x_\alpha\}], \tag{3.2}$$

$$S_{\rm sys}[X] = \int_C dz \left[\frac{1}{2}M\left(\frac{\partial X(z)}{\partial z}\right)^2 - U(X(z))\right], \tag{3.3}$$

$$S_{\rm env}[\{x_\alpha\}] = \frac{1}{2}\sum_\alpha \int_C dz \left[m_\alpha\left(\frac{\partial x_\alpha(z)}{\partial z}\right)^2 - m_\alpha\omega_\alpha^2 x_\alpha^2(z)\right], \tag{3.4}$$

$$S_{\rm int}[X;\{x_\alpha\}] = \sum_\alpha \int_C dz \left[c_\alpha x_\alpha(z)X(z) - \frac{c_\alpha^2}{2m_\alpha\omega_\alpha^2}X^2(z)\right]. \tag{3.5}$$

The set of the coordinates $\{x_\alpha\}$ describes the harmonic oscillator composing the external environment with the parameters m_α and ω_α. The coupling constant between the system

and the environment is denoted by c_α. As is discussed later, these auxiliary parameters can uniquely specify the phenomenologically given dissipation term. The partition function of the Caldeira-Leggett model is given by

$$Z_{\mathrm{CL}} = \int \mathcal{D}X\mathcal{D}x_\alpha \exp\left[\frac{i}{\hbar}S_{CL}[X;\{x_\alpha\}]\right]. \tag{3.6}$$

The Green's functions of the bath oscillators defined on the Keldysh contour C are calculated in the same way as the fermionic case;

$$\begin{pmatrix} g_\alpha^{\tilde{\mathrm{K}}}(\omega) & g_\alpha^{\mathrm{a}}(\omega) \\ g_\alpha^{\mathrm{r}}(\omega) & g_\alpha^{\mathrm{K}}(\omega) \end{pmatrix} = \begin{pmatrix} 0 & \dfrac{1}{m_\alpha(\omega^2-\omega_\alpha^2-i\omega 0^+)} \\ \dfrac{1}{m_\alpha(\omega^2-\omega_\alpha^2+i\omega 0^+)} & \dfrac{-2\pi i\coth(\beta\hbar\omega/2)}{m_\alpha^2\left(\omega^2-\omega_\alpha^2\right)^2} \end{pmatrix}, \tag{3.7}$$

with the inverse temperature β. As the action is quadratic in the bath oscillators x_α, the degrees of freedom in the environment can be exactly traced out, resulting in the self-energy

$$\begin{pmatrix} \Sigma_{\mathrm{env}}^{\tilde{\mathrm{K}}}(\omega) & \Sigma_{\mathrm{env}}^{\mathrm{a}}(\omega) \\ \Sigma_{\mathrm{env}}^{\mathrm{r}}(\omega) & \Sigma_{\mathrm{env}}^{\mathrm{K}}(\omega) \end{pmatrix} = \begin{pmatrix} 0 & -iJ(\omega) \\ iJ(\omega) & -2iJ(\omega)\coth(\beta\hbar\omega/2)) \end{pmatrix}, \tag{3.8}$$

with the spectral function

$$J(\omega) \equiv \frac{\pi}{2}\sum_\alpha \frac{c_\alpha^2}{m_\alpha\omega_\alpha}\delta(\omega-\omega_\alpha). \tag{3.9}$$

Here, we made an important assumption that the spectrum of the environmental harmonic oscillators is dense enough to be considered continuous. The auxiliary parameters introduced to describe the external environment, i.e. m_α, ω_α, and c_α, are included in the spectral function $J(\omega)$. Hence, these parameters can describe the spectral function phenomenologically specified in accordance with the system of interest. We also stress that the Keldysh component of the self-energy results from the assumption that the environment is equilibrium at inverse temperature β. This is known as the fluctuation-dissipation relation.

The action obtained after tracing out the environmental degrees of freedom is

$$\begin{aligned} S_{\mathrm{CL}}[X^{\mathrm{p}},X^{\mathrm{s}}] = \int dt \left(-MX^{\mathrm{s}}(t)\frac{\partial^2 X^{\mathrm{p}}(t)}{\partial t^2} - U^-[X^{\mathrm{p}},X^{\mathrm{s}}] + U^+[X^{\mathrm{p}},X^{\mathrm{s}}]\right) \\ -\frac{1}{2}\int dtdt' \left[X^{\mathrm{s}}(t)\Sigma_{\mathrm{env}}^{\mathrm{r}}(t,t')X^{\mathrm{p}}(t') + X^{\mathrm{p}}(t)\Sigma_{\mathrm{env}}^{\mathrm{a}}(t,t')X^{\mathrm{s}}(t') \right. \\ \left. + X^{\mathrm{s}}(t)\Sigma_{\mathrm{env}}^{\mathrm{K}}(t,t')X^{\mathrm{s}}(t')\right], \end{aligned} \tag{3.10}$$

where the physical and source components of the bosonic field are denoted by $X^{\mathrm{p}} \equiv (X^- + X^+)/2$ and $X^{\mathrm{s}} \equiv X^- - X^+$, respectively. The external environment introduces (i) the friction terms $\Sigma_{\mathrm{env}}^{\mathrm{r}}$ and $\Sigma_{\mathrm{env}}^{\mathrm{a}}$ and (ii) the fluctuation $\Sigma_{\mathrm{env}}^{\mathrm{K}}$. If we expand the action up to the linear order in X^{s}, the functional integration over X^{s} leads to the functional Dirac delta

function requiring the equation

$$M\frac{\partial^2 X^{\rm p}(t)}{\partial t^2}+\frac{\partial U[X^{\rm p}]}{\partial X^{\rm p}}+\frac{1}{2}\int dt'\left(\Sigma^{\rm r}_{\rm env}(t,t')X^{\rm p}(t')+X^{\rm p}(t')\Sigma^{\rm a}_{\rm env}(t',t)\right)=0. \tag{3.11}$$

This leads to the classical equation of motion with the friction force. The thermal and quantum fluctuation is systematically incorporated in the higher order terms in $X^{\rm q}$ as is discussed in section 3.2.

Ohmic coupling

As a simple but important case, we consider the Ohmic spectral function

$$J(\omega)=\gamma\omega, \tag{3.12}$$

which leads to the self-energy in the time representation:

$$\Sigma^{\rm r(a)}_{\rm env}(t,t')=\pm\gamma\delta(t,t')\frac{\partial}{\partial t'}, \tag{3.13}$$

$$\begin{aligned}\Sigma^{\rm K}_{\rm env}(t,t')=&-i\gamma\left(\frac{4}{\beta\hbar}+\frac{2\pi}{\beta^2\hbar^2}\int dt''\frac{1}{\sinh^2[\pi t''/\beta\hbar]}\right)\delta(t,t')\\&+\frac{2\pi i\gamma}{\beta^2\hbar^2}\frac{1}{\sinh^2[\pi(t-t')/\beta\hbar]}.\end{aligned} \tag{3.14}$$

The coefficient of the Dirac delta function of the Keldysh component is chosen to satisfy the condition

$$\int dt\Sigma^{\rm K}_{\rm env}(t)=\Sigma^{\rm K}_{\rm env}(\omega=0)=\frac{-4i\gamma}{\beta\hbar}. \tag{3.15}$$

With the aid of the retarded and the advanced self-energy (3.13), the action (3.10) becomes

$$\begin{aligned}S_{\rm CL}[X^{\rm p},X^{\rm s}]=&\int dt\left(-MX^{\rm s}(t)\frac{\partial^2 X^{\rm p}(t)}{\partial t^2}-\gamma X^{\rm s}(t)\frac{\partial X^{\rm p}(t)}{\partial t}-U^-[X^{\rm p},X^{\rm s}]+U^+[X^{\rm p},X^{\rm s}]\right)\\&+\frac{2i\gamma}{\beta\hbar}\int dt\left[(X^{\rm s}(t))^2+\frac{\pi}{4\beta\hbar}\int dt'\frac{(X^{\rm s}(t)-X^{\rm s}(t'))^2}{\sinh^2[\pi(t-t')/\beta\hbar]}\right],\end{aligned} \tag{3.16}$$

from which we recover the damped equation of motion (3.1) in the lowest order in $X^{\rm s}$. Hence, the Ohmic spectral function (3.12) produces the Ohmic dissipation within the optimal path approximation.

3.2 Classical fluctuation

In the previous section, we showed that the optimal path solution of the Caldeira-Leggett model (3.2) up to the lowest order in X^s leads to the classical damped equation of motion. The resulting equation disregards fluctuation originating from the environment. Thermal and quantum fluctuations, which are coded in the Keldysh component (3.14), are sys-

tematically incorporated in the higher-order terms in $X^{\rm s}$. In this section, we consider the fluctuation which is present in the classical limit $\hbar \to 0$.

Partition function in the classical limit

In order to properly recover the thermal fluctuation in the classical limit, it is convenient to rescale the source component as $X^{\rm s} \to \hbar X^{\rm s}$. Noting the relation

$$\frac{\pi}{2\beta\hbar}\frac{1}{\sinh^2[\pi(t-t')/\beta\hbar]} \to \delta(t-t'), \tag{3.17}$$

in the classical limit ($\hbar \to 0$), we obtain the partition as

$$\begin{aligned} Z_{\rm CL} &= \int \mathcal{D}X^{\rm p}\mathcal{D}X^{\rm s} \exp\left[\int dt \left(-iX^{\rm s}(t)\left(\left[M\frac{\partial^2}{\partial t^2}+\gamma\frac{\partial}{\partial t}\right]X^{\rm p}(t)+U'[X^{\rm p}]\right)\right)\right] \\ &\qquad \times \exp\left[-\frac{2\gamma}{\beta}\int dt\,(X^{\rm s}(t))^2\right] \\ &= \int \mathcal{D}X^{\rm p}\mathcal{D}\eta_{\rm G}\delta\left(\left[M\frac{\partial^2}{\partial t^2}+\gamma\frac{\partial}{\partial t}\right]X^{\rm p}(t)+U'[X^{\rm p}]-\eta_{\rm G}(t)\right)\exp\left[\frac{-\beta}{8\gamma}\int dt\,\eta_{\rm G}^2(t)\right], \end{aligned} \tag{3.18}$$

where the Gaussian noise $\eta_{\rm G}$ is introduced in the second line by using the Hubbard-Stratonovich transformation

$$\exp[-X^{\rm s}vX^{\rm s}] = \int \mathcal{D}\eta_{\rm G}\exp\left[-\frac{1}{4}\eta_{\rm G}v^{-1}\eta_{\rm G}+iX^{\rm s}\eta_{\rm G}\right]. \tag{3.19}$$

Stochastic differential equation

The partition function (3.18) is equivalent to the Langevin equation

$$M\frac{\partial^2 X^{\rm p}(t)}{\partial t^2}+\gamma\frac{\partial X^{\rm p}(t)}{\partial t}+U'[X^{\rm p}] = \eta_{\rm G}(t), \tag{3.20}$$

$$\Leftrightarrow \frac{\partial}{\partial t}\begin{pmatrix} X^{\rm p}(t) \\ MV^{\rm p}(t)\end{pmatrix} = \begin{pmatrix} V^{\rm p}(t) \\ -\gamma V^{\rm p}(t)-U'[X^{\rm p}]\end{pmatrix}+\begin{pmatrix} 0 \\ \eta_{\rm G}(t)\end{pmatrix}, \tag{3.21}$$

$$\boldsymbol{E}\left[\eta_{\rm G}(t)\eta_{\rm G}(t')\right] = \frac{2\gamma}{\beta}\delta(t-t'). \tag{3.22}$$

The random force $\eta_{\rm G}$ is uncorrelated with itself at different time and is referred to as a white noise. Moreover, its amplitude is given by $2\gamma/\beta$ being consistent with the fluctuation dissipation relation; a consequence of the equilibrium nature of the environment. The random force $\eta_{\rm G}$ is called the Johnson–Nyquist noise in electronic circuits. The field-theoretic formulation of stochastic processes was first proposed by Martin, Siggia, and Rose [13], and later reformulated in terms of a more transparent Lagrangian method [14–16]. The relationship with another path integral formulation proposed by Onsager and

Machlup [17] may become clear if we obtain the action

$$S_{\rm CL}[X^{\rm p}] = \frac{i\beta}{8\gamma}\int dt\left(M\frac{\partial^2 X^{\rm p}(t)}{\partial t^2}+\gamma\frac{\partial X^{\rm p}(t)}{\partial t}+U'[X^{\rm p}]\right)^2, \tag{3.23}$$

by the functional integration with respect to $\eta_{\rm G}$ in Eq. (3.18).

Free particles and trapped particles

In order to clarify the relevance of Gaussian processes to physical systems, let us consider a classical particle in the absence of the potential U. The equations for the position and the velocity (3.20) become

$$\frac{\partial X^{\rm p}}{\partial t} = V^{\rm p}(t), \tag{3.24}$$

$$\frac{\partial V^{\rm p}}{\partial t} = -\frac{\gamma}{M}V^{\rm p}(t)+\frac{\gamma}{M}\frac{1}{\sqrt{\gamma\beta}}\xi(t), \tag{3.25}$$

with $\boldsymbol{E}[\xi(t)\xi(t')] = 2\delta(t-t')$. The equation for the velocity (3.25) is called the Ornstein-Uhlenbeck process with the time constant $\tau = M/\gamma$ and the noise intensity $D = 1/\gamma\beta$. The solution is given by

$$V^{\rm p}(t) = V^{\rm p}(0)e^{-t/\tau}+\frac{\sqrt{D}}{\tau}\int_0^t dt' e^{-(t-t')/\tau}\xi(t'). \tag{3.26}$$

If we focus on the time much later than the time constant ($t \gg \tau$), the initial value is irrelevant and the lower limit of integral can be extended;

$$V^{\rm p}(t) = \frac{\sqrt{D}}{\tau}\int_{-\infty}^t dt' e^{-(t-t')/\tau}\xi(t'). \tag{3.27}$$

Then, the stationary value of the velocity is zero ($\boldsymbol{E}[V^{\rm p}(t\gg\tau)] = 0$), while the correlation of the velocity is given by

$$\boldsymbol{E}\left[V^{\rm p}(t)V^{\rm p}(t')\right] = \frac{D}{2\tau}e^{-|t-t'|/\tau}, \tag{3.28}$$

which reduces to the white noise $D\delta(t-t')$ in the limit $\tau\to 0$. The technique of tracing out the variable which rapidly relaxes to its stationary value is called the adiabatic elimination. The resulting equation for the position describes the diffusive motion with variance growing proportional to the elapsed time t.

In the presence of the harmonic potential $U[X^{\rm p}] = k(X^{\rm p}-X_0)^2/2$, the stochastic differential equation for the velocity is modified as

$$M\frac{\partial V^{\rm p}}{\partial t} = -\gamma V^{\rm p}(t)-k(X^{\rm p}(t)-X_0)+\sqrt{\frac{\gamma}{\beta}}\xi(t). \tag{3.29}$$

Here, we assume that the friction coefficient γ is much larger than the characteristic energy scales governing the internal dynamics of the particle. In the overdamped regime, the

velocity reaches its stationary value instantaneously. Using the value in the equation of the position, we find it obeying the Ornstein-Uhlenbeck process

$$\frac{\partial X^{\mathrm{p}}}{\partial t} = -\frac{k}{\gamma}(X^{\mathrm{p}}(t) - X_0) + \frac{1}{\sqrt{\gamma\beta}}\xi(t). \tag{3.30}$$

In the long-time limit, the particle is trapped around the minimum of the harmonic potential. Such a process is called mean-reverting. In striking contrast to the free particle case, there exists a stationary distribution with the bounded variance $1/k\beta$. This is consistent with the equipartition theorem $\boldsymbol{E}[k\,(X^{\mathrm{p}} - X_0)^2\,/2] = 1/2\beta$.

3.3 Path integral representation of stochastic processes

In the previous sections, probabilistic equations of a particle connected to an equilibrium environment were obtained by incorporating the fluctuation around the optimal path of the Caldeira-Leggett action. As was clear from the derivation, this argument can be inverted to reformulate a given stochastic process in terms of the path integral [13–17]. The path integral approach has an advantage of being able to proceed analytic calculations even for non-Gaussian and non-Markovian processes [3, 18]. It also provides a transparent connection between the stochastic differential equations and the deterministic time-evolution of the probability density function (PDF) such as the Fokker-Planck equation and the master equation.

In subsection 3.3.1, we provide a path integral representation of general stochastic processes using the characteristic functional defined on the Keldysh contour. In subsection 3.3.2, the Gaussian process is discussed including the important cases with the white and colored noise. In subsection 3.3.3, the Poisson processes are formulated using the field-theoretic technique.

3.3.1 Characteristic functional for stochastic processes

Let us consider the functional representation of a stochastic process $X^{\mathrm{p}}(t)$ obeying the stochastic differential equation

$$\frac{dX^{\mathrm{p}}(t)}{dt} = f(X^{\mathrm{p}}) + \eta(t). \tag{3.31}$$

Here, the random noise $\eta(t)$ is another stochastic process. The stochastic differential equation (3.31) is interpreted in the Ito sense in order to make it consistent with the discretized Keldysh contour used in the previous sections.

The stochastic process $X^{\mathrm{p}}(t)$ can be regarded as the degree of freedom of a detector perturbed by a system of interest. The realization of the random perturbation $\eta(t)$ carries fundamental information of the system. From this viewpoint, detecting the fluctuation in the system corresponds to inferring the statistical property of $\eta(t)$ from the dynamics of $X^{\mathrm{p}}(t)$. Although the statistics of η is assumed to be given in Eq. (3.31), they should be specified according to a microscopic calculation. This is one of the main subjects in chapter 4.

The expectation value of the random variable $\mathcal{O}[X^{\rm p}]$ averaged over every realization of the random noise is given in the path integral form as

$$\boldsymbol{E}[\mathcal{O}[X^{\rm p}]] = \boldsymbol{E}\left[\int \mathcal{D}X^{\rm p}\mathcal{O}[X^{\rm p}]\delta\left(\frac{dX^{\rm p}(t)}{dt} - f(X^{\rm p}) - \eta(t)\right)\right]. \tag{3.32}$$

Here, the Jacoiban associated with the change of variables in the delta functional is proven to be unity by virtue of the Ito regularization [19]. The expression is further computed as

$$\begin{aligned}\boldsymbol{E}[\mathcal{O}[X^{\rm p}]] &= \boldsymbol{E}\left[\int \mathcal{D}X^{\rm p}\mathcal{D}X^{\rm s}\mathcal{O}[X^{\rm p}]\exp\left[-i\int dtX^{\rm s}(t)\left(\frac{dX^{\rm p}(t)}{dt} - f(X^{\rm p}) - \eta(t)\right)\right]\right] \\ &= \int \mathcal{D}X^{\rm p}\mathcal{D}X^{\rm s}\mathcal{O}[X^{\rm p}]\chi[X^{\rm s}]\exp\left[-i\int dtX^{\rm s}(t)\left(\frac{dX^{\rm p}(t)}{dt} - f(X^{\rm p})\right)\right], \end{aligned}\tag{3.33}$$

where the statistics of the random noise is determined by the characteristic functional

$$\chi[X^{\rm s}] \equiv \boldsymbol{E}\left[\exp\left(i\int dtX^{\rm s}(t)\eta(t)\right)\right]. \tag{3.34}$$

The action giving the expectation value (3.33) is

$$S[X^{\rm p},X^{\rm s}] = -\int dtX^{\rm s}(t)\left(\frac{dX^{\rm p}(t)}{dt} - f(X^{\rm p})\right) - i\ln\chi[X^{\rm s}]. \tag{3.35}$$

In the following, we provide the characteristic functional of fundamental stochastic processes such as the Gaussian processes and the Poisson processes.

3.3.2 Gaussian processes

One of the most typical stochastic processes found in various applications is the Gaussian process, which is characterized by the mean function $\boldsymbol{E}[\eta(t)] = \mu(t)$ and the noise kernel $\boldsymbol{E}[\eta(t)\eta(t')] = 2\nu(t,t')$. As the mean function can be incorporated in a deterministic force $f(X^{\rm p})$, the stochastic property of the Gaussian process is determined by the noise kernel $\nu(t,t')$. The characteristic functional of the Gaussian process is given by

$$\chi_G[X^{\rm s}] = \exp\left[-\int dsds'X^{\rm s}(s)\nu(s,s')X^{\rm s}(s')\right]. \tag{3.36}$$

Substituting Eq. (3.36) for the characteristic function in Eq. (3.33), we read the action

$$S_{\rm G}[X^{\rm p},X^{\rm s}] = -\int dtX^{\rm s}(t)\left(\frac{dX^{\rm p}(t)}{dt} - f(X^{\rm p})\right) + i\int dsds'X^{\rm s}(s)\nu(s,s')X^{\rm s}(s'), \tag{3.37}$$

which is the Keldysh action for the stochastic differential equation (3.31) with the random noise obeying the Gaussian process with the noise kernel $\nu(t,t')$. An important point is that the noise kernel describes an arbitrary colored Gaussian noise.

It is readily found that the action (3.37) is closely related to the Caldeira-Leggett model (3.10). In the latter context, the time-nonlocal noise originates from the quantum fluctuation in Eq. (3.14). This implies that the quantum dynamics can be mapped to

"classical" stochastic processes. We employ this correspondence in chapter 4 to analyze the quantum fluctuation in the detector.

Gaussian process with white noise

The Langevin equation with the white Gaussian noise is recovered by choosing the noise kernel as

$$\nu(t,t') = D\delta(t-t'), \tag{3.38}$$

with the noise intensity D. The characteristic functional is simply given by

$$\chi_{\mathrm{WG}}[X^{\mathrm{s}}] = \exp\left[-D\int dt\,(X^{\mathrm{s}}(t))^2\right], \tag{3.39}$$

from which the action reads

$$S_{\mathrm{WG}}[X^{\mathrm{p}},X^{\mathrm{s}}] = -\int dt X^{\mathrm{s}}(t)\left(\frac{dX^{\mathrm{p}}(t)}{dt} - f(X^{\mathrm{p}})\right) + iD\int ds\,(X^{\mathrm{s}}(s))^2. \tag{3.40}$$

The Gaussian Langevin equation has a corresponding Fokker-Planck equation

$$\frac{\partial}{\partial t}\mathcal{P}(X^{\mathrm{p}},t) = \frac{\partial}{\partial X^{\mathrm{p}}}\left[-f[X^{\mathrm{p}}] + D\frac{\partial}{\partial X^{\mathrm{p}}}\right]\mathcal{P}(X^{\mathrm{p}},t). \tag{3.41}$$

In the following, we provide a field-theoretic derivation of the Fokker-Planck equation (3.41) by following the transfer matrix method [19]. The starting point is the action (3.40), which is understood in the Ito representation

$$S_{\mathrm{WG}}[X^{\mathrm{p}},X^{\mathrm{s}}] = \sum_j\left[-X^{\mathrm{s}}_j\left(X^{\mathrm{p}}_j - X^{\mathrm{p}}_{j-1} - \delta_t f[X^{\mathrm{p}}_{j-1}]\right) + iD\delta_t\left(X^{\mathrm{s}}_j\right)^2\right]. \tag{3.42}$$

The time stride is denoted by δ_t, and the coordinate variables are abbreviated as $X^{\mathrm{p(q)}}_j \equiv X^{\mathrm{p(q)}}(j\delta_t)$. The probability density function (PDF) at the jth step is defined as

$$\mathcal{P}_j \equiv \Pi_{i'=1}^{j-1}\Pi_{i''=1}^{j}\int \mathcal{D}X^{\mathrm{p}}_{i'}\mathcal{D}X^{\mathrm{s}}_{i''}\exp\left(iS_{\mathrm{WG}}[X^{\mathrm{p}},X^{\mathrm{s}}]\right). \tag{3.43}$$

The PDF $\mathcal{P}_j$ is related up to the first order in δ_t with $\mathcal{P}_{j-1}$ as

$$\begin{aligned}\mathcal{P}_j \simeq &\int \mathcal{D}\delta X^{\mathrm{p}}\mathcal{D}X^{\mathrm{s}}\left[1 + i\delta_t X^{\mathrm{s}} f\left[X - \delta X^{\mathrm{p}}\right]\right] \\ &\times\exp\left[-\frac{1}{2}\begin{pmatrix}\delta X^{\mathrm{p}} & X^{\mathrm{s}}\end{pmatrix}\begin{pmatrix}0 & i\\ i & 2D\delta_t\end{pmatrix}\begin{pmatrix}\delta X^{\mathrm{p}}\\ X^{\mathrm{s}}\end{pmatrix}\right]\mathcal{P}_{j-1},\end{aligned} \tag{3.44}$$

with $X \equiv X_j^{\rm p}$, $\delta X^{\rm p} \equiv X_j^{\rm p} - X_{j-1}^{\rm p}$, and $X^{\rm s} \equiv X_j^{\rm s}$. The PDF $\mathcal{P}_{j-1}$ can be further expanded as

$$\begin{aligned}\mathcal{P}_{j-1} &= \mathcal{P}[X - \delta X^{\rm p}, t_j - \delta_t] \\ &\simeq \sum_{m=0}^{\infty} \frac{(-\delta X^{\rm p})^n}{n!} \frac{\partial^n \mathcal{P}_j}{\partial X^n} - \delta_t \frac{\partial \mathcal{P}_j}{\partial t}. \end{aligned} \tag{3.45}$$

The functional integration with the Gaussian weight in Eq. (3.44) can be performed term by term. If we denote the expectation value of the variable $\mathcal{O}$ by $\langle \mathcal{O} \rangle$, the two-point correlation functions are given by

$$\langle \delta X^{\rm p} \delta X^{\rm p} \rangle = 2D\delta_t, \tag{3.46}$$

$$\langle \delta X^{\rm p} X^{\rm s} \rangle = \langle X^{\rm s} \delta X^{\rm p} \rangle = -i, \tag{3.47}$$

$$\langle X^{\rm s} X^{\rm s} \rangle = 0. \tag{3.48}$$

The two terms in Eq. (3.44) are evaluated up to the first order in δ_t using the relations

$$\begin{aligned}\langle \mathcal{P}_{j-1} \rangle &\simeq \mathcal{P}_j + \frac{1}{2} \langle \delta X^{\rm p} \delta X^{\rm p} \rangle \frac{\partial^2 \mathcal{P}_j}{\partial X^2} - \delta_t \frac{\partial \mathcal{P}_j}{\partial t} \\ &\simeq \mathcal{P}_j + D\delta_t \frac{\partial^2 \mathcal{P}_j}{\partial X^2} - \delta_t \frac{\partial \mathcal{P}_j}{\partial t}, \end{aligned} \tag{3.49}$$

and

$$\begin{aligned}\langle X^{\rm s} f[X - \delta X^{\rm p}] \mathcal{P}_{j-1} \rangle &\simeq -\langle X^{\rm s} \delta X^{\rm p} \rangle f[X] \frac{\partial \mathcal{P}_j}{\partial X} - \langle X^{\rm s} \delta X^{\rm p} \rangle f[X] \mathcal{P}_j \\ &\simeq i \frac{\partial}{\partial X} \left(f[X] \mathcal{P}_j \right). \end{aligned} \tag{3.50}$$

By taking the limit $\delta_t \to 0$, Eq. (3.44) is reduced to the Fokker-Planck equation (3.41).

Ornstein-Uhlenbeck process

Another important situation is the noise $\eta(t)$ being the Ornstein-Uhlenbeck process,

$$\frac{d\eta(t)}{dt} = \frac{1}{\tau} \left[-\eta(t) + \xi(t) \right], \tag{3.51}$$

$$\boldsymbol{E}[\xi(t)\xi(t')] = 2\delta(t - t'), \tag{3.52}$$

with the time constant τ. The correlation function of the noise is exactly computed, and it corresponds to the exponentially correlated colored noise,

$$\boldsymbol{E}[\eta(t)\eta(t')] = 2\nu(t,t') = \frac{2}{\tau} e^{-|t-t'|/\tau}. \tag{3.53}$$

Such a noise is generated by filtering a white Gaussian noise with an overdamped harmonic oscillator [see section 3.2]. The action for the stochastic process with the Ornstein-

Uhlenbeck noise is obtained as

$$S_{\rm OU}[X^{\rm p},X^{\rm s}] = -\int dt X^{\rm s}(t)\left(\frac{dX^{\rm p}(t)}{dt} - f(X^{\rm p})\right) + \frac{i}{\tau}\int dsds' X^{\rm s}(s)e^{-|s-s'|/\tau}X^{\rm s}(s'). \tag{3.54}$$

Unfortunately, it is not possible to determine the PDF of the stochastic process $X^{\rm p}$ described by the action (3.54). However, it is known that an effective Fokker-Planck equation can be derived for a small correlation time τ [19].

In the following, we perturbatively analyze the PDF for the stochastic process $X^{\rm p}$. We note that Eqs. (3.31), (3.51), and (3.52) form coupled Markovian stochastic differential equations for two stochastic variables $X^{\rm p}$ and η. If we denote the joint PDF by $\mathcal{P}(X^{\rm p},\eta,t)$, the Fokker-Planck equation is obtained as

$$\frac{\partial}{\partial t}\mathcal{P}(X^{\rm p},\eta,t) = -\frac{\partial}{\partial X^{\rm p}}\left(-f[X^{\rm p}]+\eta(t)\right)\mathcal{P}(X^{\rm p},t) + \frac{\partial}{\partial\eta}\left[\frac{1}{\tau}\eta + \frac{1}{\tau^2}\frac{\partial}{\partial\eta}\right]\mathcal{P}(X^{\rm p},t). \tag{3.55}$$

We consider a perturbative solution of Eq. (3.55) in the form

$$\mathcal{P}(X^{\rm p},\eta,t) = e^{-\frac{\eta^2\tau}{2}}\left[\mathcal{P}(X^{\rm p},t) + \eta\mathcal{N}(X^{\rm p},t)\right]. \tag{3.56}$$

Hereafter, we suppress the arguments of $\mathcal{P}(X^{\rm p},t)$ and $\mathcal{N}(X^{\rm p},t)$ for simplicity. Substituting the form in Eq. (3.55), we obtain

$$\frac{\partial}{\partial t}\left[\mathcal{P}+\eta\mathcal{N}\right] = \frac{\partial}{\partial X^{\rm p}}\left[f[X^{\rm p}]\mathcal{P}\right] - \frac{\partial}{\partial X^{\rm p}}\mathcal{N}\eta^2 - \frac{\partial}{\partial X^{\rm p}}\left(\mathcal{P}-f[X^{\rm p}]\mathcal{N}\right)\eta - \frac{1}{\tau}\mathcal{N}\eta. \tag{3.57}$$

Integrating Eq. (3.57) in terms of η with the Gaussian weight $e^{-\frac{\eta^2\tau}{2}}$, we obtain the equation for $\mathcal{P}$ as

$$\frac{\partial}{\partial t}\mathcal{P} = \frac{\partial}{\partial X^{\rm p}}\left[f[X^{\rm p}]\mathcal{P}\right] - \frac{1}{\tau}\frac{\partial}{\partial X^{\rm p}}\mathcal{N}. \tag{3.58}$$

If we integrate Eq. (3.57) after multiplying it by η, we obtain the equation

$$\frac{\partial}{\partial t}\mathcal{N} = -\frac{\partial}{\partial X^{\rm p}}\left[\mathcal{P}-f[X^{\rm p}]\mathcal{N}\right] - \frac{1}{\tau}\mathcal{N}. \tag{3.59}$$

If the correlation time τ is much smaller than the other characteristic time scales of the stochastic process, $\frac{\partial}{\partial t}\mathcal{N}$ and $f[X^{\rm p}]\mathcal{N}$ are much smaller than $\mathcal{N}/\tau$. By neglecting these terms, we find the relation $\frac{1}{\tau}\mathcal{N} = -\frac{\partial}{\partial X^{\rm p}}\mathcal{P}$. Then, Eq. (3.58) is reduced to the ordinary Fokker-Planck equation

$$\frac{\partial}{\partial t}\mathcal{P} = \frac{\partial}{\partial X^{\rm p}}\left[f[X^{\rm p}]\mathcal{P}\right] + \frac{\partial}{\partial X^{\rm p}}\mathcal{P}, \tag{3.60}$$

up to the first order in τ.

3.3.3 Poisson processes

The Poisson process is an important non-Gaussian stochastic model found in various phenomena such as electron emission from a cathode in a vacuum tube [20]. We denote the number of events which have occurred during the interval (t',t) by $N(t,t')$. Then, $N(t,t')$ is a Poisson process with rate parameter $\lambda > 0$ if it obeys a Poisson distribution with the rate parameter $\lambda(t-t')$;

$$P[N(t,t') = n] = \frac{\lambda^n (t-t')^n}{n!} e^{-\lambda(t-t')}. \tag{3.61}$$

The probability of the occurrence of the event during an infinitesimal time dt is

$$P[N(t+dt,t) = 0] = 1 - \lambda dt, \tag{3.62}$$
$$P[N(t+dt,t) = 1] = \lambda dt, \tag{3.63}$$
$$P[N(t+dt,t) = n \geq 2] = 0, \tag{3.64}$$

up to the first order in dt. Hence, the Poisson process can be viewed as a pure birth process: The events may occur in the infinitesimal time interval dt with the probability λdt independently of events outside the interval.

Shot noise with a single amplitude

We consider a particle which is perturbed by a delta pulse at each event obeying a Poisson process. The shot noise is the sequence of pulses,

$$\eta(t) = \sum_{i=1}^{N(t)} \delta(t - t_i), \tag{3.65}$$

where the events have occurred at times $t_1, t_2, \cdots, t_{N(t)}$. In order to derive the expression of the characteristic functional (3.34) for the noise, we introduce the auxiliary function

$$\chi_{\mathrm{P}}^t[X^{\mathrm{s}}] = \boldsymbol{E}\left[\exp\left[i\int_{-\infty}^{t} dt' X^s(t')\eta(t')\right]\right], \tag{3.66}$$

which is related to the characteristic functional as $\chi_{\mathrm{P}}[X^{\mathrm{s}}] = \chi_{\mathrm{P}}^{t=\infty}[X^{\mathrm{s}}]$. It satisfies the relation

$$\chi_{\mathrm{P}}^{t+dt}[X^{\mathrm{s}}] = \left((1-\lambda dt) + \lambda dt e^{iX^s(t)}\right)\chi_{\mathrm{P}}^t[X^{\mathrm{s}}], \tag{3.67}$$

which leads to the differential equation

$$\frac{d\ln\chi_{\mathrm{P}}^t[X^{\mathrm{s}}]}{dt} = \lambda\left(e^{iX^s(t)} - 1\right). \tag{3.68}$$

By integrating the equation, the characteristic functional of the Poisson noise is obtained as

$$\chi_{\mathrm{P}}[X^{\mathrm{s}}] = \exp\left[\lambda\int dt\left(e^{iX^{\mathrm{s}}(t)} - 1\right)\right]. \tag{3.69}$$

Shot noise with a random amplitude

The stochastic process for the Poisson noise is slightly generalized by considering that the amplitude of each noise is also a random variable with the probability density function $w(a)$. This variant of a Poisson process is called the compound Poisson process. The random noise is written as

$$\eta(t) = \sum_{i=1}^{N(t)} a_i \delta(t - t_i), \tag{3.70}$$

where a_i is the jump size of the particle at ith event that has occurred at t_i. The characteristic functional of the compound Poisson noise is obtained in an analogous way as

$$\begin{aligned} \chi_{\mathrm{CP}}[X^{\mathrm{s}}] &= \exp\left[\lambda \int dt \left(\int da\, w(a) e^{iaX^{\mathrm{s}}(t)} - 1 \right)\right] \\ &= \exp\left[\lambda \int dt \left(\chi_{\mathrm{J}}[X^{\mathrm{s}}(t)] - 1\right)\right], \end{aligned} \tag{3.71}$$

where the characteristic functional associated with the jump is introduced as

$$\chi_{\mathrm{J}}[X^{\mathrm{s}}(t)] \equiv \int da\, w(a) e^{iaX^{\mathrm{s}}(t)}. \tag{3.72}$$

The compound Poisson process is reduced to the Poisson process when $w(a) = \delta(a-1)$. The Keldysh action associated with the compound Poisson process is

$$S[X^{\mathrm{p}}, X^{\mathrm{s}}] = -\int dt X^{\mathrm{s}}(t) \left(\frac{dX^{\mathrm{p}}(t)}{dt} - f(X^{\mathrm{p}}) \right) - i\lambda \int dt \left(\chi_{\mathrm{J}}[X^{\mathrm{s}}(t)] - 1\right). \tag{3.73}$$

The (compound) Poisson process is a typical non-Gaussian process found in various applications. The non-Gaussian statistics of the noise is characterized by the higher-order terms in X^{s} in Eq. (3.73). If the characteristic functional for the jump is expanded up to the second order in X^{s} as

$$\chi_{\mathrm{J}}[X^{\mathrm{s}}(t)] - 1 = iX^{\mathrm{s}}(t)\boldsymbol{E}[a] - \frac{(X^{\mathrm{s}}(t))^2}{2}\boldsymbol{E}[a^2], \tag{3.74}$$

the action is reduced to the Gaussian one (3.37) with the modified deterministic force $f[X^{\mathrm{p}}] + \lambda \boldsymbol{E}[a]$ and the white noise of the intensity $\lambda \boldsymbol{E}[a^2]$. A further generalization for an arbitrarily shaped pulse is discussed in Ref. [3].

Gaussian and shot noise

We consider a stochastic process driven by noise which consists of the white Gaussian and shot noise as

$$\eta_{\rm GS}(t) = \eta_{\rm WG}(t) + \eta_{\rm CP}(t), \tag{3.75}$$

$$\boldsymbol{E}\left[\eta_{\rm WG}(t)\eta_{\rm WG}(t')\right] = 2D\delta(t-t'), \tag{3.76}$$

$$\eta_{\rm CP} = \sum_{i=1}^{N(t)} a_i \delta(t-t_i). \tag{3.77}$$

Here, D is the intensity of the white Gaussian noise, and the shot noise, whose amplitude a_i is characterized by the jump-size distribution $w(a)$, occurs at t_i according to a Poisson process with a rate parameter λ. The characteristic functional of the additive noise $\eta_{\rm GS}(t)$ is given by the product of that of the white Gaussian noise (3.39) and the shot noise (3.71);

$$\chi_{\rm GS}[X^{\rm s}] = \chi_{\rm WG}[X^{\rm s}]\chi_{\rm CP}[X^{\rm s}]. \tag{3.78}$$

Then, the action is

$$\begin{aligned} S_{\rm GS}[X^{\rm p},X^{\rm s}] = &-\int dt X^{\rm s}(t)\left(\frac{dX^{\rm p}(t)}{dt} - f(X^{\rm p})\right) + iD\int ds\,(X^{\rm s}(s))^2 \\ &- i\lambda\int dt\,(\chi_{\rm J}[X^{\rm s}(t)]-1)\,. \end{aligned} \tag{3.79}$$

In the absence of the shot noise, the time-evolution of the PDF $\mathcal{P}(X^{\rm p},t)$ is described by the Fokker-Planck equation (3.41). The Poisson noise introduces jump processes, whose dynamics is described by the master equation. In the case of the compound Poisson noise (3.73), the master equation is

$$\begin{aligned} \frac{\partial\mathcal{P}(X^{\rm p},t)}{\partial t} = &\frac{\partial}{\partial X^{\rm p}}\left[-f[X^{\rm p}] + D\frac{\partial}{\partial X^{\rm p}}\right]\mathcal{P}(X^{\rm p},t) \\ &+ \lambda_{\rm P}\int da\, w(a)\left(\mathcal{P}(X^{\rm p}-a,t) - \mathcal{P}(X^{\rm p},t)\right). \end{aligned} \tag{3.80}$$

In the following, we provide a field-theoretic derivation of the master equation (3.80). The strategy is closely analogous to the derivation for the Fokker-Planck equation discussed in subsection 3.3.2. Hereafter, we use the same notation used in Eqs. (3.42) and (3.44). The starting point is the discretized action

$$\begin{aligned} S_{\rm GS}\left[X^{\rm p},X^{\rm s}\right] = \sum_j \Big[&-X_j^{\rm s}\left(X_j^{\rm p} - X_{j-1}^{\rm p} - \delta_t f[X_{j-1}^{\rm p}]\right) + iD\delta_t\left(X_j^{\rm s}\right)^2 \\ &- i\lambda\,\delta_t\int da\, w(a)\left(e^{iaX_j^{\rm s}}-1\right)\Big]. \end{aligned} \tag{3.81}$$

The PDF (3.43) at the jth step is

$$\mathcal{P}_j \simeq \int \mathcal{D}\delta X^{\rm p}\mathcal{D}X^{\rm s}\left[1+i\delta_t X^{\rm s} f\left[X-\delta X^{\rm p}\right]+\lambda\,\delta_t\int da\, w(a)\left(e^{iaX_j^{\rm s}}-1\right)\right]$$
$$\times\exp\left[-\frac{1}{2}\begin{pmatrix}\delta X^{\rm p} & X^{\rm s}\end{pmatrix}\begin{pmatrix}0 & i\\ i & 2D\delta_t\end{pmatrix}\begin{pmatrix}\delta X^{\rm p}\\ X^{\rm s}\end{pmatrix}\right]\mathcal{P}_{j-1}. \tag{3.82}$$

The crucial difference is that we need to evaluate the higher order-terms in $X^{\rm s}$ to describe the non-Gaussian nature. With the aid of the correlation functions (3.46), (3.47), and (3.48), the non-Gaussian term in Eq. (3.82) can be evaluated as

$$\begin{aligned}\delta_t\langle e^{iaX_j^{\rm s}}-1\rangle &= \delta_t\sum_{k=1}^{\infty}\sum_{l=0}^{\infty}\frac{(ia)^k(-1)^l}{k!l!}\langle (X^{\rm s})^k(\delta X^{\rm p})^l\rangle\frac{\partial^l\mathcal{P}_j}{\partial X^l}\\ &\simeq \delta_t\sum_{k=1}^{\infty}\frac{(-a)^k}{k!}\frac{\partial^k\mathcal{P}_j}{\partial X^k}\\ &\simeq \delta_t\left(e^{-a\frac{\partial}{\partial\varphi}}-1\right)\mathcal{P}_j,\end{aligned} \tag{3.83}$$

up to the leading order in δ_t. This can be understood by noting that the cross correlation is of order 1 while the auto-correlation vanishes or is of a higher order in δ_t. This requires that the physical components to be contracted with the source ones. The number of the combination of contraction is $l!$, which is canceled with the denominator. Considering the Fokker-Planck term derived before, we can obtain the master equation (3.80) in the limit $\delta_t\to 0$.

3.4 Non-Gaussian noise in classical systems

The Gaussian Langevin equation is frequently used as a phenomenological model of fluctuating systems. For instance, the LC circuit with a dissipative environment is well described by the Langevin equation in the high-temperature limit [21]. The universality of the Langevin equation is established by the system-size expansion developed by Van Kampen [10]. On the other hand, the non-Gaussianity of fluctuation is widely recognized in various nonequilibrium systems such as electronic circuits [22, 23], granular particles [24–26], nanomagnets [27], particles in dense collides [28], and particles with long-range interactions [29]. Recently, the condition for the emergence of the non-Gaussianity and the asymptotic derivation of the non-Gaussian Langevin equation have been given by Kanazawa *et al.* [11, 12]. In this section, we review the Gaussian and non-Gaussian Langevin equations from a microscopic point of view.

3.4.1 Van Kampen's system size expansion

We review Van Kampen's theory for the Gaussian Langevin equation [10]. Let us consider dynamics of a stochastic variable $\hat{v}$, whose probability density function (PDF) is denoted

by $P(v,t) \equiv P[\hat{v}(t) = v]$. If the variable $\hat{v}$ is Markovian, the PDF obeys the master equation

$$\frac{\partial P(v,t)}{\partial t} = \int_{-\infty}^{\infty} dy \left[P(v-y,t)W(v-y;y) - P(v,t)W(v;y) \right], \tag{3.84}$$

where $W(v;y)$ is the transition rate from v with the jump size y. In general, the transition rate depends on the microscopic detail of the jump events. Here, we make a critical assumption that the transition rate is characterized by the typical jump size $\varepsilon \ll v$ and the ε-independent transition probability $\bar{W}(v;\mathcal{Y})$ with the scaled jump size $\mathcal{Y} \equiv y/\varepsilon$. More precisely, the scaled transition rate, which is defined by the relation

$$\bar{W}(v;\mathcal{Y})d\mathcal{Y} \equiv W(v;y)dy \tag{3.85}$$

$$\Leftrightarrow W(v;y) = \frac{1}{\varepsilon}\bar{W}\left(v;\frac{y}{\varepsilon}\right), \tag{3.86}$$

no longer depends on the small parameter ε. This assumption can be viewed as a separation of the characteristic scales. The Kramers-Moyal expansion of the master equation (3.84) is given by

$$\frac{\partial P(v,t)}{\partial t} = \int_{-\infty}^{\infty} d\mathcal{Y} \left[P(v-\varepsilon\mathcal{Y},t)\bar{W}(v-\varepsilon\mathcal{Y};\mathcal{Y}) - P(v,t)\bar{W}(v;\mathcal{Y}) \right] \tag{3.87}$$

$$= \sum_{n=1}^{\infty} \frac{(-\varepsilon)^n}{n!} \frac{\partial^n}{\partial v^n} \left[\alpha_n(v)P(v,t) \right], \tag{3.88}$$

with the Kramers-Moyal coefficient

$$\alpha_n(v) \equiv \int_{-\infty}^{\infty} d\mathcal{Y}\bar{W}(v;\mathcal{Y})\mathcal{Y}^n. \tag{3.89}$$

With the rescaled time $\tau \equiv \varepsilon t$ to see the coarse-grained dynamics, the master equation is approximated up to the first order as

$$\frac{\partial P(v,t)}{\partial \tau} = -\frac{\partial}{\partial v} \left[\alpha_1(v)P(v,t) \right], \tag{3.90}$$

which is identical to the deterministic equation for v. For simplicity, we assume that the $\hat{v}$ is stable around $v = 0$. If we denote the kth coefficient in the Taylor expansion of the Kramers-Moyal by $\alpha_n^{(k)}(v)$, the stability requires the relations

$$\alpha_1^{(0)} = 0, \tag{3.91}$$

$$\alpha_1^{(1)} = -\gamma < 0. \tag{3.92}$$

The fluctuation around the stationary point is incorporated in the higher-order terms in the master equation

$$\frac{\partial P(v,t)}{\partial \tau} = \frac{\partial}{\partial v} \left[\gamma v P(v,t) - \sum_{k=2}^{\infty} \frac{\alpha_1^k}{k!} v^k P(v,t) \right] + \varepsilon \sum_{n=2}^{\infty} \sum_{k=0}^{\infty} \frac{(-\varepsilon)^{n-2}}{n!k!} \alpha_n^{(k)} \frac{\partial^n}{\partial v^n} \left[v^k P(v,t) \right]. \tag{3.93}$$

We rescale the stochastic variable as $V = v/\sqrt{\varepsilon}$ so that the second term describing the fluctuation has a finite contribution in the limit $\varepsilon \to 0$. With the variable $\alpha_2^{(0)} = 2\gamma T$ and the rescaled PDF $\mathcal{P}(V,\tau)$, the master equation is reduced to

$$\frac{\partial \mathcal{P}(V,\tau)}{\partial \tau} = \gamma \frac{\partial}{\partial V}\left[V\mathcal{P}(V,\tau)\right] + \gamma T \frac{\partial^2}{\partial V^2}\mathcal{P}(V,\tau). \tag{3.94}$$

From the correspondence between the stochastic differential equation and the deterministic equation for the PDF, the Fokker-Planck equation (3.94) is found to be identical to the Gaussian Langevin equation

$$\frac{\partial V(\tau)}{\partial \tau} = -\gamma V(\tau) + \sqrt{\gamma T}\,\eta(\tau), \tag{3.95}$$

with the white noise $\boldsymbol{E}[\eta(\tau)\eta(\tau')] = 2\delta(\tau - \tau')$.

The consequence of Van Kampen's theory is general and powerful because it justifies phenomenological description of various fluctuating systems in terms of the Gaussian Langevin equation. From this viewpoint, it seems almost impossible to observe the non-Gaussian fluctuation, which we are interested in. However, it is not the case. In the next subsection, we review the universality of a non-Gaussian Langevin equation and the information which can be extracted from the distribution of the tracer particle according to the recent paper by Kanazawa *et al.* [11, 12].

3.4.2 Non-Gaussian Langevin equation

What is crucial in Van Kampen's theory is that the transition rate is characterized by a *single* parameter ε. Kanazawa *et al.* considered a particle coupled to *multiple* environments, where the amplitudes of the noise are naturally characterized by several independent parameters [11, 12]. The coexistence of thermal and athermal environments is crucial for the non-Gaussian dynamics; otherwise the noise is reduced to be Gaussian according to Van Kampen's theory. Furthermore, the sensitivity of the stochastic particle to the non-Gaussian noise allows us to probe the athermal environment by carefully considering the asymptotic behavior of the particle.

Let us consider a particle coupled to thermal and athermal environments (Fig. 3.1(a)). The coupling to the thermal environment at temperature T introduces the friction coefficient γ and the thermal noise with the intensity γT. The jump process induced by the athermal environment is characterized by the transition rate $W_\varepsilon(v;y)$ from velocity v with the jump size y. Here, the typical jump size is denoted by ε. The Markov dynamics of the particle velocity v is described by the PDF $P(v,t) \equiv P[\hat{v}(t) = v]$ obeying the master equation

$$\frac{\partial P(v,t)}{\partial t} = \gamma \frac{\partial}{\partial v}\left[v + T\frac{\partial}{\partial v}\right] P(v,t) + \int_{-\infty}^{\infty} dy\left[P(v-y,t)W_\varepsilon(v-y;y) - P(v,t)W_\varepsilon(v;y)\right]. \tag{3.96}$$

The first term is the Fokker-Planck term originating from the thermal environment. As with the case in Van Kampen's theory, we assume that the time scale of the athermal environment is well separated from that of the system. Then, we can define the ε-independent scaled

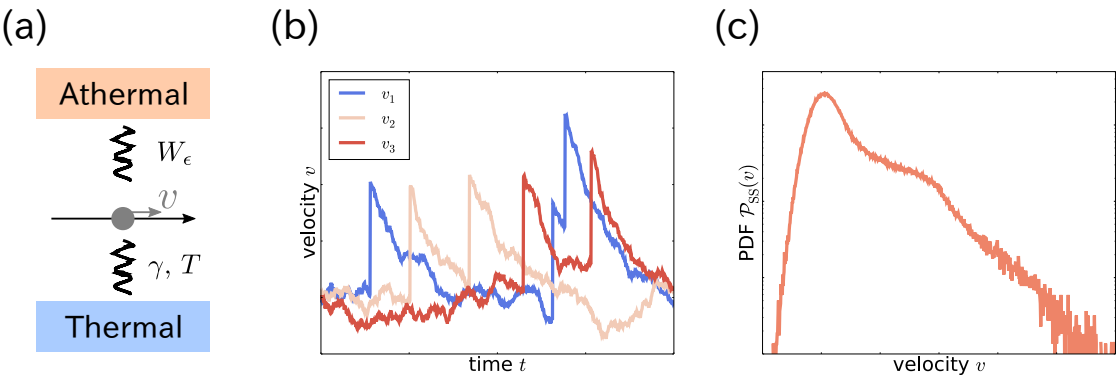

Fig. 3.1 (a) Particle coupled to both the thermal and athermal environments. (b) Typical time evolution of the particle velocity v in the presence of both the thermal and non-Gaussian noise. (c) Steady-state probability density function (PDF) with the strong non-Gaussianity.

transition rate $\bar{W}(v;\mathcal{Y})$ with $\mathcal{Y} \equiv y/\varepsilon$ from the scaling assumption

$$\bar{W}(v;\mathcal{Y})d\mathcal{Y} \equiv W_\varepsilon(v;y)dy \tag{3.97}$$

$$\Leftrightarrow W_\varepsilon(v;y) = \frac{1}{\varepsilon}\bar{W}\left(v;\frac{y}{\varepsilon}\right). \tag{3.98}$$

In the following discussion, we derive the non-Gaussian Langevin equation under the three assumptions [11, 12]:

1. *Small noise*
   The typical jump size ε is much smaller than v.

2. *Strong dissipation due to the thermal environment*
   The friction coefficient γ is independent of ε.

3. *Coexistence of thermal and athermal noises*
   There exists an ε-independent parameter $\mathcal{T}$ such that $T = \mathcal{T}\varepsilon^2$.

We introduce the scaled variable $\mathcal{V} \equiv v/\varepsilon$ and the scaled PDF $\mathcal{P}(\mathcal{V},t) \equiv \varepsilon P(v,t)$. Under the three assumptions, the master equation (3.96) is written as

$$\begin{aligned}\frac{\partial \mathcal{P}(\mathcal{V},t)}{\partial t} =& \gamma\frac{\partial}{\partial \mathcal{V}}\left[\mathcal{V} + \mathcal{T}\frac{\partial}{\partial \mathcal{V}}\right]\mathcal{P}(\mathcal{V},t) \\ &+ \sum_{n=0}^{\infty}\frac{\varepsilon^n}{n!}\int_{-\infty}^{\infty} d\mathcal{Y}\bar{W}^{(n)}(\mathcal{Y})\left[\mathcal{P}(\mathcal{V}-\mathcal{Y},t)(\mathcal{V}-\mathcal{Y})^n - \mathcal{P}(\mathcal{V},t)\mathcal{V}^n\right],\end{aligned} \tag{3.99}$$

with the expansion

$$\bar{W}(\varepsilon\mathcal{V};\mathcal{Y}) \equiv \sum_{n=0}^{\infty}\frac{\varepsilon^n}{n!}\bar{W}^{(n)}(\mathcal{Y})\mathcal{V}^n. \tag{3.100}$$

In the small-noise limit $\varepsilon \to 0$, the master equation is reduced to

$$\frac{\partial \mathcal{P}(\mathcal{V},t)}{\partial t} = \gamma \frac{\partial}{\partial \mathcal{V}} \left[\mathcal{V} + \mathcal{T} \frac{\partial}{\partial \mathcal{V}} \right] \mathcal{P}(\mathcal{V},t) + \int_{-\infty}^{\infty} d\mathcal{Y} \mathcal{W}(\mathcal{Y}) \left[\mathcal{P}(\mathcal{V}-\mathcal{Y},t) - \mathcal{P}(\mathcal{V},t) \right], \quad (3.101)$$

with the scaled transition rate $\mathcal{W}(\mathcal{Y}) \equiv \bar{W}^{(0)}(\mathcal{Y})$. The jump processes described by the scaled transition rate $\mathcal{W}(\mathcal{Y})$ are Markovian and no longer dependent on the state $\mathcal{V}$ because the environmental correlation vanishes in this limit. Moreover, the dissipation due to the friction term is dominantly induced by the thermal environment.

The steady-state PDF $\mathcal{P}_{\rm SS}(\mathcal{V}) \equiv \lim_{t\to\infty} \mathcal{P}(\mathcal{V},t)$ of the master equation (3.101) has been already known in the previous work [11, 12]. The Fourier transform of the steady-state PDF $\tilde{\mathcal{P}}_{\rm SS}(\lambda) \equiv \int d\mathcal{V} e^{i\lambda\mathcal{V}} \mathcal{P}_{\rm SS}(\mathcal{V})$ is solved as

$$\tilde{\mathcal{P}}_{\rm SS}(\lambda) = \exp\left[\int_0^\lambda ds \left(\int d\mathcal{Y}\, \mathcal{W}(\mathcal{Y}) \frac{e^{is\mathcal{Y}} - 1}{\gamma s} - \mathcal{T} s \right) \right]. \quad (3.102)$$

Moreover, the inverse formula to achieve the transition rate $\mathcal{W}(\mathcal{Y})$ from the steady-state PDF $\tilde{\mathcal{P}}_{\rm SS}(\lambda)$ can be derived as

$$\mathcal{W}(\mathcal{Y}) = \int \frac{d\lambda}{2\pi} e^{-i\lambda\mathcal{Y}} \left[\lambda^* + \gamma\mathcal{T}\lambda^2 + \gamma\lambda \frac{d}{d\lambda} \ln \tilde{\mathcal{P}}_{\rm SS}(\lambda) \right], \quad (3.103)$$

with the intensity $\lambda^* = \int d\mathcal{Y} \mathcal{W}(\mathcal{Y})$.

Employing the correspondence discussed in the section 3.3, we obtain the stochastic differential equation which corresponds to the master equation (3.101) as

$$\frac{d\hat{\mathcal{V}}}{dt} = -\gamma\hat{\mathcal{V}} + \sqrt{\gamma\mathcal{T}}\,\eta_{\rm T}(t) + \eta_{\rm NG}(t), \quad (3.104)$$

with the white Gaussian noise $\eta_{\rm T}(t)$ with $\boldsymbol{E}[\eta_{\rm T}(t)\eta_{\rm T}(t')] = 2\delta(t-t')$ and the non-Gaussian noise $\eta_{\rm NG}(t)$ whose statistics is determined by the characteristic functional

$$\chi_{\rm NG}[X^{\rm s}] = \exp\left[\int dt \int d\mathcal{Y}\, \mathcal{W}(\mathcal{Y}) \left(e^{i\mathcal{Y}X^{\rm s}(t)} - 1 \right) \right]. \quad (3.105)$$

Once the transition rate $\mathcal{W}(\mathcal{Y})$ is given, we can perform numerical simulation of the non-Gaussian Langevin equation (3.104). Typical trajectories of the velocity obtained by solving Eq. (3.104) are shown in Fig. 3.1(b). The non-Gaussian noise induces the jumps, which are subsequently decayed due to the thermal dissipation. Non-Gaussianity is clearly found in the steady-state PDF shown in Fig. 3.1(c).

The universality of the non-Gaussian Langevin equation is crucial in the context of the full counting statistics because it justifies the observability of the higher cumulants of the current through a conductor. However, there remains some points to be clarified in order to exploit the insights for the full counting statistics. First, it has not yet been clarified what is the transition rate associated with the electron transport processes. It requires a theoretical scheme to determine the transition rate from a microscopic description of the mesoscopic conductor. Second, the above discussion is limited to the classical regime while various novel phenomena of the current fluctuation are expected in the quantum

regime. In chapter 4, we address these issues to substantiate the fundamental part of the full counting statistics.

References

[1] U. Weiss, *Quantum dissipative systems*, Vol. 10 (World Scientific, 1999).

[2] A. O. Caldeira and A. J. Leggett, Physica A **121**, 587 (1983).

[3] R. P. Feynman, A. R. Hibbs, and D. F. Styer, *Quantum mechanics and path integrals* (Courier Corporation, 2005).

[4] G. Lesovik and R. Loosen, JETP Lett. **65**, 295 (1997).

[5] U. Gavish, Y. Levinson, and Y. Imry, Phys. Rev. B **62**, R10637 (2000).

[6] M. Creux, A. Crépieux, and T. Martin, Phys. Rev. B **74**, 115323 (2006).

[7] A. Zazunov, M. Creux, E. Paladino, A. Crépieux, and T. Martin, Phys. Rev. Lett. **99**, 066601 (2007).

[8] D. Chevallier, T. Jonckheere, E. Paladino, G. Falci, and T. Martin, Phys. Rev. B **81**, 205411 (2010).

[9] Y. V. Nazarov and M. Kindermann, Euro. Phys. J. B **35**, 413 (2003).

[10] N. G. Van Kampen, Can. J. Phys. **39**, 551 (1961).

[11] K. Kanazawa, T. G. Sano, T. Sagawa, and H. Hayakawa, Phys. Rev. Lett. **114**, 090601 (2015).

[12] K. Kanazawa, T. G. Sano, T. Sagawa, and H. Hayakawa, J. Stat. Phys. **160**, 1294 (2015).

[13] P. C. Martin, E. D. Siggia, and H. A. Rose, Phys. Rev. A **8**, 423 (1973).

[14] H.-K. Janssen, Z. Phys. B **23**, 377 (1976).

[15] R. Bausch, H.-K. Janssen, and H. Wagner, Z. Phys. B **24**, 113 (1976).

[16] C. De Dominicis and L. Peliti, Phys. Rev. B **18**, 353 (1978).

[17] L. Onsager and S. Machlup, Phys. Rev. **91**, 1505 (1953).

[18] P. Hänggi, Z. Phys. B **75**, 275 (1989).

[19] A. Kamenev, *Field theory of non-equilibrium systems* (Cambridge University Press Cambridge, 2011).

[20] W. Schottky, Ann. Phys. (Leipzig) **362**, 541 (1918).

[21] N. G. Van Kampen, *Stochastic processes in physics and chemistry*, Vol. 1 (Elsevier, 1992).

[22] J. Gabelli and B. Reulet, Phys. Rev. B **80**, 161203 (2009).

[23] K. Kanazawa, T. Sagawa, and H. Hayakawa, Phys. Rev. E **90**, 012115 (2014).

[24] A. Gnoli, A. Puglisi, and H. Touchette, Europhys. Lett. **102**, 14002 (2013).

[25] A. Gnoli, A. Petri, F. Dalton, G. Pontuale, G. Gradenigo, A. Sarracino, and A. Puglisi, Phys. Rev. Lett. **110**, 120601 (2013).

[26] T. G. Sano, K. Kanazawa, and H. Hayakawa, Phys. Rev. E **94**, 032910 (2016).

[27] Y. Utsumi and T. Taniguchi, Phys. Rev. Lett. **114**, 186601 (2015).

[28] E. Fodor, H. Hayakawa, P. Visco, and F. van Wijland, Phys. Rev. E **94**, 012610 (2016).

[29] I. Zaid and D. Mizuno, Phys. Rev. Lett. **117**, 030602 (2016).

Chapter 4

Detection scheme of non-Gaussian fluctuation in mesoscopic conductors

Nonequilibrium fluctuation in mesoscopic conductors has been intensively studied in both classical and quantum regimes [1, 2]. Current distribution provides exclusive information on microscopic transport processes in the mesoscopic conductors [3, 4]. Owing to the rapid progress in nanotechnology, it becomes realistic to address the current fluctuation beyond the Gaussian one [5–7]. In the classical regime, it is experimentally possible to count the number of electrons which pass through a conductor [8, 9]. The achieved histogram completely characterizes the nonequilibrium transport. The current distribution elucidates the fundamental aspects of the nonequilibrium properties such as the fluctuation theorem [10–12].

In general, it requires a sophisticated scheme to measure current fluctuation compared with the conductance measurement. The fluctuation in small systems is sensitively affected by their environments including its detector [12–18]. This is not just of theoretical interest because recent technology enables us to fabricate electronic nanostructures. In particular, on-chip devices are promising arenas to investigate the non-Gaussian noise in a well controlled manner [19–30]. So far, it has been proposed to measure the current fluctuation by using on-chip devices such as quantum point contacts [8, 9], double quantum dots [19, 21], Josephson junctions [25, 26, 31, 32], LC circuits [33–35], and RLC circuits [36, 37]. As has been reviewed in section 1.4, detailed analysis of the detector circuit is indispensable to qualitatively explain the experimental data obtained in the classical tunneling regime [12]. It is also expected that elaborate description of the detector is essential to understand the results for quantum coherent conductors [11].

In the classical regime, the detector circuit of the current fluctuation can be understood as a tracer particle under non-Gaussian noises [18, 33, 34]. A coupled mesoscopic conductor works as an athermal environment for the detector due to the nonequilibrium nature of the system. In section 3.4, we have reviewed the universal appearance of the non-Gaussian Langevin equation in such a system [38, 39]. The results are useful in that they indicate a complete connection between the dynamics of the detector and the statistical property of the non-Gaussian noise. However, there is still a gap between our insights into the non-Gaussianity in the classical [38–40] and quantum [3, 4] systems because they have been investigated separately so far. The previous works on quantum conductors [34, 36] have related the second and third cumulants of the current to those of the detector degrees

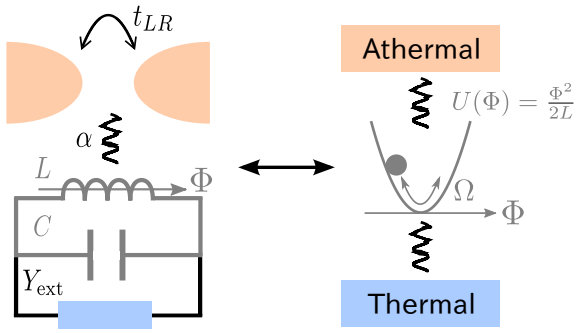

Fig. 4.1 Schematic of a QPC inductively coupled to a detector LC circuit. The flux through the LC circuit can be considered as the position of a harmonic oscillator attached to both the thermal and athermal environments.

of freedom based on a perturbative approach. Still, it is an open question whether and how the detector circuit can characterize all the cumulants of the current. What remains unclear to use the insights obtained in the classical systems is the microscopic derivation of the non-Gaussian statistics of the noise. It is also an important next step to describe the quantum dynamics of the detector circuit. Indeed, the quantum nature of the effective LC circuit was reported in the context of the Josephson qubit [41].

In this chapter, we study a detection scheme of the current fluctuation in mesoscopic conductors in the classical-quantum crossover regime. In order to proceed to a concrete discussion, we consider that the detector is described by a dissipative LC circuit, which is an effective model of the Josephson junction [41, 42]: a typical on-chip device used in various experiments [26, 27, 41–46]. As a simple and generic setup, we consider the detection of the current fluctuation in a quantum point contact (QPC). The LC circuit is subject to the fluctuation generated by the nonequilibrium transport through the QPC [18]. The problem can be interpreted as quantum Brownian motion driven by a non-Gaussian noise in terms of the correspondence between mechanical systems and electronic circuits [47]. We develop a stochastic method for describing the quantum dynamics of the detector circuit, and establish the one-to-one correspondence between the current distribution in the mesoscopic conductor and the steady-state probability density function (PDF) of the detector degrees of freedom.

This chapter is organized as follows. In Sec. 4.1, we give a microscopic description of the dissipative LC circuit coupled to the QPC based on the Keldysh formalism, and simplify the model by assuming the separation of the time scales of the subsystems. In Sec. 4.2, the dynamics of the coupled system is formulated based on a stochastic method. In Sec. 4.3, the inverse formula to infer the current distribution from the steady-state PDF of the flux in the LC circuit is extended to the quasiclassical regime by solving the master equation. In Sec. 4.4, the effect of the quantum correction on estimating the statistics of the non-Gaussian noise is numerically evaluated. We summarize the results in Sec. 4.5.

4.1 Model

4.1.1 Detector LC circuit coupled to a quantum point contact

We provide a microscopic description of a dissipative LC circuit coupled to a QPC (Fig. 4.1) based on the Keldysh formalism [see section 2.1].

Detector LC circuit

The detector LC circuit is composed of an inductance L, a capacitance C, and a resistor with admittance $Y(\omega)$. In realistic situations, the LC circuit is considered as an effective model of a SQUID device, which is frequently utilized as an on-chip detector. The basic variable of the LC circuit is the flux Φ through the inductor. If we denote the voltage across the inductor by $\hat{V}$, the flux is defined as its time integral as $\Phi(t) = \int^t dt' \hat{V}(t')$. In the absence of the resistor, the Lagrangian of the LC circuit is written as

$$\mathcal{L}_{\rm LC} = \frac{C}{2}\left(\frac{\partial\Phi}{\partial t}\right)^2 - \frac{1}{2L}\Phi^2. \tag{4.1}$$

Hence, the flux Φ is an analog of the coordinate X of a particle moving in a harmonic potential. The resistance in the circuit works as a dissipative environment for the "particle". This completely isomorphic structure indicates that the detector LC circuit is microscopically described by the Caldeira-Leggett model [48],

$$S_{\rm det}[\Phi] = \frac{1}{2}\int_C dz dz' \Phi(z)\mathcal{G}^{-1}(z,z')\Phi(z'), \tag{4.2}$$

which was discussed in section 3.1 based on the Keldysh formalism [49, 50]. The symbol $\int_C$ denotes the integration over the Keldysh contour C, and the argument z is a combination of the real time t and the Keldysh index $\rho = \mp$. The forward and backward Keldysh contours are denoted by C^- and C^+, respectively.

The physical meaning becomes quite clear if we move to the rotated Keldysh basis

$$S_{\rm det}[\Phi^{\rm p},\Phi^{\rm s}] = \int dt dt' \left[\Phi^{\rm s}(t)\left(\mathcal{G}^{-1}\right)^{\rm r}(t,t')\Phi^{\rm p}(t') + \frac{1}{2}\Phi^{\rm s}(t)\left(\mathcal{G}^{-1}\right)^{\rm K}(t,t')\Phi^{\rm s}(t')\right], \tag{4.3}$$

with the physical component $\Phi^{\rm p} \equiv \left(\Phi^- + \Phi^+\right)/2$ and source components $\Phi^{\rm s} \equiv \Phi^- - \Phi^+$. With the aid of the self-energy (3.8), the retarded and Keldysh Green's functions are obtained as

$$\left(\mathcal{G}^{-1}\right)^{\rm r}(\omega) = C(\omega^2 - \Omega^2) + iJ(\omega), \tag{4.4}$$

$$\left(\mathcal{G}^{-1}\right)^{\rm K}(\omega) = 2iJ(\omega)\coth(\beta\hbar\omega/2), \tag{4.5}$$

with the resonant frequency $\Omega \equiv 1/\sqrt{LC}$, the inverse temperature β, and the spectral function

$$J(\omega) = \frac{\sigma\omega}{1 + (\omega/\omega_{\rm D})^2}, \tag{4.6}$$

which is related with the admittance $Y(\omega)$ as $J(\omega) = \omega Y(\omega)$. Here, we assume that the coupling is Ohmic with the conductance σ in the low-frequency regime. The high-frequency cutoff is introduced using the Drude cutoff $\omega_{\rm D}$. We note that the quantum nature of the dissipative LC circuit is solely incorporated in the Keldysh component describing the fluctuation due to the linearity of the equation of motion of the flux Φ [47].

Quantum point contact

The action of the quantum point contact (QPC) consists of two parts as $S_{\rm QPC}[\bar{c},c;\Phi] = S_0[\bar{c},c] + S_T[\bar{c},c;\Phi]$. The first term S_0 describes the conduction electrons in the leads;

$$S_0[\bar{c},c] = \sum_{i=L,R}\sum_{\boldsymbol{k}}\int_C dz dz' \bar{c}_{i\boldsymbol{k}}(z) g^{-1}_{i\boldsymbol{k}}(z,z') c_{i\boldsymbol{k}}(z'), \tag{4.7}$$

where $\bar{c}_{i\boldsymbol{k}}$ [$c_{i\boldsymbol{k}}$] are the Grassmann fields for the creation [annihilation] of an electron with the wave vector $\boldsymbol{k}$ and the dispersion relation $\varepsilon_{i\boldsymbol{k}}$ for $i = L,R$. The bias voltage V is applied to the leads, which are assumed to be in equilibrium at inverse temperature $\beta_{\rm QPC}$. The chemical potentials for lead $i = L$ and R are $\mu_L = \varepsilon_{\rm F} + eV$ and $\mu_R = \varepsilon_{\rm F}$, respectively, with the Fermi energy ε_F. The Green's functions of lead electrons are given in Eq. (2.74) and (2.75) with the Fermi-Dirac distribution function

$$f_i(\omega) = \frac{1}{\exp\left[\beta_{\rm QPC}(\omega - \mu_i)\right] + 1}, \tag{4.8}$$

for lead $i = L$, R. The second term $S_{\rm T}$ describes the tunneling between the leads, accompanying an electronic excitation in the inductively coupled LC circuit [47];

$$S_{\rm T}[\bar{c},c;\Phi] = \frac{1}{N}\sum_{\boldsymbol{k},\boldsymbol{k}'}\int_C dz \left[t_{LR} e^{\frac{ie}{\hbar}\alpha\Phi(z)} \bar{c}_{R\boldsymbol{k}}(z) c_{L\boldsymbol{k}'}(z) + {\rm H.c.} \right]. \tag{4.9}$$

Here, the hopping amplitude between the leads and the coupling constant between the QPC and the LC circuit are denoted by t_{LR} and α, respectively.

As the QPC action $S_{\rm QPC}[\bar{c},c;\Phi] = S_0[\bar{c},c] + S_{\rm T}[\bar{c},c;\Phi]$ is quadratic in terms of the conduction electrons, we can exactly integrate out the fermionic degrees of freedom in the same calculations as are found in subsection 2.3.2. Then, the QPC action becomes

$$S_{\rm QPC}[\Phi] = i\hbar \int_C dz \ln\left[1 - t_{LR}^2 G_L V^\dagger[\Phi] G_R V[\Phi]\right](z,z), \tag{4.10}$$

with the vertex operator

$$V[\Phi] \equiv \exp\left(\frac{ie\alpha}{\hbar}\Phi\right). \tag{4.11}$$

Here, we used the abbreviation $(AB)(z,z') \equiv \int_C dz'' A(z,z'')B(z'',z')$. The Green's function is defined as $G_i(z,z') \equiv \frac{1}{N}\sum_{\boldsymbol{k}} g_{i\boldsymbol{k}}(z,z')$, whose retarded and Keldysh components are

$$G_i^{\mathrm{r}}(\omega) = -i\pi\rho_i, \tag{4.12}$$

$$G_i^{\mathrm{K}}(\omega) = 2\pi i\rho_i(2f_i(\omega)-1), \tag{4.13}$$

respectively. The density of states $\rho_{L(R)}$ is assumed to be independent of energy for simplicity.

Partition function

Using the actions (4.2) and (4.10), the partition function of the QPC-LC coupled system is given only in terms of the bosonic field Φ as

$$Z \equiv \int \mathcal{D}\Phi \exp\left[\frac{i}{\hbar}\left(S_{\mathrm{det}}[\Phi] + S_{\mathrm{QPC}}[\Phi]\right)\right]. \tag{4.14}$$

The calculation is exactly performed so far. However, it is not possible to perform the functional integration because the QPC action $S_{\mathrm{QPC}}[\Phi]$ contains an infinite numbers of non-linear terms with respect to the bosonic field Φ [see Eq. (4.10)].

4.1.2 Quasistationary approximation

Throughout the following analysis, we assume the separation of the time scales in the subsystems: The dynamics in the QPC is much faster than that of the LC circuit. This assumption is called the quasistationary approximation [18, 25, 51, 52]. The correlation time of the current fluctuation in the QPC is governed by either the bias voltage V or the inverse temperature β_{QPC}, while the dynamics of the LC circuit is characterized by the resonant frequency Ω and the relaxation time C/σ. If these time scales are well separated, we are allowed to consider the intermediate time scale Δt satisfying

$$\min\left(\frac{\hbar}{eV}, \hbar\beta_{\mathrm{QPC}}\right) \ll \Delta t \ll \min\left(\frac{C}{\sigma}, \frac{1}{\Omega}\right). \tag{4.15}$$

In the time interval of length Δt, we can regard the flux Φ in the QPC action Eq. (4.10) as a constant because the dynamics in the LC circuit is frozen. The action for the QPC is written on the discretized Keldysh contour as

$$S_{\mathrm{QPC}}[\Phi^{\mathrm{p}}, \Phi^{\mathrm{s}}] = i\hbar\sum_j \int_{t_j}^{t_j+\Delta t} dt' \mathrm{Tr}\ln\left[1 - t_{LR}^2 G_L \tau_z V^\dagger[\Phi_j] G_R V[\Phi_j]\tau_z\right](t',t'), \tag{4.16}$$

where Φ_j denotes the constant flux Φ in the jth time interval. If we introduce the auxiliary self-energy $\Sigma_L[\Phi_j] \equiv t_{LR}^2 V^\dagger[\Phi_j] G_R V[\Phi_j]$, it is written in the Keldysh space as

$$\Sigma_L[\Phi_j^{\mathrm{s}}] = t_{LR}^2 \begin{pmatrix} G_R^{--} & e^{-\frac{ie\alpha}{\hbar}\Phi_j^{\mathrm{s}}} G_R^{-+} \\ e^{\frac{ie\alpha}{\hbar}\Phi_j^{\mathrm{s}}} G_R^{+-} & G_R^{++} \end{pmatrix}, \tag{4.17}$$

which has the same structure as the tunneling self-energy with the counting field (2.96). Since Δt is sufficiently long for the QPC dynamics, the same calculation in deriving Eq. (2.98) from Eq. (2.95) leads to the QPC action

$$S_{\rm QPC}[\Phi^{\rm s}] = i\hbar\Delta t \sum_j \int \frac{d\omega}{2\pi} \ln\left[\det\left(1 - \boldsymbol{G}_L(\omega)\tau_x \boldsymbol{\Sigma}_L[\Phi_j](\omega)\tau_x\right)\right] \tag{4.18}$$

$$= i\hbar \int dt \int \frac{d\omega}{2\pi} \ln\Big[1 + T_{LR}\Big[f_L(\omega)(1-f_R(\omega))(e^{\frac{ie\alpha}{\hbar}\Phi^{\rm s}(t)} - 1) + f_R(\omega)(1-f_L(\omega))(e^{-\frac{ie\alpha}{\hbar}\Phi^{\rm s}(t)} - 1)\Big]\Big], \tag{4.19}$$

with the transmission coefficient $T_{LR} \equiv 4\pi^2 t_{LR}^2 \rho_L \rho_R$. Thus, we find that the QPC action has the same structure as the Levitov-Lesovik formula (1.9), which is widely known in the full counting statistics [3].

With the action of the LC circuit Eq. (4.3) and the QPC Eq. (4.24), we obtain the partition function

$$Z = \int \mathcal{D}\Phi^{\rm p}\mathcal{D}\Phi^{\rm s} \exp\left[\frac{i}{\hbar}\left(S_{\rm det}[\Phi^{\rm p}, \Phi^{\rm s}] + S_{\rm QPC}[\Phi^{\rm s}]\right)\right]. \tag{4.20}$$

The important point is that the QPC action is no longer dependent on $\Phi^{\rm p}$ as a consequence of the quasi-stationary approximation. This allows a stochastic interpretation of the QPC action as is shown in the next section. We note that the quasi-stationary approximation is violated when the time scales of the LC circuit and QPC are comparable to each other. In this regime, the dynamics of the whole system is closely related to the dynamical Coulomb blockade [53].

4.2 Stochastic analysis

In this section, we provide a stochastic interpretation of the QPC-LC coupled system by rewriting the partition function (4.20) in terms of the characteristic functionals discussed in section 3.3. The exponential of the QPC action can be associated with the characteristic functional of the compound Poisson process. The thermal and quantum fluctuations originating from the dissipative environment are incorporated in the noise kernel. The non-Gaussian Langevin equation is derived using the asymptotic scaling.

4.2.1 Characteristic functionals

Gaussian fluctuation

The Gaussian fluctuation originating from the thermal environment is described by the quadratic term in $\Phi^{\rm s}$ in the LC action Eq. (4.3). In order to recover the thermal fluctuation in the classical limit [see subsection 3.2], we scale the fields as $\Phi^{\rm s}(t) \equiv (\hbar/e\gamma)\varphi^{\rm s}(s)$ and $\Phi^{\rm p}(t) \equiv (e/C\Omega)\varphi^{\rm p}(s)$ with the dimensionless time $s \equiv \Omega t$ and the dimensionless friction coefficient $\gamma \equiv \sigma/C\Omega$. The contribution from the $(\Phi^{\rm s})^2$ term in the action is identical to

the Gaussian characteristic functional (3.36)

$$\chi_{\rm G}[\varphi^{\rm s}] \equiv \exp\left[-\frac{T}{\gamma}\int ds ds' \varphi^{\rm s}(s)\nu(s-s')\varphi^{\rm s}(s')\right], \tag{4.21}$$

with the dimensionless temperature $T \equiv C/e^2\beta$ and the noise kernel

$$\nu(s) \equiv \frac{\beta\hbar}{2\sigma\Omega}\int_{-\infty}^{\infty}\frac{d\omega}{2\pi}J(\omega)\coth\left(\frac{\beta\hbar\omega}{2}\right)e^{-is\omega/\Omega}. \tag{4.22}$$

Using the Ohmic spectral function with the Drude cutoff (4.6), the noise kernel becomes

$$\nu(s) = \frac{\omega_{\rm c}}{2}e^{-|s|\omega_{\rm c}} + \sum_{k=1}^{\infty}\frac{1}{(k/\tau\omega_{\rm c})^2-1}\left(\omega_{\rm c}e^{-|s|\omega_{\rm c}} - \frac{k}{\tau}e^{-k|s|/\tau}\right), \tag{4.23}$$

where $\omega_{\rm c} \equiv \omega_{\rm D}/\Omega$ and $\tau \equiv \beta\hbar\Omega/2\pi$ are the dimensionless cutoff and the quantum-mechanical time scale, respectively. The cutoff frequency $\omega_{\rm D}$ is usually assumed to be much larger than the resonant frequency Ω ($\omega_{\rm c} \gg 1$) so that the first term on the right hand side of Eq. (4.23) may become a Dirac delta function. The second term is the non-Markovian quantum correction, which becomes relevant at sufficiently low temperatures $1/\beta$ of the order $\hbar\Omega$. In the classical limit ($\tau \to 0$ and $\omega_c \to \infty$), the second term vanishes and the noise kernel is solely determined by the thermal noise $(T/\gamma)\delta(s)$. As will be shown later, the existence of the cutoff $\omega_{\rm c}$ and the exponentially decaying form of the second term are crucial to analyze the quantum correction.

Non-Gaussian fluctuation

As was already discussed in the introduction 1.2.2, the Levitov-Lesovik formula is interpreted as a compound Poisson process by introducing the transition rate W_n using the following relations

$$S_{\rm QPC}[\varphi^{\rm s}] \equiv -i\sum_{n=-\infty}^{\infty}\int dt\; W_n(e^{\frac{i\alpha}{\gamma}n\varphi^{\rm s}(t)} - 1). \tag{4.24}$$

Then, the contribution from the QPC action in the partition function (4.20) is given by

$$\chi_{\rm NG}[\varphi^{\rm s}] \equiv \exp\left[\lambda_{\rm P}\int ds\left[\int dy\; w(y)\left(e^{iy\varphi^{\rm s}(s)} - 1\right)\right]\right], \tag{4.25}$$

where we defined the rate parameter $\lambda_{\rm P} \equiv \sum_n w_n$ and the jump size distribution

$$w(y) \equiv \frac{1}{\lambda_{\rm P}}\sum_{n=-\infty}^{\infty} w_n\delta\left(y - \frac{n\alpha}{\gamma}\right), \tag{4.26}$$

with the dimensionless transition rate $w_n \equiv W_n/\hbar\Omega$ ($n \in \mathbb{Z}$). The functional $\chi_{\rm NG}$ is identical to the characteristic fuctional for the compound Poisson processes (3.71).

In the weak tunneling regime, dominant contributions of the non-Gaussian noise comes from the lowest-order terms of the transition rate Eq. (4.24);

$$\begin{aligned} W_{+1} &= \hbar T_{LR} \int \frac{d\omega}{2\pi} (1 - f_R(\omega)) f_L(\omega) \\ &= \frac{T_{LR}}{2\pi} \frac{eV}{1 - e^{-eV\beta_{\mathrm{QPC}}}}, \end{aligned} \tag{4.27}$$

$$\begin{aligned} W_{-1} &= \hbar T_{LR} \int \frac{d\omega}{2\pi} f_R(\omega)(1 - f_L(\omega)), \\ &= \frac{T_{LR}}{2\pi} \frac{eV}{e^{eV\beta_{\mathrm{QPC}}} - 1}. \end{aligned} \tag{4.28}$$

The transition rate W_1 (W_{-1}) is proportional to the probability for an electron to be transmitted from the left (right) lead to the right (left) one.

As the non-Gaussian characteristic functional is structurally equivalent to the cumulant generating functional (1.9) for the QPC without the detector, the transition rate W_n is directly related to the current fluctuations. According to the full counting statistics, the higher-order cumulants of the current fluctuation are generated by introducing the counting field χ. If we consider the weak-tunneling regime for simplicity, the QPC action is expanded in terms of the counting field as

$$\begin{aligned} iS_{\mathrm{QPC}}(\chi) &\simeq \left[W_{+1} \left(e^{i\chi} - 1 \right) + W_{-1} \left(e^{-i\chi} - 1 \right) \right] \\ &= (W_{+1} - W_{-1})(i\chi) + (W_{+1} + W_{-1})(i\chi)^2 + O(\chi^3). \end{aligned} \tag{4.29}$$

The current and noise through the QPC are obtained as the coefficients, which are related to the transition rate W_n as

$$I = \frac{e}{\hbar} (W_{+1} - W_{-1}), \tag{4.30}$$

$$S = \frac{e^2}{\hbar} (W_{+1} + W_{-1}), \tag{4.31}$$

respectively.

Stochastic interpretation

In the following discussions, we consider the overdamped regime ($\gamma \gg 1$). The partition function Eq. (4.20) is written in terms of the two characteristic functionals (4.21) and (4.25) as

$$Z = \int \mathcal{D}\varphi^{\mathrm{p}} \mathcal{D}\varphi^{\mathrm{s}} \chi_{\mathrm{G}}[\varphi^{\mathrm{s}}] \chi_{\mathrm{NG}}[\varphi^{\mathrm{s}}] \exp \left[i \int ds \varphi^{\mathrm{s}}(s) \left(-\frac{\partial}{\partial s} - \frac{1}{\gamma} \right) \varphi^{\mathrm{p}}(s) \right]. \tag{4.32}$$

In deriving the equation of motion of the LC circuit, we used the fact that the friction kernel becomes Markovian under the assumption of the large cutoff $\omega_{\mathrm{c}} \gg 1$. The action

for the total system is

$$S[\varphi^{\mathrm{p}},\varphi^{\mathrm{s}}] = \int ds\varphi^{\mathrm{s}}(s)\left[-\frac{\partial}{\partial s}-\frac{1}{\gamma}\right]\varphi^{\mathrm{p}}(s)+\frac{iT}{\gamma}\int dsds'\varphi^{\mathrm{s}}(s)\nu(s-s')\varphi^{\mathrm{s}}(s') - i\lambda_{\mathrm{P}}\int ds\int dy\, w(y)\left(e^{iy\varphi^{\mathrm{s}}(s)}-1\right). \tag{4.33}$$

As the characteristic functional is the product of the Gaussian and Poissonian ones, the "tracer particle" is considered to be driven by the two independent noises obeying the Gaussian and Poisson statistics. The stochastic differential equation corresponding to the action (4.33) is

$$\frac{\partial\varphi^{\mathrm{p}}(s)}{\partial s} = -\frac{1}{\gamma}\varphi^{\mathrm{p}}(s)+\sqrt{\frac{T}{\gamma}}\eta_{\mathrm{G}}(s)+\sum_i y_i\delta(s-s_i), \tag{4.34}$$

$$\langle\eta_G(s)\eta_G(s')\rangle = 2\nu(s-s'). \tag{4.35}$$

The statistical property of the Poisson noise, which is often referred to as shot noise, is determined by the non-Gaussian characteristic functional χ_{NG}. There are two random variables to determine the shot noise; a set of the arrival times $\{s_i\}$ and the amplitudes $\{y_i\}$. The arrival time s_i obeys the Poisson process with a rate parameter λ_{P}. The amplitude of the noise y_i is chosen according to the jump-size distribution $w(y)$. In our model, the noise amplitude at each event takes the value $n\alpha/\gamma$ with the probability w_n/λ_{P}.

The physical meaning of the Gaussian and shot noise is as follows. As is clear from the derivation, the Gaussian noise is induced by the dissipative environment of the detector circuit. In the classical limit, it is reduced to the Gaussian white noise, i.e. the thermal noise. The non-Markovian nature of the Gaussian noise is a consequence of the quantum nature of the environment, which is expected to be relevant at sufficiently low temperatures [see the discussion below Eq. (4.23)]. The quantum correction to the thermal noise is discussed later. On the other hand, the origin of the shot noise is the nonequilibrium current through the QPC. According to Ampere's law, the instantaneous current produces a magnetic field, which perturbs the flux in the inductively coupled LC circuit. All the information of the current fluctuation in the QPC is coded in the shot noise. Hence, the detection of the current distribution is equivalent to determining the statistics of the shot noise. This is a reminiscent of the virtual spin $1/2$ galvanometer reviewed in section 1.3. Our model is a more realistic model of the detector by taking its internal dynamics into account. We note that the statistical property of the shot noise is decoupled from the state of the LC circuit as a consequence of the separation of the time scales.

4.2.2 Asymptotic scaling

The detector LC circuit coupled to the QPC can be considered as a quantum particle which is coupled to both thermal and athermal environments. As was reviewed in section 3.4, a particle coupled to a number of environments has been studied in the previous works [38, 39], which clarified the three conditions for the non-Gaussianity to emerge:

1. The typical jump size ε induced by the non-Gaussian noise is small.
2. The thermal friction coefficient γ does not depend on ε.

3. The thermal noise is smaller than or of the same order as ε^2.

It is straightforward to confirm these conditions in our case. The jump-size distribution (4.26) indicates that the characteristic size of the jump is given by $\varepsilon \equiv \alpha/\gamma$, which is small in the regime of weak inductive coupling and large damping. The condition 1 is satisfied if it is possible to neglect the higher-order terms in the jump-size distribution. This holds when the transmission coefficient is small; $T_{LR} \ll 1$. The condition 2 is trivially satisfied because the thermal friction coefficient γ is irrelevant to the QPC, i.e. the athermal environment. The condition 3 requires the temperature T at the detector to be scaled as ε^2, allowing to define the ε-independent scaled temperature $\mathcal{T} \equiv T/\varepsilon^2$.

With the rescaled variables $\phi \equiv \varphi^{\mathrm{p}}/\varepsilon$, $\phi^{\mathrm{s}} \equiv \varepsilon\varphi^{\mathrm{s}}$ and $\mathcal{Y} \equiv y/\varepsilon$, the action (4.33) is scaled as

$$\begin{aligned} S[\phi,\phi^{\mathrm{s}}] = &\int ds\phi^{\mathrm{s}}(s)\left[-\frac{\partial}{\partial s}-\frac{1}{\gamma}\right]\phi(s)+\frac{i\mathcal{T}}{\gamma}\int dsds'\phi^{\mathrm{s}}(s)\nu(s-s')\phi^{\mathrm{s}}(s') \\ &-i\lambda_{\mathrm{P}}\int ds\int d\mathcal{Y}\mathcal{W}(\mathcal{Y})\left(e^{i\mathcal{Y}\phi^{\mathrm{s}}(s)}-1\right), \end{aligned} \tag{4.36}$$

with the rescaled jump-size distribution

$$\begin{aligned} \mathcal{W}(\mathcal{Y}) &\equiv \varepsilon w(y) \\ &= \frac{1}{\lambda_{\mathrm{P}}}\sum_{n=-\infty}^{\infty} w_n\delta(\mathcal{Y}-n). \end{aligned} \tag{4.37}$$

This is equivalent to consider the partition function

$$Z = \int \mathcal{D}\phi^{\mathrm{p}}\mathcal{D}\phi^{\mathrm{s}}\chi_{\mathrm{G}}[\phi^{\mathrm{s}}]\chi_{\mathrm{NG}}[\phi^{\mathrm{s}}]\exp\left[i\int ds\phi^{\mathrm{s}}(s)\left(-\frac{\partial}{\partial s}-\frac{1}{\gamma}\right)\phi^{\mathrm{p}}(s)\right], \tag{4.38}$$

with the scaled characteristic functionals

$$\ln\chi_{\mathrm{G}}[\phi^{\mathrm{s}}] = -\frac{\mathcal{T}}{\gamma}\int dsds'\phi^{\mathrm{s}}(s)\nu(s-s')\phi^{\mathrm{s}}(s'), \tag{4.39}$$

$$\begin{aligned} \ln\chi_{\mathrm{NG}}[\phi^{\mathrm{s}}] &= \lambda_{\mathrm{P}}\int ds\int d\mathcal{Y}\mathcal{W}(\mathcal{Y})\left(e^{i\mathcal{Y}\phi^{\mathrm{s}}(s)}-1\right) \\ &= -\int ds\int\frac{d\omega}{2\pi\Omega}\ln\Big[1+T_{LR}\Big[f_L(\omega)(1-f_R(\omega))(e^{i\phi^{\mathrm{s}}(s)}-1) \\ &\qquad +f_R(\omega)(1-f_L(\omega))(e^{-i\phi^{\mathrm{s}}(s)}-1)\Big]\Big]. \end{aligned} \tag{4.40}$$

The corresponding Langevin equation is

$$\frac{\partial\phi(s)}{\partial s} = -\frac{1}{\gamma}\phi(s)+\sqrt{\frac{\mathcal{T}}{\gamma}}\eta_{\mathrm{G}}(s)+\eta_{\mathrm{P}}(s), \tag{4.41}$$

with the Gaussian noise η_{G}, whose statistical property is given as (4.35), and the shot noise

$$\eta_{\mathrm{P}}(s) = \sum_i \mathcal{Y}_i\delta(s-s_i). \tag{4.42}$$

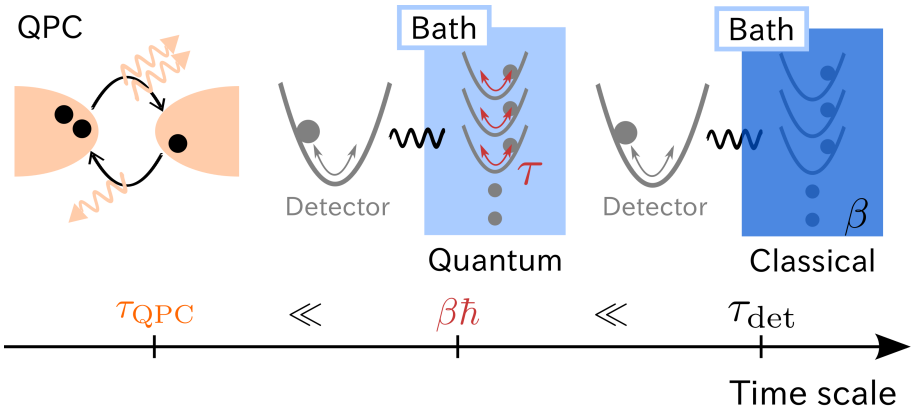

Fig. 4.2 Time scales.

The rescaled shot-noise amplitude $\mathcal{Y}_i$ takes an integer value with the jump-size distribution $\mathcal{W}(\mathcal{Y})$, while the arrival time s_i is determined by the Poisson process with a rate parameter λ_{P}.

4.2.3 Fluctuation theorem

The fluctuation theorem [see subsection 1.2.3 and Ref. [10] for details] imposes strict constraints on the statistics of the shot noise. With the aid of the identity $f_L(\omega)(1-f_R(\omega)) = e^{eV\beta_{\mathrm{QPC}}} f_R(\omega)(1-f_L(\omega))$, the non-Gaussian characteristic functional (4.40) satisfies the relation

$$\chi_{\mathrm{NG}}[\phi^{\mathrm{s}}] = \chi_{\mathrm{NG}}\left[-\phi^{\mathrm{s}} + ieV\beta_{\mathrm{QPC}}\right]. \tag{4.43}$$

By expanding the non-Gaussian characteristic functional in terms of the transition probability, the forward and backward processes represented by the transition rate $W_{\pm n}$ are mutually related as

$$W_n = W_{-n} e^{neV\beta_{\mathrm{QPC}}}, \tag{4.44}$$

for $n \in \mathbb{Z}$. This relation is nothing but the detailed balance of the transition rate. We note that Eq. (4.43) is a consequence of the fluctuation theorem in the QPC.

4.2.4 Quantum fluctuation

In the following, we consider the dynamics of the detector circuit away from the classical limit. The relevant time scales are shown in Fig. 4.2. The characteristic time scale of the detector LC circuit is determined by the resonant frequency and the decay time constant as $\tau_{\mathrm{det}} = \min(C/\sigma, 1/\Omega)$. In the classical regime, the fluctuation induced by the thermal bath can be described by the inverse temperature β. The quantum nature of the dissipative LC circuit becomes relevant at sufficiently low temperatures such that $\tau = \beta\hbar\Omega/2\pi \neq 0$. Here, $\beta\hbar$ can be understood as the quantum-mechanical correlation time of the thermal bath which is composed of an infinite numbers of harmonic oscillators. We note that the QPC time scale $\tau_{\mathrm{QPC}} = \min(\hbar/eV, \hbar\beta_{\mathrm{QPC}})$ is assumed to be much smaller than the other

time scales so that the quasistationary approximation Eq. (4.15) is applicable. In addition, we need not consider the memory effect of the friction kernel as the cutoff is sufficiently large ($\omega_c \gg 1$).

The quantum effect is incorporated via the second term on the right-hand side of Eq. (4.23), whose kth term gives the contribution

$$\frac{\mathcal{T}}{\gamma}\frac{1}{(k/\tau\omega_c)^2-1}\left(\omega_c e^{-\omega_c|s|}-\frac{k}{\tau}e^{-k|s|/\tau}\right). \tag{4.45}$$

The exponentially decaying colored noise is a hallmark of the Ornstein-Uhlenbeck process discussed in section 3.3. The auxiliary variables $\eta_k^{\mu=\pm}$ obeying the Ornstein-Uhlenbeck processes

$$\frac{\partial\eta_k^\mu(s)}{\partial s}=\frac{-\eta_k^\mu(s)+\xi_k^\mu(s)}{\tau_k^\mu}, \tag{4.46}$$

$$\langle\xi_k^\mu(s)\xi_{k'}^{\mu'}(s')\rangle=2\delta(s-s')\delta_{kk'}\delta_{\mu\mu'}, \tag{4.47}$$

with $\tau_k^+\equiv 1/\omega_c$, $\tau_k^-\equiv\tau/k$, and the Kronecker delta $\delta_{kk'}$ and $\delta_{\mu\mu'}$, have the same statistical properties as the fluctuation in Eq. (4.45);

$$\langle\eta_k^\mu(s)\eta_{k'}^{\mu'}(s')\rangle=\frac{1}{\tau_k^\mu}\exp\left(-|s-s'|/\tau_k^\mu\right)\delta_{kk'}\delta_{\mu\mu'}. \tag{4.48}$$

Hence, it is possible to consider that the quantum fluctuation is decomposed into the mutually independent auxiliary variables η_k^μ. This discussion is substantiated in the field-theoretic treatment by applying the Hubbard-Stratonovich transformation.

The overdamped Langevin equation with the quantum correction is

$$\frac{\partial\phi(s)}{\partial s}=-\frac{1}{\gamma}\phi(s)+\sqrt{\frac{\mathcal{T}}{\gamma}}\eta_0(s)+\sum_{k=1}^{\infty}\sqrt{\frac{\mathcal{T}_k}{\gamma}}\left[\eta_k^+(s)+i\eta_k^-(s)\right]+\eta_P(s), \tag{4.49}$$

with the noise amplitude $\mathcal{T}_k=\mathcal{T}/((k/\tau\omega_c)^2-1)$ the thermal noise η_0 whose statistics is given by

$$\langle\eta_0(s)\eta_0(s')\rangle=2\delta(s-s'). \tag{4.50}$$

We note that the η_k^- term is pure-imaginary because the second term of Eq. (4.45) is negative. Thus, we were able to map the quantum dynamics of the detector coupled to the QPC into the linearly-coupled non-Gaussian Langevin equations with the auxiliary variables.

4.3 Master equation

In this section, we perturbatively solve the stochastic equations (4.42), (4.48), (4.49), and (4.50) by mapping them to a deterministic equation of the probability density function (PDF), i.e. the master equation. In section 3.3, we showed that the Gaussian processes are

described by the Fokker-Planck terms and the non-Gaussian noise introduces additional jump processes. The master equation (3.80) for a single variable is straightforwardly generalized to a multivariate case.

We denote the PDF [1] by $\mathcal{P}(\phi, \boldsymbol{\eta}, s)$ with the flux ϕ, a set of the auxiliary variables $\boldsymbol{\eta}$, and the rescaled time s. The corresponding master equation is

$$\begin{aligned}\frac{\partial \mathcal{P}(\phi,\boldsymbol{\eta},s)}{\partial s} =& \frac{1}{\gamma}\frac{\partial}{\partial\phi}\left[\phi\mathcal{P}(\phi,\boldsymbol{\eta},s)\right] + \frac{\mathcal{T}}{\gamma}\frac{\partial^2\mathcal{P}(\phi,\boldsymbol{\eta},s)}{\partial\phi^2} \\ &+ \sum_{k=1}^{\infty}\sum_{\mu=\pm}\left(\sqrt{\frac{\mu\mathcal{T}_k}{\gamma}}\eta_k^\mu\frac{\partial}{\partial\phi} + \frac{1}{\tau_k^\mu}\frac{\partial}{\partial\eta_k^\mu}\left[\eta_k^\mu + \frac{1}{\tau_k^\mu}\frac{\partial}{\partial\eta_k^\mu}\right]\right)\mathcal{P}(\phi,\boldsymbol{\eta},s) \\ &+ \lambda_{\mathrm{P}}\int d\mathcal{Y}\mathcal{W}(\mathcal{Y})\left(e^{\mathcal{Y}\frac{\partial}{\partial\phi}} - 1\right)\mathcal{P}(\phi,\boldsymbol{\eta},s). \end{aligned} \tag{4.51}$$

The first two terms on the right-hand side of Eq. (4.51) is identical to the Fokker-Planck equation in the classical limit. The second line, which essentially originates from the quantum nature of the thermal environment, describes the coupling between the flux ϕ and the auxiliary variables η_k^μ we sell as their diffusive motion. The last term is the consequence of the jump processes induced by the shot noise.

The multivariate master equation Eq. (4.51) is reduced to a single-variate one using the technique discussed in subsection 3.3.2. In this case, the conditions for the short time constant and the positive coupling constant [50] are expressed as $\tau_k^\mu \ll 1$ and $\mathcal{T}_k > 0$ for an arbitrary natural number $k \in \mathcal{N}$ and $\mu = \pm$. The former condition leads to the inequalities $1/\omega_{\mathrm{c}} \ll 1$ and $\tau \ll 1$. The latter one further requires a cutoff frequency to filter the quantum-mechanical energy scale ($\tau\omega_{\mathrm{c}} < 1$). Under these assumptions, we can construct a perturbative solution from the classical limit as

$$\mathcal{P}(\phi,\boldsymbol{\eta},s) \simeq \exp\left[-\sum_{k=1}^{\infty}\sum_{\mu=\pm}\frac{\tau_k^\mu\left(\eta_k^\mu\right)^2}{2}\right]\left[\mathcal{P}(\phi,s) + \sum_{k=1}^{\infty}\sum_{\mu=\pm}\eta_k^\mu N_k^\mu(\phi,s)\right]. \tag{4.52}$$

The coupled master equations for $\mathcal{P}(\phi,s)$ and $N_k^\mu(\phi,s)$ are given by

$$\begin{aligned}\frac{\partial\mathcal{P}(\phi,s)}{\partial s} =& \left[\frac{1}{\gamma}\left(1+\phi\frac{\partial}{\partial\phi}\right) + \frac{\mathcal{T}}{\gamma}\frac{\partial^2}{\partial\phi^2} + \lambda_{\mathrm{P}}\int d\mathcal{Y}\mathcal{W}(\mathcal{Y})\left(e^{\mathcal{Y}\frac{\partial}{\partial\phi}} - 1\right)\right]\mathcal{P}(\phi,s) \\ &+ \sum_{k=1}^{\infty}\sum_{\mu=\pm}\frac{1}{\tau_k^\mu}\sqrt{\frac{\mu\mathcal{T}_k}{\gamma}}\frac{\partial N_k^\mu(\phi,s)}{\partial\phi}, \end{aligned} \tag{4.53}$$

$$\begin{aligned}\tau_k^\mu\frac{\partial N_k^\mu(\phi,s)}{\partial s} =& \left[\frac{1}{\gamma}\left(1+\phi\frac{\partial}{\partial\phi}\right) + \frac{\mathcal{T}}{\gamma}\frac{\partial^2}{\partial\phi^2} + \lambda_{\mathrm{P}}\int d\mathcal{Y}\mathcal{W}(\mathcal{Y})\left(e^{\mathcal{Y}\frac{\partial}{\partial\phi}} - 1\right) - \frac{1}{\tau_k^\mu}\right]N_k^\mu(\phi,s) \\ &+ \sqrt{\frac{\mu\mathcal{T}_k}{\gamma}}\frac{\partial\mathcal{P}(\phi,s)}{\partial\phi}, \end{aligned} \tag{4.54}$$

[1] The classical interpretation of the PDF fails in the quantum regime. In this case, we need to consider the density matrix of the quantum circuit [4].

respectively. The equation for the steady-state PDF $\mathcal{P}_{\rm SS}(\phi)$ is given up to the first order in τ_k^μ as

$$0 = \left[\left(1+\phi\frac{\partial}{\partial\phi}\right)+\mathcal{T}\frac{\partial^2}{\partial\phi^2}+\gamma\lambda_{\rm P}\int d\mathcal{Y}\mathcal{W}(\mathcal{Y})\left(e^{\mathcal{Y}\frac{\partial}{\partial\phi}}-1\right)\right. \\ \left.-\left[1-\sum_k\frac{\mathcal{T}_k\tau_k}{\gamma}\frac{\partial^2}{\partial\phi^2}\right]^{-1}\sum_k\mathcal{T}_k\left[1-\frac{\tau_k}{\gamma}\right]\frac{\partial^2}{\partial\phi^2}\right]\mathcal{P}_{\rm SS}(\phi), \tag{4.55}$$

with $\tau_k \equiv 1/\omega_{\rm c} - \tau/k$. With the Fourier transform of the steady-state PDF $\tilde{\mathcal{P}}_{\rm SS}(\lambda)$ and the cumulant generating function $\tilde{\mathcal{F}}_{\rm SS}(\lambda) \equiv \ln\tilde{\mathcal{P}}_{\rm SS}(\lambda)$, Eq. (4.55) is solved as

$$\tilde{\mathcal{F}}_{\rm SS}(\lambda) = \ln\tilde{\mathcal{K}}(\lambda) + \tilde{\mathcal{F}}^{\rm cl}_{\rm SS}(\lambda). \tag{4.56}$$

Here, the solution in the classical limit is known in Refs. [38, 39] as

$$\tilde{\mathcal{F}}^{\rm cl}_{\rm SS}(\lambda) = -\frac{\mathcal{T}\lambda^2}{2}+\gamma\lambda_{\rm P}\int d\mathcal{Y}\mathcal{W}(\mathcal{Y})\int_0^\lambda d\lambda'\frac{e^{i\mathcal{Y}\lambda'}-1}{\lambda'}. \tag{4.57}$$

The additional kernel describing the quantum correction is

$$\tilde{\mathcal{K}}(\lambda) \equiv \left(\frac{1}{1+\theta^2\lambda^2}\right)^k, \tag{4.58}$$

with the parameters

$$\theta \equiv \left(\frac{\mathcal{T}\tau}{\gamma}\left[\psi(1+\tau\omega_{\rm c})-\psi(1)\right]\right)^{1/2}, \tag{4.59}$$

$$k \equiv \frac{1}{2}\left[\frac{\mathcal{T}}{2\theta^2}\left(1-\frac{\pi\tau\omega_{\rm c}}{\tan(\pi\tau\omega_{\rm c})}\right)-\frac{1}{\gamma}\right]. \tag{4.60}$$

Here, $\psi(x) \equiv \frac{d}{dx}\ln\Gamma(x)$ is the digamma function with the gamma function $\Gamma(x) \equiv \int_0^\infty dt\, t^{x-1}e^{-t}$. The factor of $\tilde{\mathcal{K}}$ is determined by the normalization of the PDF $\tilde{\mathcal{P}}_{\rm SS}(0) = 1$. The quantum correction kernel Eq. (4.58) is identical to the characteristic functional of the difference of the two independent random variables obeying the identical gamma distribution with the scale parameter θ and the shape parameter k. The parameters θ and k are associated with the amplitude and the arrival rate of the quantum fluctuation, respectively. The quantum correction does not modulate the mean but the fluctuation of the flux ϕ. The quantum correction vanishes in the classical limit, i.e. $\ln\tilde{\mathcal{K}}(\lambda) = 0$ for $\tau = 0$.

The kernel $\tilde{\mathcal{K}}$ can be Fourier transformed for $k > 0$ as

$$\mathcal{K}(\phi) = \frac{1}{\sqrt{\pi}\Gamma(k)\theta}\left(\frac{|\phi|}{2\theta}\right)^{k-1/2}K_{k-1/2}\left(|\phi|/\theta\right), \tag{4.61}$$

with the modified Bessel function of the second kind $K_\nu(z)$. The steady-state PDF with the quantum correction $\mathcal{K}(\phi)$ is related with the classical solution as

$$\mathcal{P}_{\rm SS}(\phi) = \int d\phi' \mathcal{K}(\phi - \phi') \mathcal{P}^{\rm cl}_{\rm SS}(\phi'). \tag{4.62}$$

The steady-state PDF of the quasiclassical LC circuit is determined if the detailed information of the non-Gaussian noise is given as $\mathcal{W}(\mathcal{Y})$.

As was discussed in the previous work [38, 39], the steady-state PDF of the classical particle can be utilized to probe the non-Gaussianity of the athermal environment. This also holds for the quasiclassical particle; we can derive the formula to determine $\mathcal{W}(\mathcal{Y})$ from $\mathcal{P}_{\rm SS}(\phi)$ by using Eqs. (4.56), (4.57), and (4.58). The inverse formula is

$$\mathcal{W}(\mathcal{Y}) = \frac{1}{\gamma\lambda_{\rm P}} \int \frac{d\lambda}{2\pi} e^{-i\mathcal{Y}\lambda} \left[\gamma\lambda_{\rm P} + \left(\mathcal{T} + \frac{2k\theta^2}{1+\theta^2\lambda^2} \right) \lambda^2 + \lambda \frac{d}{d\lambda} \tilde{\mathcal{F}}_{\rm SS}(\lambda) \right]. \tag{4.63}$$

The classical limit is recovered for $\tau = 0$. The quantum correction becomes significant when the temperature of the LC circuit is comparable to the variance of the quantum correction ($\mathcal{T} \sim 2k\theta^2$). Equation (4.63) is one of the main results of this chapter.

4.4 Results

4.4.1 Quantum correction without non-Gaussian noise

First, we discuss how the quantum correction (4.61) affects the steady-state PDF of the detector circuit. In order to discern it from the effect of the non-Gaussian noise, we suppose that there is no transmission in the QPC ($T_{LR} = 0$). The steady-state PDF $\mathcal{P}_{\rm SS}(\phi)$ for the LC circuit in this setup is shown in Fig. 4.3(a). In the absence of the non-Gaussian noise, the flux in the LC circuit is driven by the thermal and quantum fluctuations. The amplitude of the thermal noise is $\mathcal{T} = 0.01$, and the cutoff is $\omega_{\rm c} = 10$. We examine various quantum-mechanical scales: $\tau = 0$, 0.01, 0.02, 0.03, 0.04, and 0.05. As is shown in Fig. 4.3(a), the quantum fluctuation broadens the steady-state PDF. The behavior of the quantum kernel can be qualitatively understood as the increase of the temperature of order $2k\theta^2$. We note that this interpretation is not perfect because of the λ-dependence of the quantum correction. The variance of the PDF $\sigma_\phi^2 \equiv \langle (\phi - \langle\phi\rangle)^2 \rangle$ normalized with its classical value $\mathcal{T}$ is plotted in Fig. 4.3(b) for various values of $\omega_{\rm c}$. The cutoff effectively modulates the quantum effect by controlling the filtering. The τ dependence of the variance indicates that the quantum fluctuation grows as τ increases. This implies that the quantum effect cannot be filtered by the cutoff, and the effective temperature becomes higher than the real temperature.

4.4.2 Non-Gaussian noise in the weak tunneling regime

The non-Gaussian noise produced by the instantaneous current through the QPC significantly modifies the steady-state PDF. For simplicity, we consider the weak tunneling regime ($T_{LR} \ll 1$) so that the lowest-order terms ($w_{\pm 1}$) are dominant. As is reviewed in subsection 1.2.2, the non-Gaussian noise obeys a bidirectional Poisson process [10] in this

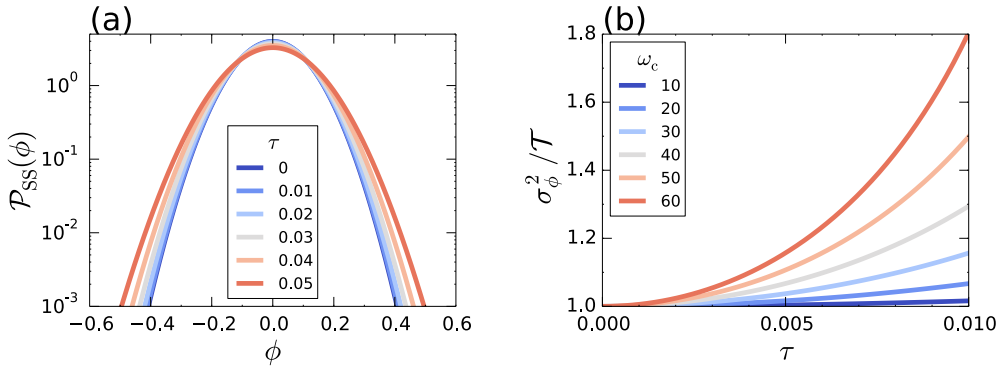

Fig. 4.3 (a) The steady-state PDF $\mathcal{P}_{\rm SS}$ without the non-Gaussian noise for various quantum-mechanical time scales τ with the cutoff $\omega_{\rm c} = 10$. (b) The dependence of the variance σ_ϕ^2 normalized with the thermal noise amplitude $\mathcal{T}$ on τ for various $\omega_{\rm c}$. The other parameters are set to $T_{\rm LR} = 0$, $\gamma = 2.0$, and $\mathcal{T} = 0.01$.

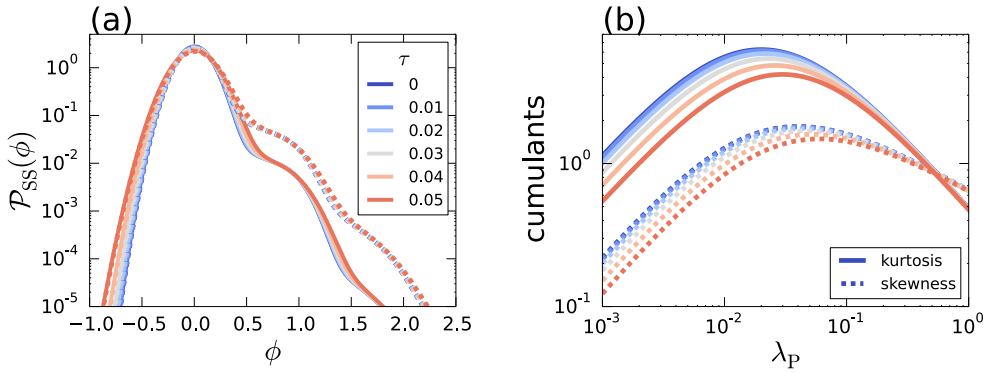

Fig. 4.4 (a) The steady-state PDF of the flux in the detector LC circuit coupled to the QPC at large bias voltage ($eV/2\pi\hbar\Omega = 10^3$). The solid and dashed lines correspond to $T_{LR} = 4 \cdot 10^{-6}$ and $T_{LR} = 1.6 \cdot 10^{-5}$, respectively. (b) The dependence of the skewness (dashed lines) and the kurtosis (solid lines) on $\lambda_{\rm P}$ for various values of τ. The notation of the colors is the same as the left panel. The other parameters are given by $\gamma = 2.0$, $\mathcal{T} = 0.02$, $\omega_{\rm c} = 10$, and $2\pi\hbar\Omega\beta_{\rm QPC} = 10^3$.

regime: The rate parameter $\lambda_{\rm P}$ is reduced to $\lambda_{\rm P} = w_{+1} + w_{-1}$, and the amplitudes of the shot noise take two values ± 1 with the probability $w_{\pm 1}/\lambda_{\rm P}$ [see also Eq. (1.19)].

High bias voltage

With the aid of Eqs. (4.27) and (4.28), the transition probability and the rate parameter at zero-temperature are computed as

$$\frac{w_{\pm 1}}{\lambda_{\rm P}} = \theta(\pm eV), \tag{4.64}$$

$$\lambda_{\rm P} = \frac{T_{LR}}{2\pi}\frac{e|V|}{\hbar\Omega}, \tag{4.65}$$

respectively. The sign of the shot-noise amplitude is determined by that of the bias voltage as the current flows unidirectionally at zero-temperature due to the Fermi statistics. The

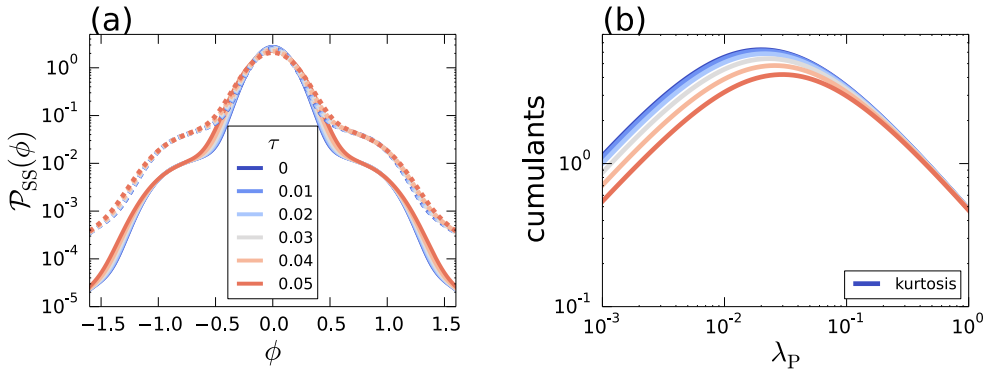

Fig. 4.5 (a) The steady-state PDF of the flux in the detector LC circuit coupled to the QPC without the bias voltage ($V = 0$) and at finite temperature ($2\pi\hbar\Omega\beta_{\rm QPC} = 10^{-3}$). The solid and dashed lines correspond to $T_{LR} = 4 \cdot 10^{-6}$ and $T_{LR} = 1.6 \cdot 10^{-5}$, respectively. (b) The dependence of the kurtosis on $\lambda_{\rm P}$ for corresponding τ. The other parameters are set to $\gamma = 2.0$, $\mathcal{T} = 0.02$, and $\omega_{\rm c} = 10$.

rate parameter is given by the product of the attempt rate $e|V|/2\pi\hbar\Omega$ and the transmission coefficient T_{LR}. The steady-state PDF for the detector LC circuit coupled to the QPC in the shot-noise regime ($2\pi\hbar\Omega\beta_{\rm QPC} = 10^3$ and $eV/2\pi\hbar\Omega = 10^3$) is shown in Fig. 4.4(a). The curves are plotted for various quantum-mechanical time scales τ. The rate parameter is estimated as $\lambda_{\rm P} \approx 0.004$ ($\lambda_{\rm P} \approx 0.016$) for $T_{LR} = 4 \cdot 10^{-6}$ ($T_{LR} = 1.6 \cdot 10^{-5}$), respectively. Hence, the variance induced by the shot noise is smaller than or comparable to that of the thermal noise ($\mathcal{T} = 0.02$). As can be understood by comparing the results with and without the shot noise (Figs. 4.3(a) and 4.4(a)), the shot noise induces the shift and asymmetry of the PDF; it has a long tail for the positive region of ϕ. Moreover, the PDF exhibits a characteristic step around $\phi = 1$ because the amplitude of the shot noise is discretized due to the granularity of the electron transport in the QPC. The quantum correction smoothens the non-Gaussian structures of the PDF. Nevertheless, the τ dependence is weak around $\phi \simeq 1$, where the shot noise is dominant.

The non-Gaussianity of the steady-state PDF is quantified in terms of the skewness $\langle(\phi - \langle\phi\rangle)^3\rangle/\sigma_\phi^3$ and the kurtosis $\langle(\phi - \langle\phi\rangle)^4\rangle/\sigma_\phi^4 - 3$). The dependence of the skewness and the kurtosis on the rate parameter $\Lambda_{\rm P}$ is shown in Fig. 4.4(b) as dashed and solid lines, respectively. The notation of the colors is the same as in Fig. 4.4(a) in that each color represents the curve with corresponding values of τ. In the regime where the shot noise coexists with the thermal noise ($\lambda_{\rm P} \leq \mathcal{T} = 0.02$), the non-Gaussianity develops as the rate parameter $\lambda_{\rm P}$ increases. When the shot noise becomes dominant over the thermal noise, the non-Gaussianity begins to be suppressed. This is consistent with Van Kampen's theory reviewed in subsection 3.4.1 because the flux is effectively driven by a single environment. The broadening of the steady-state PDF due to the quantum fluctuation manifests itself as the decrease of the non-Gaussianity for larger values of τ.

Finite temperature without bias voltage

The non-Gaussian noise is induced by the QPC even at high temperatures without the bias voltage because of its nonlinear coupling to the LC circuit. The transition probability and

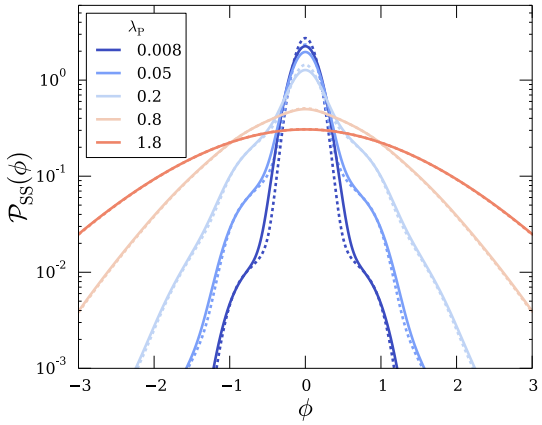

Fig. 4.6 The transition of the steady-state PDF from the non-Gaussian to the Gaussian distribution for large $\lambda_P = T_{LR}/\pi\hbar\Omega\beta_{QPC}$ with the fixed inverse temperature $2\pi\hbar\Omega\beta_{QPC} = 10^{-3}$. The solid and dashed lines correspond to $\tau = 0.05$ and $\tau = 0$, respectively. The other parameters are set to the same values as in Fig. 4.5.

the rate parameter are computed as

$$\frac{w_{\pm 1}}{\lambda_P} = \frac{1}{2}, \tag{4.66}$$

$$\lambda_P = \frac{T_{LR}}{\pi\hbar\Omega\beta_{QPC}}. \tag{4.67}$$

At finite temperatures without the bias voltage, the shot noise amplitude becomes either positive or negative with the same probability because the current through the QPC is bidirectional and unbiased. The rate parameter is proportional to the product of the temperature and the transmission coefficient. The rate parameters for the solid lines ($T_{LR} = 4 \cdot 10^{-6}$) and dashed lines ($T_{LR} = 1.6 \cdot 10^{-5}$) are estimated as $\lambda_P \approx 0.008$ and $\lambda_P \approx 0.032$, respectively, in the steady-state PDF for $2\pi\hbar\Omega\beta_{QPC} = 10^{-3}$ shown in Fig. 4.5(a). The characteristic structures of the PDF around $\phi = \pm 1$ is smoothened by the quantum fluctuation as τ increases. The reduction of the non-Gaussianity by the quantum fluctuation is also confirmed in the kurtosis plotted in Fig. 4.5(b).

4.4.3 Relation to the central limit theorem

As is expected from Van Kampen's theory, the steady-state PDF approaches Gaussian as the rate parameter λ_P becomes larger: If the arrival interval of the intermittent noise is much shorter than the decay time, it is piled up to be Gaussian. The steady-state PDF of the detector circuit coupled with the equilibrium QPC with a relatively large transmission coefficient is shown in Fig. 4.6. The solid lines are for the case with the quantum fluctuation ($\tau = 0.05$), while the dotted lines indicate the corresponding classical limit ($\tau = 0$). The rate parameters are approximately evaluated as $\lambda_P \approx 0.008$, 0.05, 0.2, 0.8, and 1.8. The characteristic step around $\phi = \pm 1$ are smoothened as λ_P increases. Moreover, the quantum correction becomes less relevant when the non-Gaussian noise plays a dominant role in

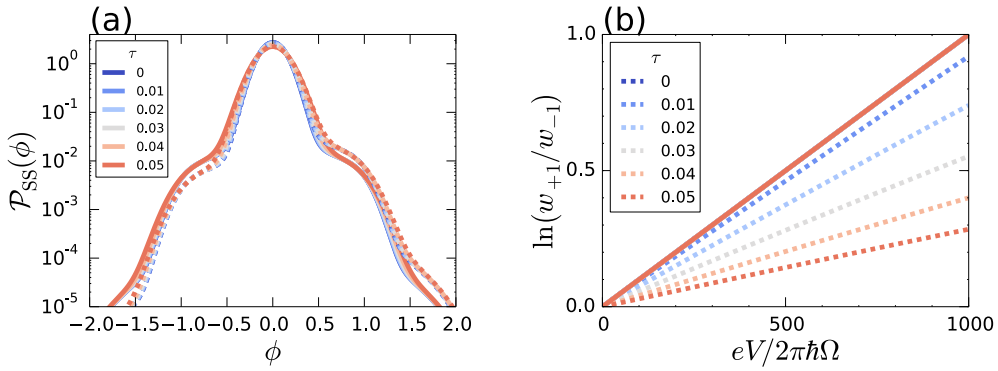

Fig. 4.7 The steady-state PDF of the flux in the detector LC circuit coupled to the QPC with the finite temperature ($2\pi\hbar\Omega\beta_{\rm QPC} = 0.001$) and the bias voltage [$eV/2\pi\hbar\Omega = 100$ (1000) for solid (dashed) lines]. (b) the logarithm of the ratio w_{+1}/w_{-1} estimated by the inverse formula Eq. (4.63). The solid curves are obtained by properly incorporating the quantum correction, which is neglected in the dashed lines. Parameters: $\gamma = 2.0$, $\mathcal{T} = 0.02$, $\omega_{\rm c} = 10$, and $T_{LR} = 4.0 \cdot 10^{-6}$.

determining the PDF. The behavior is consistent with the $\lambda_{\rm P}$-dependence of the kurtosis shown in Fig. 4.5(b).

4.4.4 Estimation of current distribution

Finally, we come back to our original problem to detect the full counting statistics in the QPC from the steady-state PDF $\mathcal{P}_{\rm SS}(\phi)$. This can be done by estimating the transition rate $w_{\pm 1}$ with the aid of the inverse formula Eq. (4.63). As a demonstration, we estimate the transition rate in the QPC at a finite temperature ($2\pi\hbar\Omega\beta_{\rm QPC} = 0.001$) and a finite bias voltage. The steady-state PDF for the LC circuit coupled to the QPC in this parameter regime is plotted in Fig. 4.7(a). The solid and dashed lines correspond to $eV/2\pi\hbar\Omega = 100$ and 1000, respectively. In contrast to the case without the bias voltage [see Fig. 4.5(a)], the bias voltage introduces asymmetry of the PDF by modulating the transition rate $w_{\pm 1}$. Nevertheless, the transition rates are rigidly related with each other as

$$\ln\left(\frac{w_{+1}}{w_{-1}}\right) = eV\beta_{\rm QPC}, \tag{4.68}$$

because of the fluctuation theorem discussed in subsection 4.2.3. The logarithm of the ratio estimated by using the inverse formula Eq. (4.63) is plotted in Fig. 4.7(b) as solid lines, which perfectly agree with the theoretical prediction Eq. (4.68). In general, the transition rate which is estimated by neglecting the quantum correction is no longer correct. The approximate estimate for various values of τ is shown as dashed lines in Fig. 4.7(b). The curve for the classical limit ($\tau = 0$) is consistent with the fluctuation theorem, while the ratio gradually deviates from the correct value for larger τ. This result indicates that the quantum correction is essential to correctly estimate the transition rate by the inverse formula.

4.5 Discussion

In this chapter, we have studied a detection scheme of the current distribution through a quantum point contact (QPC) by using an inductively coupled detector LC circuit. With the assumption that the detector dynamics is much slower than the QPC dynamics, the detector can be considered as a quantum particle driven by the non-Gaussian noise: the instantaneous current through the QPC generates a non-Gaussian fluctuation in the circuit. The statistics of the non-Gaussian fluctuation is solely determined by the current distribution in the QPC as a consequence of the time-scale separation. The quantum nature of the dissipative circuit becomes also relevant at low temperatures. We have used a stochastic approach to determine the statistics of the non-Gaussian and quantum fluctuations from a microscopic viewpoint. The quantum correction of the steady-state probability density function (PDF) is perturbatively evaluated, and is found to smoothen the non-Gaussian structure of the steady-state PDF. This behavior is qualitatively understood as the increase of an effective temperature. We have derived the inverse formula to infer the non-Gaussian noise from the steady-state PDF. The formula establishes a one-to-one correspondence between the PDF of the detector circuit and the current distribution in the mesoscopic conductor even in the classical-quantum crossover regime. The numerical results indicate that the quantum correction is essential to correctly estimate the statistical property of the current fluctuation.

As typical values of the bias voltage applied to quantum conductors are set to $|eV| \leq 50\mu eV \sim 12$GHz in shot-noise experiments, the resonant frequency of the detector we used is estimated as $\Omega \simeq 10$ MHz. If the QPC and the detector circuit are placed at sufficiently low temperature $T \simeq 10\text{mK} \sim 0.2$GHz to observe the quantum shot noise, the quantum-mechanical time scale is approximately given as $\tau \simeq 0.008$. Hence, the quantum correction is relevant for the realistic parameter region. We note that our analysis cannot be directly applied to the experiment which have tested the fluctuation theorem in a coherent Aharonov-Bohm ring [see [11] and section 1.4]. In order to reduce undesirable noises such as the $1/f$ and the random telegraph noises, the authors of Ref. [11] used the finite-frequency current fluctuation, which is not available in our setup. It is necessary to go beyond the quasistationary approximation to detect the current fluctuation in the dynamical regime [54, 55]. In this regime, the strong electromagnetic coupling between the conductor and the detector results in the dynamical Coulomb blockade [53]. Further studies are needed to tell whether the proper treatment of the quantum correction can explain the discrepancies between the theoretical predictions and the experimental results [11].

References

[1] J. P. Pekola, Nat. Phys. **11**, 118 (2015).

[2] Y. Blanter and M. Büttiker, Phys. Rep. **336** (2000).

[3] L. S. Levitov, H. Lee, and G. B. Lesovik, J. Math. Phys. **37**, 4845 (1996).

[4] Y. V. Nazarov and M. Kindermann, Euro. Phys. J. B **35**, 413 (2003).

[5] B. Reulet, J. Senzier, and D. Prober, Phys. Rev. Lett. **91**, 196601 (2003).

[6] G. Gershon, Y. Bomze, E. V. Sukhorukov, and M. Reznikov, Phys. Rev. Lett. **101**, 016803 (2008).

[7] J. Gabelli and B. Reulet, Phys. Rev. B **80**, 161203 (2009).

[8] T. Fujisawa, T. Hayashi, R. Tomita, and Y. Hirayama, Science **312**, 1634 (2006).

[9] S. Gustavsson, R. Leturcq, B. Simovič, R. Schleser, T. Ihn, P. Studerus, K. Ensslin, D. C. Driscoll, and A. C. Gossard, Phys. Rev. Lett. **96**, 076605 (2006).

[10] M. Esposito, U. Harbola, and S. Mukamel, Rev. Mod. Phys. **81**, 1665 (2009).

[11] S. Nakamura, Y. Yamauchi, M. Hashisaka, K. Chida, K. Kobayashi, T. Ono, R. Leturcq, K. Ensslin, K. Saito, Y. Utsumi, and A. C. Gossard, Phys. Rev. Lett. **104**, 080602 (2010).

[12] B. Küng, C. Rössler, M. Beck, M. Marthaler, D. S. Golubev, Y. Utsumi, T. Ihn, and K. Ensslin, Phys. Rev. X **2**, 011001 (2012).

[13] Y. Utsumi, D. S. Golubev, M. Marthaler, K. Saito, T. Fujisawa, and G. Schön, Phys. Rev. B **81**, 125331 (2010).

[14] S.-H. Ouyang, C.-H. Lam, and J. Q. You, Phys. Rev. B **81**, 075301 (2010).

[15] D. S. Golubev, Y. Utsumi, M. Marthaler, and G. Schön, Phys. Rev. B **84**, 075323 (2011).

[16] G. Bulnes Cuetara, M. Esposito, G. Schaller, and P. Gaspard, Phys. Rev. B **88**, 115134 (2013).

[17] C. W. J. Beenakker, M. Kindermann, and Y. V. Nazarov, Phys. Rev. Lett. **90**, 176802 (2003).

[18] Y. Utsumi, D. S. Golubev, M. Marthaler, G. Schön, and K. Kobayashi, Phys. Rev. B **86**, 075420 (2012).

[19] R. Aguado and L. P. Kouwenhoven, Phys. Rev. Lett. **84**, 1986 (2000).

[20] E. Onac, F. Balestro, L. H. W. van Beveren, U. Hartmann, Y. V. Nazarov, and L. P. Kouwenhoven, Phys. Rev. Lett. **96**, 176601 (2006).

[21] S. Gustavsson, M. Studer, R. Leturcq, T. Ihn, K. Ensslin, D. C. Driscoll, and A. C. Gossard, Phys. Rev. Lett. **99**, 206804 (2007).

[22] M. Hashisaka, Y. Yamauchi, S. Nakamura, S. Kasai, T. Ono, and K. Kobayashi, Phys. Rev. B **78**, 241303 (2008).

[23] N. Ubbelohde, C. Fricke, C. Flindt, F. Hohls, and R. J. Haug, Nat. Commun. **3**, 612 (2012).

[24] Y. Jompol, P. Roulleau, T. Jullien, B. Roche, I. Farrer, D. Ritchie, and D. Glattli, Nat. Commun. **6**, 6130 (2015).

[25] J. Tobiska and Y. V. Nazarov, Phys. Rev. Lett. **93**, 106801 (2004).

[26] J. P. Pekola, Phys. Rev. Lett. **93**, 206601 (2004).

[27] R. Deblock, E. Onac, L. Gurevich, and L. P. Kouwenhoven, Science **301**, 203 (2003).

[28] T. T. Heikkilä, P. Virtanen, G. Johansson, and F. K. Wilhelm, Phys. Rev. Lett. **93**, 247005 (2004).

[29] E. Onac, F. Balestro, B. Trauzettel, C. F. J. Lodewijk, and L. P. Kouwenhoven, Phys. Rev. Lett. **96**, 026803 (2006).

[30] P.-M. Billangeon, F. Pierre, H. Bouchiat, and R. Deblock, Phys. Rev. Lett. **96**, 136804 (2006).

[31] G. Lesovik, JETP Lett. **60**, 820 (1994).

[32] T. Ojanen and T. T. Heikkilä, Phys. Rev. B **73**, 020501 (2006).

[33] U. Gavish, Y. Levinson, and Y. Imry, Phys. Rev. B **62**, R10637 (2000).

[34] G. Lesovik and R. Loosen, JETP Lett. **65**, 295 (1997).

[35] M. Creux, A. Crépieux, and T. Martin, Phys. Rev. B **74**, 115323 (2006).

[36] A. Zazunov, M. Creux, E. Paladino, A. Crépieux, and T. Martin, Phys. Rev. Lett. **99**, 066601 (2007).

[37] D. Chevallier, T. Jonckheere, E. Paladino, G. Falci, and T. Martin, Phys. Rev. B **81**, 205411 (2010).

[38] K. Kanazawa, T. G. Sano, T. Sagawa, and H. Hayakawa, Phys. Rev. Lett. **114**, 090601 (2015).

[39] K. Kanazawa, T. G. Sano, T. Sagawa, and H. Hayakawa, J. Stat. Phys. **160**, 1294 (2015).

[40] K. Kanazawa, T. Sagawa, and H. Hayakawa, Phys. Rev. Lett. **108**, 210601 (2012).

[41] J. Johansson, S. Saito, T. Meno, H. Nakano, M. Ueda, K. Semba, and H. Takayanagi, Phys. Rev. Lett. **96**, 127006 (2006).

[42] I. Chiorescu, P. Bertet, K. Semba, Y. Nakamura, C. Harmans, and J. Mooij, Nature **431**, 159 (2004).

[43] V. E. Manucharyan, J. Koch, L. I. Glazman, and M. H. Devoret, Science **326**, 113 (2009).

[44] J. Basset, H. Bouchiat, and R. Deblock, Phys. Rev. Lett. **105**, 166801 (2010).

[45] A. A. Houck, H. E. Türeci, and J. Koch, Nat. Phys. **8**, 292 (2012).

[46] J. Basset, A. Y. Kasumov, C. P. Moca, G. Zaránd, P. Simon, H. Bouchiat, and R. Deblock, Phys. Rev. Lett. **108**, 046802 (2012).

[47] U. Weiss, *Quantum dissipative systems*, Vol. 10 (World Scientific, 1999).

[48] A. O. Caldeira and A. J. Leggett, Physica A **121**, 587 (1983).

[49] K. Chou, Z. Su, B. Hao, and L. Yu, Phys. Rep. **118**, 1 (1985).

[50] A. Kamenev, *Field theory of non-equilibrium systems* (Cambridge University Press, 2011).

[51] S. Pilgram, A. N. Jordan, E. V. Sukhorukov, and M. Büttiker, Phys. Rev. Lett. **90**, 206801 (2003).

[52] Y. Nazarov, Ann. Phys. (Leipzig) **16**, 720 (2007).

[53] H. Grabert and M. H. Devoret, *Single charge tunneling: Coulomb blockade phenomena in nanostructures*, Vol. 294 (Springer Science & Business Media, 2013).

[54] J. Gabelli, G. Fève, J.-M. Berroir, B. Plaçais, A. Cavanna, B. Etienne, Y. Jin, and D. Glattli, Science **313**, 499 (2006).

[55] E. Bocquillon, V. Freulon, J.-M. Berroir, P. Degiovanni, B. Plaçais, A. Cavanna, Y. Jin, and G. Feve, Science **339**, 1054 (2013).

Chapter 5

Current noise of a charge-fluctuating quantum dot system

Remarkable advance in nanotechnology enables us to investigate the non-linear transport in interacting systems. Among mesoscopic conductors, quantum dot systems offer experimentally well-controlled situations to study the interplay of nonequilibrium fields and two-body interaction. The interacting resonant-level model (IRLM), which was originally introduced as a variant of the Kondo model [1], is an archetypal model to describe a quantum dot dominated by the charge fluctuations. The nontrivial transport property which has been confirmed by a vast amount of works on the IRLM [2–9] is the appearance of universal power-law behavior in the nonlinear regime. In the scaling regime, where the lead bandwidth Δ is much larger than any other energy scales, the I-V characteristic shows a power-law decay whose exponent depends on the strength of the two-body interaction [2–4, 6–9]. This is a consequence of a renormalization effect due to the charge fluctuation in the quantum dot system.

While a unified understanding on the current through the IRLM has been established, the research of the current fluctuation has been just started recently. A perturbative approach based on the Keldysh technique was put forward in Ref. [10] to understand the current noise. Important insights for the noise were gained at a special parameter point where the model has self-duality [11]. With the aid of this symmetry, the IRLM can be mapped to a solvable model even under a finite bias voltage [4]. The analysis on the shot noise using field-theoretic techniques and the density-matrix renormalization-group method consistently indicates that the quasi-particles with the effective charge $e^* = 2e$ are formed at the self-dual point [12–14]. This is in clear contrast to the noninteracting limit $e^* = e$. Away from the self-dual point, the bias-voltage dependence of the current noise of the IRLM is still an open question. In addition, finite-temperature effects have not been investigated so far. Considering this situation, it is strongly desirable to clarify the current noise through the IRLM in general parameter regions.

In this chapter, we study a renormalization effect on the current noise of the IRLM in wide parameter regions using the nonequilibrium functional renormalization group (FRG) method [15]. Logarithmic divergences, which are major obstacles to go deep into the scaling regime, are consistently removed in the FRG framework [6, 7]. It is also found that the renormalization of the hopping between the dot and the leads can be described using a surprisingly simple approximation [6]. In this chapter, we obtain and solve the

flow equations of the current vertex functions (2.159) to determine the current noise. For the on-resonance transport, an artificial divergence of the vertex correction found in plain perturbation theory with respect to the interaction is consistently removed in our FRG scheme. Away from the particle-hole symmetric point, a severe divergence which occurs in the perturbation theory when the dot energy level is aligned with the chemical potentials is shifted to higher orders. These achievements allow us to gain a comprehensive picture of the zero-frequency current noise in the scaling limit. We show that the current noise is governed by a universal power-law scaling in the large bias-voltage regime with an exponent which, to the leading order in the interaction, is the same as that of the current. The temperature dependence of the current noise is incorporated consistently with the fluctuation-dissipation theorem. In addition, the effective charge is discussed by combining analytic considerations with numerical results of the vertex correction. We conclude that $e^* = e\left[1+\mathcal{O}(u^2)\right]$ with the dimensionless amplitude of the interaction u.

This chapter is organized as follows. In section 5.1, we describe the model and the FRG scheme to compute the current noise. In section. 5.2, the results for the noise are presented. A discussion of the results is given in Sec. 5.3.

5.1 Model and formalism

5.1.1 Model

We consider the charge-fluctuating quantum dot system without the spin degrees of freedom. The minimal interaction in this situation is the Coulomb interaction between the spinless fermion in the quantum dot and those in the leads. The interacting resonant level model (IRLM) describes such a localized fermion capacitively coupled to delocalized ones in the left and right leads (see Fig. 5.1). In the following discussions, we use a three-site system, in which a fermion in the quantum dot, i.e. the central site, feels the interaction with those in adjacent ones. The hopping amplitudes $t_{\alpha=L,R}$ between the three-site region and the leads are assumed to be much larger than the inter-site one t such that the left (right) site is effectively incorporated into the left (right) lead. The single-site model studied in [1] is recovered in this limit [6, 7, 16, 17]. The action of the IRLM is given by

$$\begin{aligned} S = &\sum_{i,j=1}^{3}\int dzdz'\bar{d}_i(z)\boldsymbol{g}^{-1}_{dij}(z,z')d_j(z') + \sum_{\alpha=L,R}\sum_{\boldsymbol{k}}\int dzdz'\bar{c}_{\alpha\boldsymbol{k}}(z)g^{-1}_{\alpha\boldsymbol{k}}(z,z')c_{\alpha\boldsymbol{k}}(z') \\ &-\frac{1}{\sqrt{N}}\sum_{\boldsymbol{k}}\int dz\Big[t_L\bar{d}_1(z)c_{L\boldsymbol{k}}(z)+t_R\bar{d}_3(z)c_{R\boldsymbol{k}}(z)+\text{H.c.}\Big]+S_U. \end{aligned} \tag{5.1}$$

The Grassmann fields $\bar{d}_i(z)$ ($d_i(z)$) defined on the Keldysh contour C (Fig. 2.1) create [annihilate] a spinless fermion on the site i. The creating and annihilating Grassmann fields of the delocalized fermions in the lead α with the momentum $\boldsymbol{k}$ are denoted by $\bar{c}_{\alpha\boldsymbol{k}}(z)$ and $c_{\alpha\boldsymbol{k}}(z)$, respectively. The retarded component of the Green's functions of the isolated dot is

$$\left(\boldsymbol{g}^{\mathrm{r}}_d\right)^{-1}(\omega) = \begin{pmatrix} \omega+U/2 & -t & 0 \\ -t & i\frac{d}{dz'}-(\varepsilon-U) & -t \\ 0 & -t & \omega+U/2 \end{pmatrix}. \tag{5.2}$$

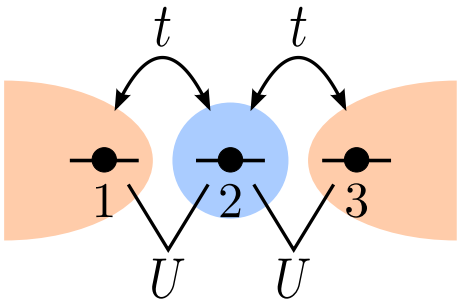

Fig. 5.1 Schematic of the interacting resonant level model (IRLM).

The energy level of the localized site and its hopping amplitude with adjacent sites are denoted by ε and t, respectively. The energy level ε is defined such that $\varepsilon = 0$ corresponds to the particle-hole symmetric case. The third term of the action Eq. (5.1) describes the hopping between the three-site region and the leads with N sites. As was discussed in subsection 2.3.1, the lesser component of the isolated three-site system is irrelevant in the steady-state. The retarded and lesser Green's functions for the noninteracting delocalized fermion are given by Eqs. (2.74) and (2.75), respectively. We use units with $k_B = 1$ and $\hbar = 1$ and elementary charge $e = 1$. The interaction part is given by

$$S_U \equiv -U \int dz \left(\bar{d}_2(z) d_2(z) \bar{d}_1(z) d_1(z) + \bar{d}_2(z) d_2(z) \bar{d}_3(z) d_3(z) \right). \tag{5.3}$$

The noninteracting reservoirs can be integrated out yielding the action

$$S = \sum_{i,j=1}^{3} \int dz dz' \bar{d}_i(z) \boldsymbol{G}_{0ij}^{-1}(z,z') d_j(z') + S_U, \tag{5.4}$$

where $\boldsymbol{G}_0^{-1}(z,z') \equiv \boldsymbol{g}_d^{-1}(z,z') - \boldsymbol{\Sigma}_0^{-1}(z,z')$. The tunneling self-energy is given as

$$\boldsymbol{\Sigma}_0(z,z') = \begin{pmatrix} \Sigma_L(z,z') & 0 & 0 \\ 0 & 0 & 0 \\ 0 & 0 & \Sigma_R(z,z') \end{pmatrix}, \tag{5.5}$$

with Eq. (2.101). We suppose that a bias voltage V is applied symmetrically to the equilibrium leads at the inverse temperature β. The Fermi-Dirac distribution is given by $f_\alpha(\omega) = 1/(e^{\beta(\omega-\mu_\alpha)}+1)$, where the chemical potentials are $\mu_L = \varepsilon_F + V/2$ and $\mu_R = \varepsilon_F - V/2$ with the Fermi energy ε_F. The Fourier transforms of the tunneling self-energies are obtained as

$$\boldsymbol{\Sigma}_0^{\mathrm{r}}(\omega) = \begin{pmatrix} -\frac{i\Delta_L}{2} & 0 & 0 \\ 0 & 0 & 0 \\ 0 & 0 & -\frac{i\Delta_R}{2} \end{pmatrix}, \tag{5.6}$$

$$\boldsymbol{\Sigma}_0^{\mathrm{K}}(\omega) = \begin{pmatrix} i\Delta_L(2f_L(\omega)-1) & 0 & 0 \\ 0 & 0 & 0 \\ 0 & 0 & i\Delta_R(2f_R(\omega)-1) \end{pmatrix}. \tag{5.7}$$

Here, we suppose that the bandwidth $\Delta_\alpha \equiv 2\pi\rho_\alpha t_\alpha^2$ with the frequency-independent density of states ρ_α. For simplicity, we assume $\Delta_L = \Delta_R \equiv \Delta$. As the particle-hole symmetry $\varepsilon = 0$ corresponds to the resonant transport, we often refer to this case as the on-resonance situation.

5.1.2 Functional renormalization group approach

Reservoir cutoff scheme

In setting up the functional renormalization group approach discussed in subsection 2.4.4, we utilize the reservoir-cutoff scheme [16, 17]. One of the most crucial advantage of this scheme is that the KMS condition is automatically satisfied, enabling the calculations consistent with the fluctuation-dissipation theorem. In the reservoir-cutoff scheme, the regulator function R_Λ [see Eq. (2.141)] is introduced as

$$\boldsymbol{R}^{\mathrm{r}}_\Lambda(\omega) = \frac{i\Lambda}{2}\mathbf{1}, \tag{5.8}$$

$$\boldsymbol{R}^{\mathrm{K}}_\Lambda(\omega) = -i\Lambda\left[2f_{\mathrm{aux}}(\omega) - 1\right]\mathbf{1}, \tag{5.9}$$

where $f_{\mathrm{aux}}(\omega)$ is the Fermi-Dirac distribution function at the inverse temperature β_{aux} and $\mathbf{1}$ is the identity matrix of dimension three. This prescription is equivalent to consider additional structureless reservoirs (see Fig. 5.2). It was shown in the previous work [18, 19] that results for the current are independent of the choice of β_{aux}. In the following, we use the auxiliary reservoirs at infinite temperature, i.e. $f_{\mathrm{aux}}(\omega) = 1/2$, so that the Keldysh component of the regulator function vanishes. The full Green's function with the interaction-induced self-energy $\boldsymbol{\Sigma}_{U,\Lambda}$ is obtained by the Dyson equation

$$\left(\boldsymbol{G}^{\mathrm{r}}_\Lambda\right)^{-1}(\omega) = \left(\boldsymbol{G}^{\mathrm{r}}_0\right)^{-1}(\omega) + \boldsymbol{R}^{\mathrm{r}}_\Lambda(\omega) - \boldsymbol{\Sigma}^{\mathrm{r}}_{U,\Lambda}(\omega), \tag{5.10}$$

$$\boldsymbol{G}^{\mathrm{K}}_\Lambda(\omega) = \boldsymbol{G}^{\mathrm{r}}_\Lambda(\omega)\left[\boldsymbol{\Sigma}^{\mathrm{K}}_0(\omega) + \boldsymbol{\Sigma}^{\mathrm{K}}_{U,\Lambda}(\omega)\right]\boldsymbol{G}^{\mathrm{a}}_\Lambda(\omega). \tag{5.11}$$

The retarded and the Keldysh components of the scale-dependent propagator $\boldsymbol{S}_\Lambda(z, z')$ [see Eq. (2.156)] are obtained as

$$\boldsymbol{S}^{\mathrm{r}}_\Lambda(\omega) = \frac{-i}{2}\boldsymbol{G}^{\mathrm{r}}_\Lambda(\omega)\boldsymbol{G}^{\mathrm{r}}_\Lambda(\omega), \tag{5.12}$$

$$\boldsymbol{S}^{\mathrm{K}}_\Lambda(\omega) = \frac{-i}{2}\boldsymbol{G}^{\mathrm{r}}_\Lambda(\omega)\boldsymbol{G}^{\mathrm{K}}_\Lambda(\omega) + \frac{i}{2}\boldsymbol{G}^{\mathrm{K}}_\Lambda(\omega)\boldsymbol{G}^{\mathrm{a}}_\Lambda(\omega). \tag{5.13}$$

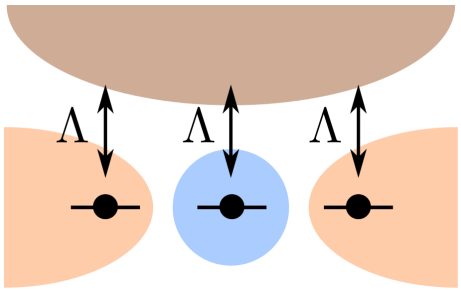

Fig. 5.2 Reservoir-cutoff scheme.

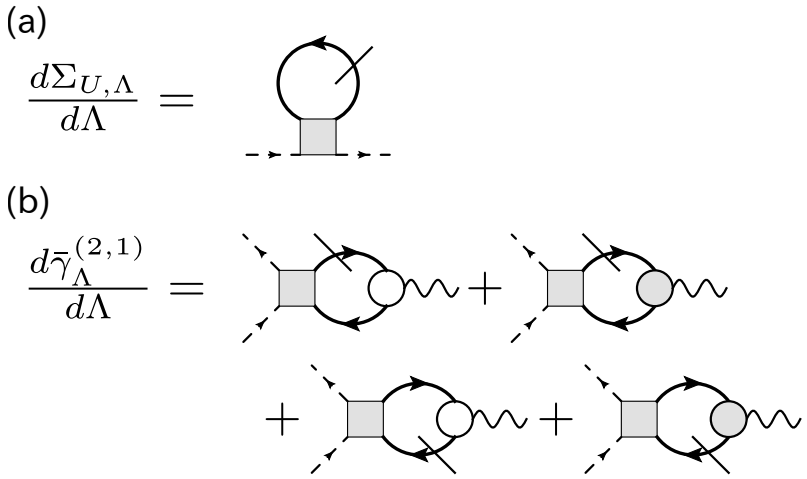

Fig. 5.3 Diagrammatic representation of the flow equations of (a) the self-energy and (b) the three-point current-vertex function in the static approximation. The gray square represents the bare two-particle interaction. The open and gray circles are diagrammatic representations of the bare and the dressed three-point current vertex functions, respectively. The inner line denotes the Green's function $\boldsymbol{G}_\Lambda$ while the slashed one denotes the scale-dependent propagator $\boldsymbol{S}_\Lambda$.

Truncation of the flow equation

In order to implement numerical calculations, we need to truncate the infinite hierarchy of the flow equations (2.152). In the following, we use the lowest-order truncation, which is known as the static approximation [15], to determine the flow equations of the self-energy and current-vertex functions. We consider the Hartree-Fock-type diagram for the self-energy and the RPA-type diagram for the vertex function [see Fig. 5.3]. In the static approximation, the flow equation of the four-point vertex function is ignored, and its value is replaced by the anti-symmetrized bare two-particle interaction $U_{ik;jl}$. In spite of its simplicity, this truncation for the self-energy is known to describe rich properties of the I-V characteristics due to the built-in renormalization effect [15]. In particular, logarithmic divergences found in the plain perturbation theory are consistently resummed to power laws [6]. Hence, we expect that it is a good starting point to examine the current noise by solving the flow equation of the current vertex functions within the static approximation. We note that higher-order corrections can be systematically included in principle by incorporating flow equations of higher-order vertices.

The flow equation of the self-energy is obtained as

$$\frac{d}{d\Lambda}\left(\boldsymbol{\Sigma}^{\mathrm{r}}_{U,\Lambda}\right)_{ij} = \frac{iU_{ik;jl}}{2}\int\frac{d\omega}{2\pi}\left(\boldsymbol{S}^{\mathrm{K}}_{\Lambda}\right)_{lk}(\omega). \tag{5.14}$$

Within the present approximation, the self-energy is independent of the frequency due to the structure of the right-hand side. Hence, the single-particle Green's functions can be interpreted as effective noninteracting ones with renormalized parameters.

As we are interested in the current fluctuation in the steady state, we focus on the vertex functions related with the current from the left reservoir to the quantum dot region. The flow equation of the retarded component of the interaction-induced part of the three-point

vertex function (2.123) is given by

$$\frac{d}{d\Lambda}\left(\bar{\boldsymbol{\gamma}}_{\Lambda}^{(2,1)}\right)_{ij;L}^{\mathrm{r;s}} = \frac{iU_{ik;jl}}{2}\left[\left(\boldsymbol{\Phi}_{\Lambda}^{(2,1)}\right)_{lk}^{\mathrm{K}} + \left(\boldsymbol{\Phi}_{\Lambda}^{(2,1)}\right)_{lk}^{\tilde{\mathrm{K}}}\right], \tag{5.15}$$

with

$$\begin{aligned}\left(\boldsymbol{\Phi}_{\Lambda}^{(2,1)}\right)^{\mathrm{K}} \equiv \int\frac{d\omega}{2\pi}\Big[&\boldsymbol{S}_{\Lambda}^{\mathrm{r}}(\omega)\left(\boldsymbol{\gamma}_{\Lambda}^{(2,1)}\right)_{;L}^{\mathrm{r;s}}\boldsymbol{G}_{\Lambda}^{\mathrm{K}}(\omega) + \boldsymbol{S}_{\Lambda}^{\mathrm{K}}(\omega)\left(\boldsymbol{\gamma}_{\Lambda}^{(2,1)}\right)_{;L}^{\mathrm{a;s}}\boldsymbol{G}_{\Lambda}^{\mathrm{a}}(\omega)\\ &+\boldsymbol{S}_{\Lambda}^{\mathrm{r}}(\omega)\left(\boldsymbol{\gamma}_{\Lambda}^{(2,1)}\right)_{;L}^{\mathrm{K;s}}\boldsymbol{G}_{\Lambda}^{\mathrm{a}}(\omega) + \boldsymbol{S}_{\Lambda}^{\mathrm{K}}(\omega)\left(\boldsymbol{\gamma}_{\Lambda}^{(2,1)}\right)_{;L}^{\tilde{\mathrm{K}};\mathrm{s}}\boldsymbol{G}_{\Lambda}^{\mathrm{K}}(\omega) + (\boldsymbol{S}\leftrightarrow\boldsymbol{G})\Big],\end{aligned} \tag{5.16}$$

and

$$\left(\boldsymbol{\Phi}_{\Lambda}^{(2,1)}\right)^{\tilde{\mathrm{K}}} \equiv \int\frac{d\omega}{2\pi}\left[\boldsymbol{S}_{\Lambda}^{\mathrm{a}}(\omega)\left(\boldsymbol{\gamma}_{\Lambda}^{(2,1)}\right)_{;L}^{\tilde{\mathrm{K}};s}\boldsymbol{G}_{\Lambda}^{\mathrm{r}}(\omega) + (\boldsymbol{S}\leftrightarrow\boldsymbol{G})\right]. \tag{5.17}$$

The abbreviation $(\boldsymbol{S}\leftrightarrow\boldsymbol{G})$ denotes the terms which are obtained by mutually replacing $\boldsymbol{S}$ and $\boldsymbol{G}$ in the preceding ones in the same parentheses. Similarly, the flow equation of the Keldysh component is obtained as

$$\frac{d}{d\Lambda}\left(\bar{\boldsymbol{\gamma}}_{\Lambda}^{(2,1)}\right)_{ij;L}^{\mathrm{K;s}} = \frac{iU_{ik;jl}}{2}\left[\left(\boldsymbol{\Phi}_{\Lambda}^{(2,1)}\right)_{lk}^{\mathrm{r}} + \left(\boldsymbol{\Phi}_{\Lambda}^{(2,1)}\right)_{lk}^{\mathrm{a}}\right], \tag{5.18}$$

with

$$\left(\boldsymbol{\Phi}_{\Lambda}^{(2,1)}\right)^{\mathrm{r}} \equiv \int\frac{d\omega}{2\pi}\left[\boldsymbol{S}_{\Lambda}^{\mathrm{r}}(\omega)\left(\boldsymbol{\gamma}_{\Lambda}^{(2,1)}\right)_{;L}^{\mathrm{r;s}}\boldsymbol{G}_{\Lambda}^{\mathrm{r}}(\omega) + \boldsymbol{S}_{\Lambda}^{\mathrm{K}}(\omega)\left(\boldsymbol{\gamma}_{\Lambda}^{(2,1)}\right)_{;L}^{\tilde{\mathrm{K}};\mathrm{s}}\boldsymbol{G}_{\Lambda}^{\mathrm{r}}(\omega) + (\boldsymbol{S}\leftrightarrow\boldsymbol{G})\right], \tag{5.19}$$

$$\left(\boldsymbol{\Phi}_{\Lambda}^{(2,1)}\right)^{\mathrm{a}} \equiv \int\frac{d\omega}{2\pi}\left[\boldsymbol{S}_{\Lambda}^{\mathrm{a}}(\omega)\left(\boldsymbol{\gamma}_{\Lambda}^{(2,1)}\right)_{;L}^{\mathrm{a;s}}\boldsymbol{G}_{\Lambda}^{\mathrm{a}}(\omega) + \boldsymbol{S}_{\Lambda}^{\mathrm{a}}(\omega)\left(\boldsymbol{\gamma}_{\Lambda}^{(2,1)}\right)_{;L}^{\tilde{\mathrm{K}};\mathrm{s}}\boldsymbol{G}_{\Lambda}^{\mathrm{K}}(\omega) + (\boldsymbol{S}\leftrightarrow\boldsymbol{G})\right]. \tag{5.20}$$

The argument of the three-point vertex functions is omitted as these turn out to be independent of the frequency in the static approximation. In contrast to the self-energy, these vertex functions do not have a simple interpretation in reference to a noninteracting model.

Using the initial condition and the flow equation, we can prove the symmetry relations for the three-point current-vertex functions;

$$\left[\left(\boldsymbol{\gamma}_{\Lambda}^{(2,1)}\right)_{ij;L}^{\mathrm{r;s}}\right]^{*} = -\left(\boldsymbol{\gamma}_{\Lambda}^{(2,1)}\right)_{ji;L}^{\mathrm{a;s}}, \tag{5.21}$$

$$\left[\left(\boldsymbol{\gamma}_{\Lambda}^{(2,1)}\right)_{ij;L}^{\mathrm{K;s}}\right]^{*} = \left(\boldsymbol{\gamma}_{\Lambda}^{(2,1)}\right)_{ji;L}^{\mathrm{K;s}}, \tag{5.22}$$

$$\left[\left(\boldsymbol{\gamma}_{\Lambda}^{(2,1)}\right)_{ij;L}^{\tilde{\mathrm{K}};\mathrm{s}}\right]^{*} = \left(\boldsymbol{\gamma}_{\Lambda}^{(2,1)}\right)_{ji;L}^{\tilde{\mathrm{K}};\mathrm{s}}. \tag{5.23}$$

In the static approximation, we can derive the additional relations

$$\left(\bar{\boldsymbol{\gamma}}_{\Lambda}^{(2,1)}\right)^{\mathrm{r;s}}_{ij;L} = \left(\bar{\boldsymbol{\gamma}}_{\Lambda}^{(2,1)}\right)^{\mathrm{a;s}}_{ij;L}, \tag{5.24}$$

$$\left(\bar{\boldsymbol{\gamma}}_{\Lambda}^{(2,1)}\right)^{\mathrm{K;s}}_{ij;L} = \left(\bar{\boldsymbol{\gamma}}_{\Lambda}^{(2,1)}\right)^{\tilde{\mathrm{K}};\mathrm{s}}_{ij;L}. \tag{5.25}$$

Hence, it is sufficient to determine the retarded and the Keldysh components of the three-point vertex function.

We determine the self-energy and the three-point current-vertex functions by solving these flow equations numerically, and use the functions at $\Lambda = 0$ in the formula of the current noise given in Eqs. (2.130)-(2.134).

Initial condition

We consider the model with $\Lambda_{\mathrm{init}} \to \infty$ as the initial one of the flow as all the vertex functions defined in Eq. (2.120) can be calculated exactly in this limit. The initial conditions of the self-energy and the vertex functions are computed in the following. The set of coupled flow equations has to be integrated down to $\Lambda = 0$ at which the auxiliary reservoirs are decoupled and the original model is restored.

The initial condition of the self-energy for $\Lambda_{\mathrm{init}} \to \infty$ is written as

$$\left(\boldsymbol{\Sigma}^{\mathrm{r}}_{U,\Lambda_{\mathrm{init}}}\right)_{11}(\omega) = U_1 n_2, \tag{5.26}$$

$$\left(\boldsymbol{\Sigma}^{\mathrm{r}}_{U,\Lambda_{\mathrm{init}}}\right)_{22}(\omega) = U_1 n_1 + U_3 n_3, \tag{5.27}$$

$$\left(\boldsymbol{\Sigma}^{\mathrm{r}}_{U,\Lambda_{\mathrm{init}}}\right)_{33}(\omega) = U_3 n_2, \tag{5.28}$$

$$\left(\boldsymbol{\Sigma}^{\mathrm{K}}_{U,\Lambda_{\mathrm{init}}}\right)_{ij}(\omega) = 0, \tag{5.29}$$

where n_i is the occupation of the ith site.

As all the internal propagator is suppressed in the limit of $\Lambda_{\mathrm{init}} \to \infty$, the initial current-vertex functions are identical to those of the noninteracting system;

$$\left(\boldsymbol{\gamma}^{(2,n)}_{\Lambda_{\mathrm{init}}}\right)^{\rho_1'\rho_1;\mathrm{s}\cdots\mathrm{s}}_{ij;\alpha_1\cdots\alpha_n}(t_1',t_1;t_1''\cdots t_n'') = \left(\boldsymbol{\gamma}^{(2,n)}_{0}\right)^{\rho_1'\rho_1;\mathrm{s}\cdots\mathrm{s}}_{ij;\alpha_1\cdots\alpha_n}(t_1',t_1;t_1''\cdots t_n'') \quad (\text{for } n>0). \tag{5.30}$$

The noninteracting current-vertex functions can be determined using the Ward-Takahashi identity

$$\left(\boldsymbol{\gamma}^{(2,1)}_{0}\right)_{11;L}(z',z;z'') = i\left[\delta(z',z'') - \delta(z,z'')\right](\boldsymbol{\Sigma}_0)_{11}(z',z). \tag{5.31}$$

The other components of the three-point vertex functions are zero because the source field $A_L(z)$ is only included in the (1,1)-component of the tunneling self-energy Eq. (5.5). The

initial conditions of the three-point current-vertex functions are obtained as

$$\left(\boldsymbol{\gamma}^{(2,1)}_{\Lambda_{\rm init}}\right)^{\rm r;s}_{ij;\alpha_1}(\omega_1,\omega_1;0) = -\delta_{i1}\delta_{j1}\delta_{\alpha_1 L}\Delta_L(1-2f_L(\omega_1)), \tag{5.32}$$

$$\left(\boldsymbol{\gamma}^{(2,1)}_{\Lambda_{\rm init}}\right)^{\rm a;s}_{ij;\alpha_1}(\omega_1,\omega_1;0) = \delta_{i1}\delta_{j1}\delta_{\alpha_1 L}\Delta_L(1-2f_L(\omega_1)), \tag{5.33}$$

$$\left(\boldsymbol{\gamma}^{(2,1)}_{\Lambda_{\rm init}}\right)^{\rm K;s}_{ij;\alpha_1}(\omega_1,\omega_1;0) = -\delta_{i1}\delta_{j1}\delta_{\alpha_1 L}\Delta_L, \tag{5.34}$$

$$\left(\boldsymbol{\gamma}^{(2,1)}_{\Lambda_{\rm init}}\right)^{\tilde{\rm K};{\rm s}}_{ij;\alpha_1}(\omega_1,\omega_1;0) = \delta_{i1}\delta_{j1}\delta_{\alpha_1 L}\Delta_L. \tag{5.35}$$

Here, we show only the case with $\omega_1 = \omega_1'$ because we focus on the zero-frequency current noise in this chapter. We note that $\left(\boldsymbol{\gamma}^{(2,1)}_{\Lambda_{\rm init}}\right)^{\tilde{\rm K};{\rm s}}$ does not need to be zero. The multi-point current vertices are determined by recursively using the Ward-Takahashi identity, and the initial conditions for four-point current-vertex functions are

$$\left(\boldsymbol{\gamma}^{(2,2)}_{\Lambda_{\rm init}}\right)^{\rm r;ss}_{ij;\alpha_1\alpha_2}(\omega_1,\omega_1;0,0) = 2i\delta_{i1}\delta_{j1}\delta_{\alpha_1 L}\delta_{\alpha_2 L}\Delta_L, \tag{5.36}$$

$$\left(\boldsymbol{\gamma}^{(2,2)}_{\Lambda_{\rm init}}\right)^{\rm a;ss}_{ij;\alpha_1\alpha_2}(\omega_1,\omega_1;0,0) = -2i\delta_{i1}\delta_{j1}\delta_{\alpha_1 L}\delta_{\alpha_2 L}\Delta_L, \tag{5.37}$$

$$\left(\boldsymbol{\gamma}^{(2,2)}_{\Lambda_{\rm init}}\right)^{\rm K;ss}_{ij;\alpha_1\alpha_2}(\omega_1,\omega_1;0,0) = 2i\delta_{i1}\delta_{j1}\delta_{\alpha_1 L}\delta_{\alpha_2 L}\Delta_L(1-2f_L(\omega_1)), \tag{5.38}$$

$$\left(\boldsymbol{\gamma}^{(2,2)}_{\Lambda_{\rm init}}\right)^{\tilde{\rm K};{\rm ss}}_{ij;\alpha_1\alpha_2}(\omega_1,\omega_1;0,0) = -2i\delta_{i1}\delta_{j1}\delta_{\alpha_1 L}\delta_{\alpha_2 L}\Delta_L(1-2f_L(\omega_1)). \tag{5.39}$$

The initial conditions of the four-point and higher-point vertex functions are determined by the bare action. If we denote the anti-symmetrized bare two-particle interaction [20] by $U_{ij;kl}$, these vertex functions are written as

$$\left(\boldsymbol{\gamma}^{(4,0)}_{\Lambda_{\rm init}}\right)^{\rho_1'\rho_2';\rho_1\rho_2}_{ij;kl}(\omega_1',\omega_2';\omega_1,\omega_1'+\omega_2'-\omega_1) = \begin{cases} -\rho_1' U_{ij;kl} & \text{if } \rho_1'=\rho_2'=\rho_1=\rho_2, \\ 0 & \text{otherwise.} \end{cases} \tag{5.40}$$

$$\left(\boldsymbol{\gamma}^{(4,m)}_{\Lambda_{\rm init}}\right)^{\rho_1'\rho_2';\rho_1\rho_2;\rho_1''\cdots\rho_m''}_{ij;kl;\alpha_1\cdots\alpha_m}(\omega_1',\omega_2';\omega_1,\omega_2;\omega_1'',\cdots,\omega_m'') = 0 \ \ (m>0). \tag{5.41}$$

5.2 Results

In the following discussions, we focus on the scaling regime where the bandwidth Δ is much larger than any other energy scales. It was established by earlier studies that the universal features of the steady-state current, such as the power-law behavior at large bias voltages, manifest themselves in the scaling limit [2–4, 6–9]. The characteristic energy scale governing the low-energy physics of the IRLM is introduced as $T_{\rm K} \equiv 8|\bar{t}^{\rm ren}|^2/\Delta$ with the renormalized hopping amplitude $\bar{t}^{\rm ren} \equiv t + \boldsymbol{\Sigma}^{\rm r}_{12}|_{T=V=\varepsilon=0}$ obtained at the end of the flow (see e.g. Ref. [6]). An alternative definition of the scale using the susceptibility is discussed in Appendix 5.A. The current shows a crossover from the linear-response regime to a power-law decay at $V \simeq T_{\rm K}$ [4, 6].

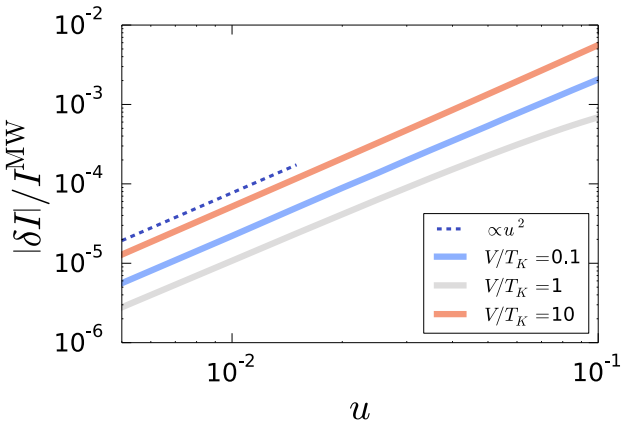

Fig. 5.4 The dependence of δI on the dimensionless interaction u for various values of V/T_{K}. The parameters are set to $t/\Delta = 0.001$, $\varepsilon/T_{\mathrm{K}} = 0$, and $T/T_{\mathrm{K}} = 0$.

5.2.1 Consistency with the Meir-Wingreen formula

A standard approach to compute the current through an interacting system is to use the Meir-Wingreen formula with the self-energy [21]. In this subsection, it is shown that an alternative FRG formulation can be developed by solving the flow equation for the current (2.160). We show that the current thus determined is indeed consistent with the results with the Meir-Wingreen formula up to the controlled order. As the three-point current-vertex functions enter the flow equation for the current, this consistency validates our reformulation of the transport in terms of the FRG approach.

The explicit expression of the current using the Meir-Wingreen formula is given as

$$I_\Lambda^{\mathrm{MW}} = \frac{1}{2\pi}\int d\omega \left[T_{LR}^\Lambda(\omega)(f_L(\omega)-f_R(\omega)) + T_{L\mathrm{aux}}^\Lambda(\omega)(f_L(\omega)-f_{\mathrm{aux}}(\omega))\right], \tag{5.42}$$

with

$$T_{LR}^\Lambda(\omega) = \Delta_L\Delta_R\,(\boldsymbol{G}_\Lambda^{\mathrm{r}})_{13}(\omega)\,(\boldsymbol{G}_\Lambda^{\mathrm{a}})_{31}(\omega), \tag{5.43}$$

$$T_{L\mathrm{aux}}^\Lambda(\omega) = \Delta_L\Lambda\,(\boldsymbol{G}_\Lambda^{\mathrm{r}}\boldsymbol{G}_\Lambda^{\mathrm{a}})_{11}(\omega). \tag{5.44}$$

This should be equivalent to the current obtained by solving its flow equation, which is denoted by $I_\Lambda^{\mathrm{flow}}$. If we denote their difference by $\delta I_\Lambda \equiv I_\Lambda^{\mathrm{MW}} - I_\Lambda^{\mathrm{flow}}$, its flow equation is given by

$$\begin{aligned}\frac{d\delta I_\Lambda}{d\Lambda} = \frac{-i}{2}\int\frac{d\omega}{2\pi}\Bigg[&(\boldsymbol{S}_\Lambda)_{ij}^{\mathrm{r}}\left(\bar{\boldsymbol{\gamma}}_\Lambda^{(2,1)}\right)_{ji;L}^{\mathrm{r;s}} + (\boldsymbol{S}_\Lambda)_{ij}^{\mathrm{a}}\left(\bar{\boldsymbol{\gamma}}_\Lambda^{(2,1)}\right)_{ji;L}^{\mathrm{a;s}} + (\boldsymbol{S}_\Lambda)_{ij}^{\mathrm{K}}\left(\bar{\boldsymbol{\gamma}}_\Lambda^{(2,1)}\right)_{ji;L}^{\tilde{\mathrm{K}};\mathrm{s}} \\ &- \Delta_L(2f_L-1)\left(\boldsymbol{G}_\Lambda^{\mathrm{r}}\frac{d\boldsymbol{\Sigma}_U^{\mathrm{r}}}{d\Lambda}\boldsymbol{G}_\Lambda^{\mathrm{r}} - \boldsymbol{G}_\Lambda^{\mathrm{a}}\frac{d\boldsymbol{\Sigma}_U^{\mathrm{a}}}{d\Lambda}\boldsymbol{G}_\Lambda^{\mathrm{a}}\right)_{11}\left(\boldsymbol{G}_\Lambda^{\mathrm{r}}\frac{d\boldsymbol{\Sigma}_U^{\mathrm{r}}}{d\Lambda}\boldsymbol{G}_\Lambda^{\mathrm{K}}\right)_{11} \\ &+\Delta_L\left(\boldsymbol{G}_\Lambda^{\mathrm{K}}\frac{d\boldsymbol{\Sigma}_U^{\mathrm{a}}}{d\Lambda}\boldsymbol{G}_\Lambda^{\mathrm{a}}\right)_{11}\Bigg].\end{aligned} \tag{5.45}$$

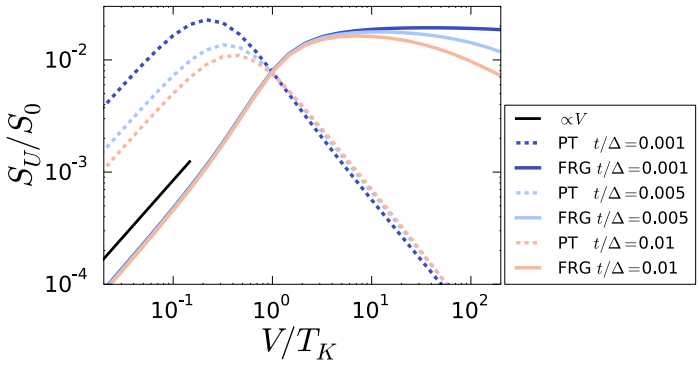

Fig. 5.5 The vertex correction S_U calculated using the FRG scheme (solid lines) and the plain perturbation theory (dashed lines) for various values of t as a function of V. The parameters are set to $u = 0.1$, $\varepsilon/T_{\rm K} = 0$, and $T/T_{\rm K} = 0$.

with the initial condition $\delta I_{\Lambda_{\rm init}} = 0$. The right-hand side should be zero within the approximations that we use.

Equation (5.45) together with the expression for the self-energy Eq. (5.14) as well as the vertex functions Eqs. (5.15) and (5.18) can be solved numerically. The resulting value of the relative difference, $|\delta I|/I^{\rm MW}$ as a function of the dimensionless interaction $u \equiv U/\Delta$ is plotted in Fig. 5.4. Within the static approximation the difference should be of second order in u, i.e. $\delta I \equiv \delta I_{\Lambda=0} = \mathcal{O}(u^2)$, which is confirmed in Fig. 5.4 for various values of V. This finding indicates that we can consistently determine the current by solving its flow equation and that the flow of the current-vertex function was properly implemented. Hence, we can correctly reproduce all the known results for the current, e.g. a power-law scaling with a U-dependent exponent at large voltages from the current determined by the new scheme.

5.2.2 On-resonance current noise

As the current is governed by the single universal energy scale $T_{\rm K}$, it is natural to expect it as the characteristic energy scale of the current noise as well. As long as we are concerned with the zero-frequency current noise in the steady state, it is sufficient to focus on the component $S \equiv S_{LL}(\omega = 0)$ due to the charge conservation. If we denote the zero-frequency bubble term (2.130) and the vertex correction (2.131) by $S_0 \equiv S^0_{LL}(\omega = 0)$ and $S_U \equiv S^U_{LL}(\omega = 0)$, respectively, the current noise can be written as

$$S = S_0 + S_U. \tag{5.46}$$

In this subsection, we consider the current noise for the on-resonance transport ($\varepsilon = 0$).

Necessity of renormalization group treatment

In order to calculate the current noise, we need to determine the current-vertex functions, which enter the expression for the vertex correction [see Eq. (2.131) and Fig. 2.5(b)]. The three-point vertex function can be computed either by using plain perturbation theory or

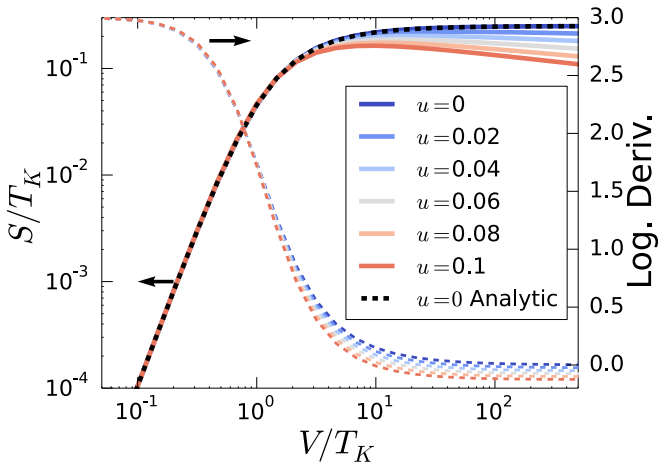

Fig. 5.6 The dependence of noise S and its logarithmic derivative $d\ln S(V)/d\ln V$ on V for various values of u. The parameters are set to $\varepsilon/T_{\rm K}=0$, $t/\Delta=0.001$, and $T/T_{\rm K}=0$.

by solving the flow equations (5.15) and (5.18). It is established in the previous study that the self-energy is plagued by a logarithmic divergence when it is computed in the plain perturbation theory [6]. To avoid this known problem, we use the propagators with the self-energy computed within the FRG scheme. Thus, we single out a possible divergence of a perturbatively calculated three-point vertex function. The V-dependence of the vertex correction S_U obtained by perturbation theory and FRG is compared in Fig. 5.5 for various values of t/Δ. The both vertex corrections are divided by the bubble term S_0, which is free from artificial divergences. A significant difference is that the results obtained by perturbation theory in the linear-response regime becomes gradually larger as we go deeper in the scaling regime $t/\Delta \ll 1$. The artificial divergence around $V=0$ prohibits us to correctly analyze the scaling limit with the plain perturbation theory. The vertex corrections calculated using FRG for the three-point vertex are free of this problem and collapse into a single curve if rescaled by $T_{\rm K}$. This indicates that the FRG regularizes the divergences of the vertex correction as is the case for the self-energy.

Zero-temperature current noise in the presence of the bias voltage

The dependence of the zero-frequency current noise on the bias voltage V is shown in Fig. 5.6 for various u. Both the self-energy and the vertex function are determined by numerically solving their flow equations. The logarithmic derivative of the noise $d\ln[S(V)]/d\ln(V)$ is also plotted to read off the exponent with respect to the bias voltage V. At small bias voltages $V<T_{\rm K}$, the curves for the current noise scaled with $T_{\rm K}$ are proportional to V^3 and collapse into a single one. This indicates that the prefactor of the leading term proportional to $(V/T_{\rm K})^3$ is independent of the two-particle interaction. For $u=0$, the current noise computed in our three-site problem agrees with the analytic result for a lattice model discussed in Ref. [22] [see the thick dashed line in Fig. 5.6].

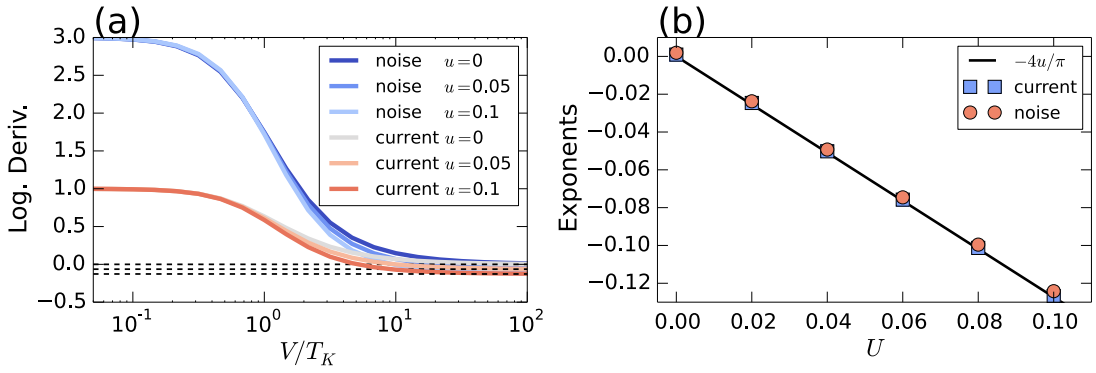

Fig. 5.7 (a) The dependence of the logarithmic derivative of the current and noise on V for various values of u. (b) The exponents for the current (blue squares) and noise (red circles) read off at large bias voltages for various values of u. The black dashed (solid) lines in the left (right) panel are the analytic result for the current [see Eq. (5.47)]. The parameters are $\varepsilon/T_{\mathrm{K}} = 0$, $t/\Delta = 0.001$, and $T/T_{\mathrm{K}} = 0$.

It is established that the current shows a power-law decay at high bias voltages

$$I/T_{\mathrm{K}} \sim (V/T_{\mathrm{K}})^{-\frac{4u}{\pi}}, \tag{5.47}$$

whose exponent is correct up to the first order in u. The constant logarithmic derivative of the noise at large voltages ($V \gg T_{\mathrm{K}}$) in Fig. 5.6 indicates that the current noise exhibits power-law behavior in the same regime. The exponents read off from the logarithmic derivatives of the current and noise at large bias voltage are compared in Fig. 5.7. The dashed lines in Fig. 5.7(a) and the solid line in Fig. 5.7(b) are the analytically obtained exponent for the current $-4u/\pi$ [6]. The exponent of the noise is found to reach the same value as that of the current at sufficiently large bias voltages. Previous works employing FRG showed that the behavior of the current can be understood from an effective noninteracting model with a renormalized hopping amplitude [6]. However, whether the effective noninteracting model can also describe the noise is not obvious because the current-vertex corrections enter its expression. The contribution of the vertex correction to the current noise is discussed in more detail in the next section.

Finite temperature current noise

The dependence of the equilibrium thermal noise S on T is shown as the solid lines in Fig. 5.8. The fluctuation-dissipation theorem states that the thermal noise is related with the linear conductance $G \equiv d\,I/dV|_{V=0}$ as $S = 4TG$, which are plotted as the dashed lines. The excellent agreement confirms that the fluctuation dissipation relation is indeed guaranteed in the reservoir-cutoff scheme. The observed power-law decay of the thermal noise at high temperatures in Fig. 5.8 can be understood as a renormalization of the transmission amplitude.

The finite-temperature current noise as a function of V is plotted for $T \ll T_{\mathrm{K}}$ and $T \gg T_{\mathrm{K}}$ in Fig. 5.9(a) and (b), respectively. The black dashed lines in Fig. 5.9(a) are the thermal noise calculated via the fluctuation-dissipation theorem $4TG$ for each temperature. The current noise obeys the fluctuation dissipation relation in the zero-bias limit; $S(V \to$

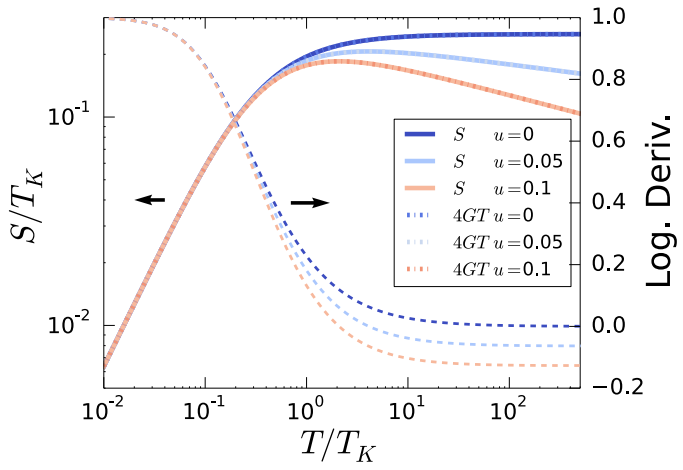

Fig. 5.8 The dependence of the equilibrium noise S (solid lines) and its logarithmic derivative $d\ln S(T)/d\ln T$ (dashed lines) on T for various values of u. The fluctuation dissipation theorem requires the equilibrium noise to be related with the conductance G as $S = 4GT$, which are plotted as dash-dot lines. The parameters are set to $\varepsilon/T_{\rm K} = 0$, $V/T_{\rm K} = 0$, and $t/\Delta = 0.001$.

$0) = 4TG$. The crossover from thermal to shot noise occurs around voltages such that $S_3V^3 \sim TG$, where S_3 is the coefficient of the V^3 term in the current noise S. The power-law decay of the current noise is observed in the high-bias regime as it is for the zero-temperature noise. The current noise at high temperatures $T \gg T_{\rm K}$ is shown in Fig. 5.9(b). The power-law decay at high-bias voltages still survives when the bias voltage is larger than T. It is found that the current noise exhibits a power-law decay at sufficiently large voltages; $V \gg \max\{T, T_{\rm K}\}$. Due to this renormalization effect, the value of the current noise at high voltages can become even smaller than the value in the zero bias limit. We note, however, that the current is suppressed as well with the same exponent.

Effective charge in the weak interaction regime

The ratio between the noise and the current can be interpreted as an effective charge of carriers when the transport is governed by the Poisson statistics [23]. At the particle-hole symmetric point, the effective charge is defined as the ratio between the noise and the backscattering current [12, 13] as

$$e^* = \lim_{V\to 0} \frac{S(V)}{2I_{\rm BS}(V)}, \tag{5.48}$$

with the backscattering current

$$I_{\rm BS} \equiv GV - I. \tag{5.49}$$

In the noninteracting case $u = 0$, the effective charge e^* is e as is expected for the resonant level model [see subsection 2.3.1 for details]. The self-dual point [12, 13] is another solvable case reached at a relatively large interaction in the presence of the particle-hole symme-

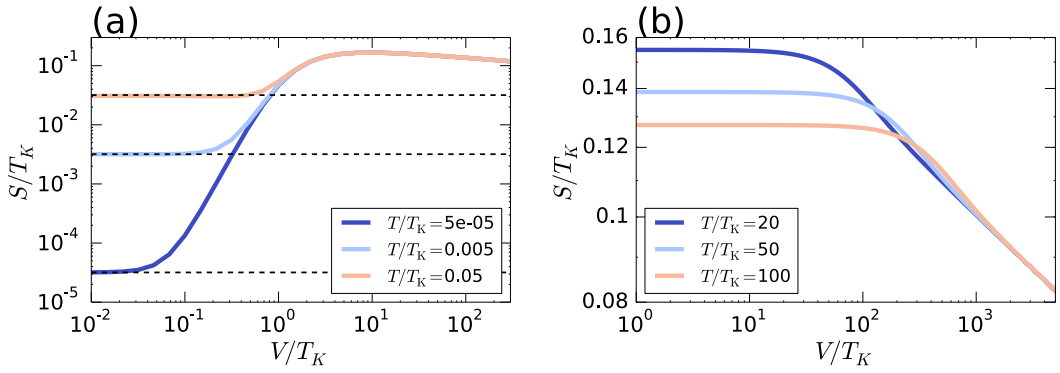

Fig. 5.9 The dependence of the noise on V for (a) $T \ll T_K$ and (b) $T \gg T_K$ for various values of u and T. The parameters are set to $u = 0.01$, $\varepsilon/T_K = 0$ and $t/\Delta = 0.001$.

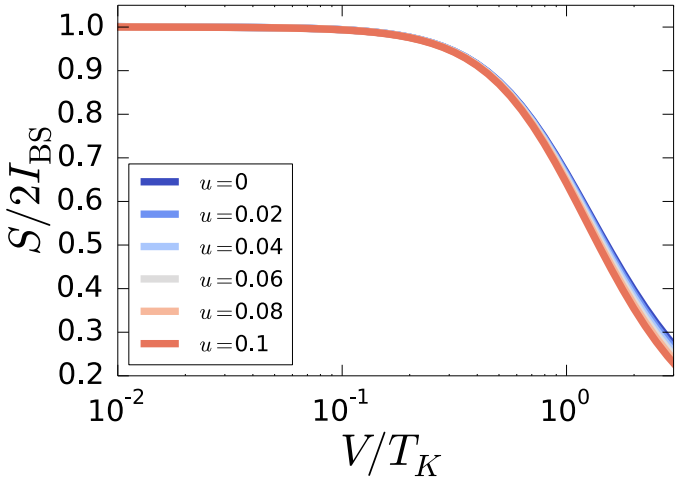

Fig. 5.10 The dependence of the ratio between the noise S and the backscattering current I_{BS} on V for various values of u. The parameters are set to $\varepsilon/T_K = 0$, $t/\Delta = 0.001$, and $T/T_K = 0$.

try. At this point, field-theoretical techniques and the density-matrix renormalization-group approach were utilized to show that the effective charge is $2e$. However, It is totally unknown so far how e^* develops from e to $2e$ when u is increased. In this subsection, we study this issue using our FRG scheme. Since our scheme is based on an expansion in terms of the interaction strength (on the right-hand side of RG flow equations), we are bound to small to intermediate u.

The dependence of the ratio $S/2I_{BS}$ on V is shown in Fig. 5.10 for various values of u. The value of e^*/e can be read off at $V/T_K = 10^{-2}$. It is found that e^* does not depend on the interaction in our approximation. As all the contributions to linear order in u are kept in our FRG scheme, we conclude that $e^*/e = 1 + \mathcal{O}(u^2)$. This numerical observation can be substantiated by combined with the following analytic considerations.

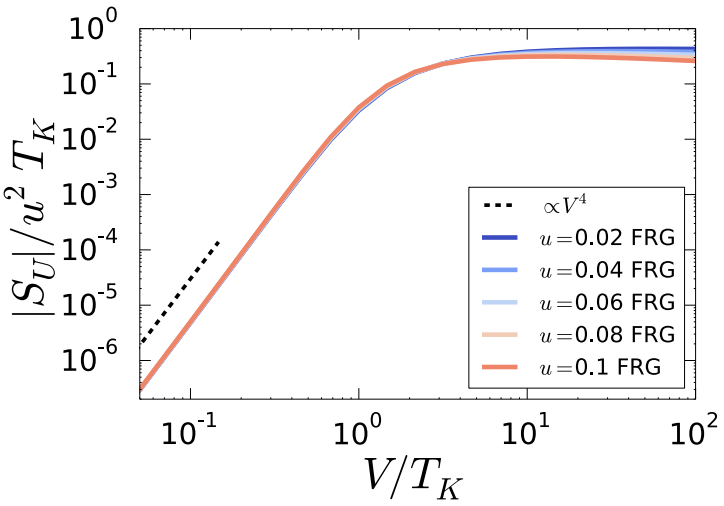

Fig. 5.11 The vertex correction S_U divided by $u^2 S_0$ calculated using our FRG scheme for various values of u as a function of V. The parameters are set to $\varepsilon/T_\mathrm{K} = 0$, $t/\Delta = 0.001$, and $T/T_\mathrm{K} = 0$.

We, first, consider the leading term of the backscattering current I_BS with respect to the bias voltage V. In the linear-response regime, the transmission amplitude

$$T_{LR}(\omega) \equiv \Delta_L \Delta_R \left(\boldsymbol{G}^\mathrm{r}\right)_{13}(\omega) \left(\boldsymbol{G}^\mathrm{a}\right)_{31}(\omega). \tag{5.50}$$

can be expanded in terms of the bias voltage as

$$T_\mathrm{LR} = T_\mathrm{LR}^{(0)} - T_\mathrm{LR}^{(2)} \left(\frac{V}{T_\mathrm{K}}\right)^2 + \cdots. \tag{5.51}$$

Here, the frequency dependence of the transmission amplitude is neglected as we focus on the small bias-voltage regime ($V \ll T_\mathrm{K}$). Since we are concerned with the on-resonance transport, the first term is unity $T_\mathrm{LR}^{(0)} = 1$. The second-order coefficient is obtained as $T_\mathrm{LR}^{(2)} = 1/3$ because field-theoretical considerations [24] have shown that the backscattering current is given by

$$\frac{2\pi I_\mathrm{BS}}{T_\mathrm{K}} = \frac{1}{3}\left[1 + \mathcal{O}(u^2)\right]\left(\frac{V}{T_\mathrm{K}}\right)^3 - \frac{1}{5}\left[1 - \frac{20}{3}\frac{u}{\pi} + \mathcal{O}(u^2)\right]\left(\frac{V}{T_\mathrm{K}}\right)^5 + \mathcal{O}\left(\left[\frac{V}{T_\mathrm{K}}\right]^7\right), \tag{5.52}$$

which is consistently obtained by FRG (see footnote [52] of Ref. [24]; for a similar analysis of the current as function of temperature see Ref. [19]). We note that this result can be reproduced by our numerical calculations with the properly chosen T_K (see Appendix 5.A). This shows that the nonlinear coefficient of the current and noise can be reliably obtained by our numerical calculation.

As for the bubble term of the current noise, the lowest-order contribution in V at zero-temperature ($T = 0$) and on resonance ($T_{\mathrm{LR}}^{(0)} = 1$) is obtained as

$$\frac{S_0}{T_{\mathrm{K}}} = \frac{1}{\pi}\left(\frac{V}{T_{\mathrm{K}}}\right)^3 T_{\mathrm{LR}}^{(2)}. \tag{5.53}$$

Then, the effective charge (5.48) is directly associated with the vertex correction S_U as

$$e^* = 1 + \left.\frac{3\pi S_U}{(V/T_{\mathrm{K}})^3}\right|_{V=0}. \tag{5.54}$$

This relation shows that the U-dependence of the effective charge is incorporated via the vertex correction.

The remaining question is whether the leading $(V/T_{\mathrm{K}})^3$ term in the vertex correction has an correction of order u. The answer is negative as is numerically seen in Fig. 5.11, in which the vertex correction divided by u^2 is plotted for various values of u. From this figure, it is evident that S_U depends on u and V as $|S_U|/T_{\mathrm{K}} \propto u^2(V/T_{\mathrm{K}})^4$ in the linear-response regime ($V < T_{\mathrm{K}}$). Because of the prefactor of order u^2 , the vertex correction is not under control within the static approximation which only contains terms of order u. However, the vertex correction does not contribute to the effective charge because it is of order V^4 while the bubble term scales as V^3 in the linear-response regime ($V < T_{\mathrm{K}}$). These analytic and numerical considerations on the effective charge and the numerical observation of the vertex correction consistently lead us to the conclusion that the effective charge e^* shown in Fig. 5.10 is not dependent on the two-body interaction u up to the first order. In order to discern whether the correct u^2 term is proportional to V^3 or not, we have to use the higher order truncation schemes.

5.2.3 Current noise away from particle hole symmetric point

In this subsection, we investigate the current noise away from the particle-hole symmetric point ($\varepsilon \neq 0$).

Breakdown of plain perturbation theory away from resonance

We start by considering how the plain perturbation theory breaks down in the particle-hole asymmetric case. The bias-voltage dependence of the noise with the three-point vertex functions calculated with plain perturbation theory is shown in Fig. 5.12(a) for different values of u and t/Δ. Here, all propagators entering in the current vertex function are computed in the FRG scheme to suppress the artificial divergence originating from the self-energy. The peak located around $V/2 \sim \varepsilon$ divergently develops as we go deeper into the scaling regime ($t/\Delta \ll 1$). The vertex correction S_U divided by the product of the two-body interaction u and the bubble term S_0 is shown in Fig. 5.12(b), in which the diverging peak is found to have a prefactor of order u. The plain perturbation theory cannot be used to study the current noise away from particle-hole symmetry in the scaling limit even for very small u.

The current noise and its vertex correction determined by solving their flow equations Eqs. (5.15) and (5.18) are shown in Fig. 5.13. The divergent behavior of the current noise

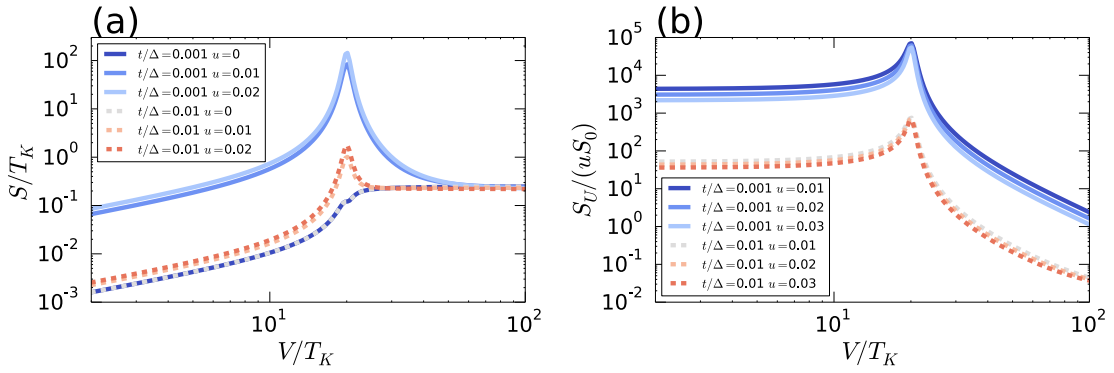

Fig. 5.12 (a) The current noise S and (b) the vertex correction S_U divided by uS_0 calculated from a plain perturbation theory for various values of u and t away from the particle-hole symmetric point as a function of V. The parameters are set to $\varepsilon/T_\mathrm{K} = 10$ and $T/T_\mathrm{K} = 0$.

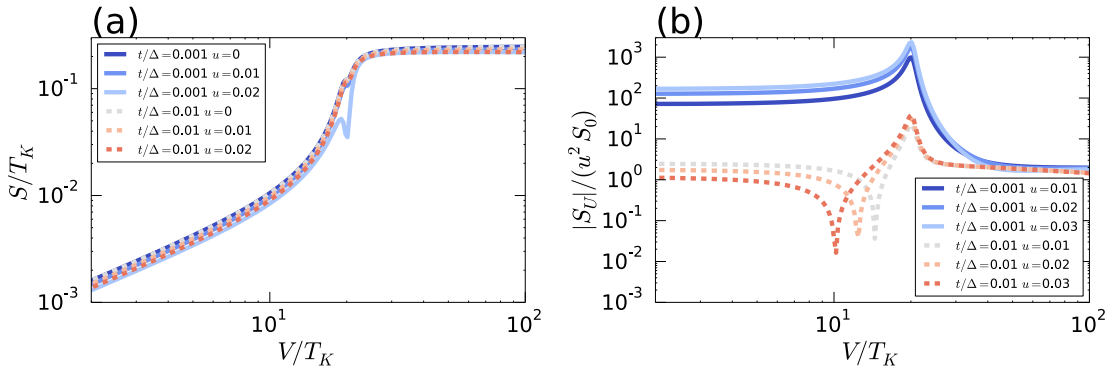

Fig. 5.13 (a) The current noise S and (b) the vertex correction S_U divided by u^2S_0 calculated using our FRG scheme for various values of u and t away from the particle-hole symmetric point as a function of V. The parameters are set to $\varepsilon/T_\mathrm{K} = 10$ and $T/T_\mathrm{K} = 0$.

observed in Fig. 5.12(a) is essentially removed for the curves in Fig. 5.13(a) for $t/\Delta = 0.01$. This indicates that our FRG scheme regularizes the leading-order divergences as for the self-energy. In order to analyze the weak features still visible in the deep scaling regime $t/\Delta = 0.001$, we plot the vertex correction S_U divided by u^2S_0 in Fig. 5.13(b). This figure shows that the divergence with a prefactor of order u of plain perturbation theory [see Fig. 5.12(b)] is pushed to order u^2 within the FRG scheme. We cannot get rid of the artificial divergence of order u^2 within the static approximation which is valid up to the linear order in u. This second-order divergence manifests itself as the artificial dip of the noise appearing in Fig. 5.13(a) in the deep scaling regime ($t/\Delta = 0.001$). In the subsequent discussions, we take $t/\Delta = 0.01$, where this artifact of order u^2 is negligibly smaller than the bubble term.

Off-resonance current noise

The current noise as a function of V is shown in Fig. 5.14 for various values of u. In the linear-response regime ($V < T_\mathrm{K}$), the current noise is proportional to V in contrast to the resonant transport [see Fig. 5.6]. At large bias voltages, the current crosses over to a

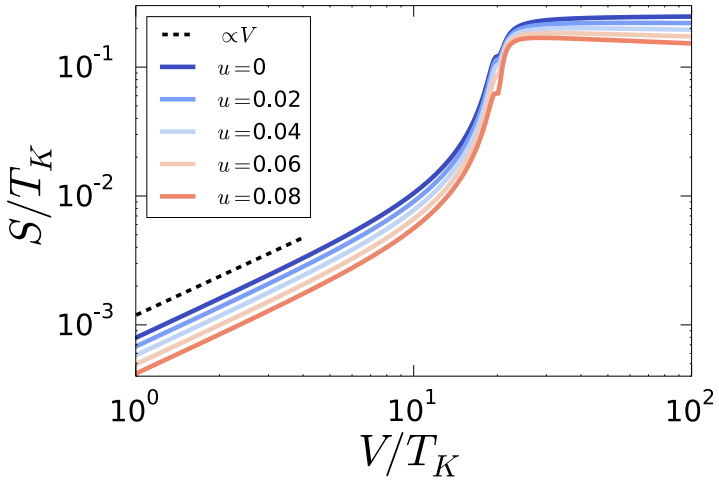

Fig. 5.14 The dependence of the current noise S on V for various values of u away from the particle-hole symmetric point. The parameters are set to $\varepsilon/T_{\rm K} = 10$, $t/\Delta = 0.01$, and $T/T_{\rm K} = 0$.

power-law decay with an interaction-dependent exponent $\alpha_S = -4u/\pi$. This accordance with the on-resonant case $\varepsilon = 0$ is reasonable as the bias voltage dominates the transport regardless of the presence or absence of ε for $V \gg \varepsilon$.

The dependence of the current noise on ε at a fixed value of V is shown in Fig. 5.15. The noise is constant for $\varepsilon \ll V$ as the level is placed inside the bias window. The ε-dependence of the noise is visible when the level energy is away from the bias window ($\varepsilon \gtrsim V/2$). For large $\varepsilon \gg T_{\rm K}$, the noise crosses over to a power-law decay as a function of ε as the level position works as the cutoff of the renormalization in this case. For $u = 0$ the exponent is -2 and the interacting part of the exponent is found to be twice as large as that of the V-dependence; see the logarithmic derivative shown in Fig. 5.15 for $\varepsilon/T_{\rm K} \leq 1$ and $\varepsilon/T_{\rm K} \geq 10$.

5.3 Discussion

In this chapter, we have investigated the current noise through a charge-fluctuating quantum dot system. The minimal model for the interacting spinless fermion in the quantum dot is given by the interacting resonant-level model (IRLM), where the transmission amplitude between the dot and the leads is significantly renormalized by the two-particle interaction u. We have developed a nonequilibrium functional renormalization-group (FRG) scheme to investigate the current fluctuation in wide parameter regions which previous works could not have addressed. In contrast to the current which is solely determined by the self-energy, the current noise requires computation of the current vertex function. We start with the lowest-order truncation with respect to the two-particle interaction u to derive and solve the flow equation of the current vertex function. The simple approximation allows a unified picture of the current noise through the IRLM in the wide parameter regions including the case without the particle-hole symmetry.

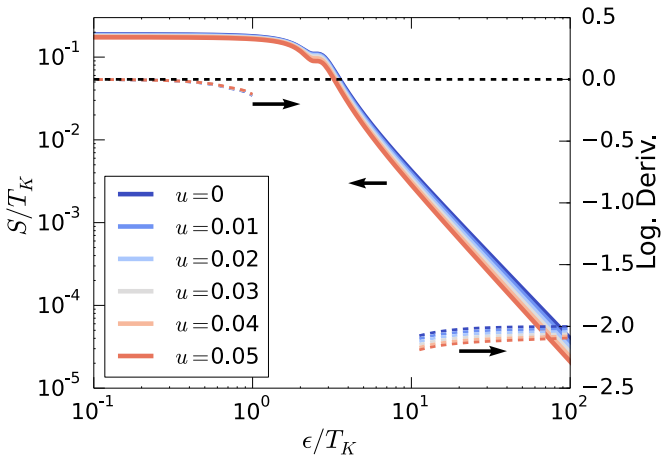

Fig. 5.15 The dependence of the current noise and its logarithmic derivative on ε for various values of u. The parameters are set to $V/T_{\mathrm{K}} = 5$, $t/\Delta = 0.01$, and $T/T_{\mathrm{K}} = 0$.

In the scaling limit, where the bandwidth of the lead is much larger than any other energy scales, the current noise calculated in plain perturbation theory is plagued by artificial divergences. We have confirmed that the divergence originates from the vertex function which enters in the vertex correction to the current noise. Our FRG method removes the divergence at the particle-hole symmetric point, allowing a reliable analysis in the deep scaling limit. In this regime, the current noise at high bias voltages shows a power-law decay with the same exponent as that of the current. A finite-temperature effect on the current noise is also incorporated consistently with the fluctuation-dissipation theorem. The effective charge associated with the on-resonance transport through IRLM is found to be independent of the interaction in the linear order in u. In the absence of the particle-hole symmetry, a severe leading-order divergence found in the plain perturbation theory is consistently replaced by $\mathcal{O}(u^2)$ one, which is out of control in our lowest-order approximation. Although the remaining order u^2 divergence prohibits us to go deep in the scaling limit, we obtain reliable results down to $t/\Delta = 0.01$. We found that the current noise robustly shows a power-law decay for $\max\{V, \varepsilon\} \gg T_{\mathrm{K}}$.

The remaining problem is that we are bound to the regime where the two-body interaction is weak or intermediate. Higher-order calculations are desirable in the future to discuss the crossover of the effective charge from the noninteracting case ($e^*/e = 1$) to the self-dual point ($e^*/e = 2$) realized at relatively large values of u [12]. Furthermore, the higher-order contributions need to be taken into account to remove a diverging term of order u^2 away from the particle-hole symmetric point. Another promising step is to extend the FRG framework to determine the full counting statistics of interacting fermion systems [13, 25, 26].

Appendix 5.A Definition of T_{K}

There is an alternative definition of the characteristic energy scale T_{K} other than $T_{\mathrm{K}} \equiv 8|t + \mathbf{\Sigma}^{\mathrm{r}}_{12}|_{T=V=\varepsilon=0}|^2/\Delta$ used in the main text. The definition used in previous papers

[6, 7, 18, 19] is related with the susceptibility as

$$T_{\mathrm{K}}^{\mathrm{sus}} \equiv -\frac{2}{\pi}\left(\left.\frac{d\langle n_2\rangle}{d\varepsilon}\right|_{T=V=\varepsilon=0}\right)^{-1}, \tag{5.55}$$

where $\langle n_2\rangle$ is the occupation of the central site. Both definitions can equivalently be used when comparing with field-theoretical results obtained for $t/\Delta \to 0$ in the scaling regime. We found that results rescaled with the T_{K} obtained with the renormalized hopping are weakly dependent on t/Δ and are closer to the field-theoretical predictions.

References

[1] P. Schlottmann, Phys. Rev. B **25**, 4815 (1982).

[2] B. Doyon, Phys. Rev. Lett. **99**, 076806 (2007).

[3] L. Borda, K. Vladár, and A. Zawadowski, Phys. Rev. B **75**, 125107 (2007).

[4] E. Boulat, H. Saleur, and P. Schmitteckert, Phys. Rev. Lett. **101**, 140601 (2008).

[5] A. Nishino, T. Imamura, and N. Hatano, Phys. Rev. Lett. **102**, 146803 (2009).

[6] C. Karrasch, M. Pletyukhov, L. Borda, and V. Meden, Phys. Rev. B **81**, 125122 (2010).

[7] C. Karrasch, S. Andergassen, M. Pletyukhov, D. Schuricht, L. Borda, V. Meden, and H. Schoeller, Europhys. Lett. **90**, 30003 (2010).

[8] S. Andergassen, M. Pletyukhov, D. Schuricht, H. Schoeller, and L. Borda, Phys. Rev. B **83**, 205103 (2011).

[9] A. Nishino, N. Hatano, and G. Ordonez, Phys. Rev. B **91**, 045140 (2015).

[10] A. Golub, Phys. Rev. B **76**, 193307 (2007).

[11] P. Fendley, A. W. W. Ludwig, and H. Saleur, Phys. Rev. B **52**, 8934 (1995).

[12] A. Branschädel, E. Boulat, H. Saleur, and P. Schmitteckert, Phys. Rev. Lett. **105**, 146805 (2010).

[13] S. T. Carr, D. A. Bagrets, and P. Schmitteckert, Phys. Rev. Lett. **107**, 206801 (2011).

[14] S. T. Carr, P. Schmitteckert, and H. Saleur, Phys. Scr. **2015**, 014009 (2015).

[15] W. Metzner, M. Salmhofer, C. Honerkamp, V. Meden, and K. Schönhammer, Rev. Mod. Phys. **84**, 299 (2012).

[16] S. G. Jakobs, M. Pletyukhov, and H. Schoeller, J. Phys. A: Math. Theor. **43**, 103001 (2010).

[17] S. G. Jakobs, M. Pletyukhov, and H. Schoeller, Phys. Rev. B **81**, 195109 (2010).

[18] D. M. Kennes, S. G. Jakobs, C. Karrasch, and V. Meden, Phys. Rev. B **85**, 085113 (2012).

[19] D. M. Kennes and V. Meden, Phys. Rev. B **87**, 075130 (2013).

[20] J. W. Negele and H. Orland, *Quantum many-particle systems* (Westview, 1988).

[21] Y. Meir and N. S. Wingreen, Phys. Rev. Lett. **68**, 2512 (1992).

[22] A. Branschädel, E. Boulat, H. Saleur, and P. Schmitteckert, Phys. Rev. B **82**, 205414 (2010).

[23] Y. Blanter and M. Büttiker, Phys. Rep. **336**, 1 (2000).

[24] L. Freton and E. Boulat, Phys. Rev. Lett. **112**, 216802 (2014).

[25] A. O. Gogolin and A. Komnik, Phys. Rev. B **73**, 195301 (2006).

[26] A. O. Gogolin and A. Komnik, Phys. Rev. Lett. **97**, 016602 (2006).

Chapter 6

Summary and conclusion

In this thesis, we have investigated the nonequilibrium current fluctuation in mesoscopic conductors. In chapter 1, we have reviewed the full counting statistics [1] and shown that rich information on the microscopic transport processes is accessed by utilizing the current fluctuation. The recent knowledge established by theoretical and experimental works have motivated us to clarify two important aspects of the current fluctuation: a detection of the full counting statistics and renormalization effect due to the two-body interaction. These are essentially concerned with interacting mesoscopic systems. In order to microscopically discuss the current fluctuation in such systems, a systematic method has been developed in chapter 2 based on the Keldysh path integral formulation. In chapter 3, we have overviewed the recent insights into the non-Gaussian stochastic equation which describes a particle coupled to multiple environments. Chapters 4 and 5 are devoted to the topics of our main interest. We summarize the results in the following.

Detection of non-Gaussian fluctuation

In chapter 4, we have studied a realistic detection scheme of full counting statistics in mesoscopic conductors. We consider the simple problem of determining the current distribution through a quantum point contact (QPC) by using an inductively coupled LC circuit as a detector. We use a critical assumption that the characteristic time scale of the detector is much larger than that of the QPC. With the aid of the quasi-stationary approximation, we can obtain a stochastic picture in which the flux through the detector circuit is perturbed by a non-Gaussian noise generated by the current through the QPC. In the classical limit, the detector can be considered as a stochastic particle driven by the thermal and the non-Gaussian noise. At low temperatures, the quantum nature of the dissipative circuit becomes significant as well. We used a stochastic approach to microscopically describe the dynamics of the particle in the presence of the thermal, quantum, and non-Gaussian noises. Based on this, we have shown that the steady-state probability density function (PDF) of the detector circuit can fully characterize the statistical properties of the non-Gaussian noise even in the classical-quantum crossover regime. It is also clarified that the quantum correction is essential to correctly estimate the current fluctuation in the mesoscopic conductor.

The result of this thesis has established the observability of the current distribution by using a realistic on-chip device. The information on the full counting statistics, which looked too abstract to be determined at first sight, is completely encoded in the dynamics

of the detector circuit. We have provided the inverse relation to infer the statistics of the current fluctuation from the steady state PDF of the detector circuit even in the presence of the weak quantum fluctuation. It is an important future work to use the formalism for coherent conductors such as the Aharonov-Bohm ring [2]. A possible drawback of our analysis is that it is restricted to the time-averaged current fluctuations. When the time scale of the detector is comparable to that of the conductor, the transport through the conductor are significantly affected by the photon exchange between the subsystems [3, 4]. We need to go beyond the quasi-stationary approximation to discuss the time-dependent transport [5, 6] and the finite-frequency full counting statistics [7].

Current noise in a charge-fluctuating quantum dot

In chapter 5, we have studied nonequilibrium current noise through a charge-fluctuating quantum-dot system. The quantum dot in this regime is well described by the interacting resonant-level model (IRLM), where the capacitive coupling between the quantum dot and leads results in significant renormalization effect on the transmission amplitude. Although the nonlinear I-V characteristic has been established by various methods [8–14], little work has been done on the current noise except for a self-dual point [15–17]. We have developed a functional renormalization group (FRG) approach [11, 18] to describe the current fluctuation in the IRLM in wide parameter regions. The flow equations of the current-vertex functions are derived and solved to determine the current noise. Our FRG method consistently removes artificial divergences found in the plain perturbation theory, allowing a comprehensive understanding of the current noise in the scaling regime. It is found that the current noise exhibits universal power-law decay, whose exponent is dependent on the strength of the two-body interaction. We also analyze the effective charge in the weak coupling regime and find that it is only modified to the second or higher orders in the two-particle interaction.

Our results indicate that novel renormalization effect manifests itself in the current noise in the interacting quantum-dot systems. The nonequilibrium FRG approach developed in this thesis offers a versatile method to discuss the full counting statistics in interacting systems [16, 19, 20]. What remains unclear in our analysis is the higher-order contributions in terms of the two-body interaction. An important question for future studies is to clarify the microscopic scattering process of Fermi liquids in nonequilibrium situations [21].

References

[1] L. S. Levitov, H. Lee, and G. B. Lesovik, J. Math. Phys. **37**, 4845 (1996).

[2] S. Nakamura, Y. Yamauchi, M. Hashisaka, K. Chida, K. Kobayashi, T. Ono, R. Leturcq, K. Ensslin, K. Saito, Y. Utsumi, and A. C. Gossard, Phys. Rev. Lett. **104**, 080602 (2010).

[3] H. Grabert and M. H. Devoret, *Single charge tunneling: Coulomb blockade phenomena in nanostructures*, Vol. 294 (Springer Science & Business Media, 2013).

[4] Y. Nazarov, Ann. Phys. (Leipzig) **16**, 720 (2007).

[5] J. Gabelli, G. Fève, J.-M. Berroir, B. Plaçais, A. Cavanna, B. Etienne, Y. Jin, and D. Glattli, Science **313**, 499 (2006).

[6] E. Bocquillon, V. Freulon, J.-M. Berroir, P. Degiovanni, B. Plaçais, A. Cavanna, Y. Jin, and G. Feve, Science **339**, 1054 (2013).

[7] N. Ubbelohde, C. Fricke, C. Flindt, F. Hohls, and R. J. Haug, Nat. Commun. **3**, 612 (2012).

[8] B. Doyon, Phys. Rev. Lett. **99**, 076806 (2007).

[9] L. Borda, K. Vladár, and A. Zawadowski, Phys. Rev. B **75**, 125107 (2007).

[10] E. Boulat, H. Saleur, and P. Schmitteckert, Phys. Rev. Lett. **101**, 140601 (2008).

[11] C. Karrasch, M. Pletyukhov, L. Borda, and V. Meden, Phys. Rev. B **81**, 125122 (2010).

[12] C. Karrasch, S. Andergassen, M. Pletyukhov, D. Schuricht, L. Borda, V. Meden, and H. Schoeller, Europhys. Lett. **90**, 30003 (2010).

[13] S. Andergassen, M. Pletyukhov, D. Schuricht, H. Schoeller, and L. Borda, Phys. Rev. B **83**, 205103 (2011).

[14] A. Nishino, N. Hatano, and G. Ordonez, Phys. Rev. B **91**, 045140 (2015).

[15] A. Branschädel, E. Boulat, H. Saleur, and P. Schmitteckert, Phys. Rev. Lett. **105**, 146805 (2010).

[16] S. T. Carr, D. A. Bagrets, and P. Schmitteckert, Phys. Rev. Lett. **107**, 206801 (2011).

[17] S. T. Carr, P. Schmitteckert, and H. Saleur, Phys. Scr. **2015**, 014009 (2015).

[18] W. Metzner, M. Salmhofer, C. Honerkamp, V. Meden, and K. Schönhammer, Rev. Mod. Phys. **84**, 299 (2012).

[19] A. O. Gogolin and A. Komnik, Phys. Rev. B **73**, 195301 (2006).

[20] A. O. Gogolin and A. Komnik, Phys. Rev. Lett. **97**, 016602 (2006).

[21] A. Oguri, J. Phys. Soc. Jpn. **74**, 110 (2005).